Computational modelling of molecular nexopathies

Konstantinos Georgiadis

A dissertation submitted in partial fulfillment

of the requirements for the degree of

Doctor of Philosophy

of

University College London.

Department of Medical Physics and Biomedical Engineering

University College London

February 11, 2020

I, Konstantinos Georgiadis, confirm that the work presented in this thesis is my own. Where information has been derived from other sources, I confirm that this has been indicated in the work.

Abstract

Neurodegenerative diseases are an ever-increasing health problem, requiring substantial human and financial resources. They are caused by pathogenic proteins, which accumulate and spread in the brain's neural network, causing neuronal loss and brain atrophy. However, the mechanisms that govern pathogenic protein accumulation, spread, and toxic effects are still poorly understood, and many competing hypotheses regarding them have been presented by researchers. A better understanding of these mechanisms can help inform which hypotheses are more likely to be true, improve prognosis tools, and assist in drug development.

Clinically, brain atrophy follows specific spatiotemporal patterns in each neurodegenerative disease, and each disease is linked to specific pathogenic proteins. This observation led to the 'molecular nexopathies' hypothesis, which states that clinical phenotypes can be predicted if the specific pathogenic protein variant and the neural network characteristics are both known. However, little computational work has been done that links pathogenic protein mechanisms, the brain's neural network, and clinical phenotypes.

In this thesis, I developed computational models for a variety of hypotheses regarding pathogenic protein mechanisms of accumulation, spread, and toxic effects on the brain, which occur at the neuronal scale, while linking them to neuroimaging data, which is acquired at the brain scale. After running simulations with the modelled mechanisms within a neural network, I compared simulation results over time against empirical data for Alzheimer's disease and three genetic variants of frontotemporal dementia.

For each disease, the model that best fitted its atrophy progression was found,

discovering differences among diseases with regards to what degree each mechanism played a role. I also analysed how each mechanism affected disease progression, discovered each disease's seed location, and found mechanisms that showed potential as candidate targets for therapies, in particular, increasing the firing frequency of neurons.

Impact Statement

In this thesis, I present a framework for linking neuronal scale mechanisms of pathogenic proteins to brain scale disease phenotypes (with more work required for a more substantial impact). The current work could have an impact in the short term primarily in the academic field. At its core, the aim of this work was to discover which hypotheses regarding pathogenic protein mechanisms hold more validity against patient neuroimaging data, providing evidence in favour of some hypotheses and against others, which is a common application for computational modelling. Thus, this work can suggest which hypotheses should have priority for further neurobiological research. Similarly, neurobiological research improves our understanding of pathogenic protein mechanisms would result in more accurate computational models. This cyclical effect could be best exploited within a collaborative and multidisciplinary effort between neurobiologists and modellers. Publishing of this work's results in multidisciplinary journals would increase their visibility to neurobiologists.

Assuming this work is further progressed in the future, it has a lot of potential in the long term. After creating sufficiently refined and accurate models of pathogenic protein mechanisms, their behaviour would become predictable. Computational modelling has been used before in pharmaceutical research, and with the further development of this work, it will be possible to make suggestions regarding which specific mechanisms hold promise as therapeutic targets by simulating therapies that directly affect the mechanisms in some manner, and then checking which therapies ended up delaying disease progression. In addition, with further improvement of this work's modelling, it is possible to have improved prognosis, including

prognosis for individual subjects, which would be useful in a clinical and academic context.

Acknowledgements

I would like to thank my primary supervisor, Dr. Marc Modat, as well as my secondary supervisors, Prof. Jason D. Warren, and Prof. Sébastien Ourselin for always being helpful, for their enthusiasm and their insight.

I would like to thank those who directly collaborated with me, in particular: Selina Wray, Carla Semedo, Alexandra Young, Michael Hütel, Adeel Razi, Daniel Alexander, and Jonathan Schott. In addition, I would like to thank Ted Carnevale for his help with the NEURON simulator, as well as Sam Neymotin and Bill Lytton for their help with their cortical column network code, which I used for my work.

I would also like to thank my friends and labmates, especially Marta Ranzini, Stefano Moriconi, Jonas Pichat, Irina Grigorescu, Kerstin Stinkiii Klaser, Liane Canas, Stephen Morrell, Maria Robu, Joao Ramalhinho, Nooshin Ghavami, Irme Groothuis, Marzia Scelsi, and Alessia Atzeni.

Finally, I would like to thank my parents, Christos and Maria, and my brother, Giorgos.

Contents

List of Figures

List of Tables

List of abbreviations and mathematical notation

Abbreviations

AD Alzheimer's disease

ADNI Alzheimer's Disease Neuroimaging Initiative

ApoE Apolipoprotein E

APP amyloid precursor protein

ASY asymmetry

BOLD blood-oxygen-level dependent

bvFTD behavioural variant frontotemporal dementia

C9orf72 chromosome 9 open reading frame 72

CJD Creutzfeldt-Jakob disease

CT computed tomography

EBM event based model

fMRI functional MRI

FS fast spiking (inhibitory neuron)

FTD frontotemporal dementia

GBP great british pound

GDS geodesic distance to the seed

GRN Progranulin

IB intrinsically bursting (excitatory neuron)

LTS low-threshold spiking (inhibitory neuron)

lvPPA logopenic variant PPA

MAPT microtubule-associated protein tau

MR magnetic resonance

MRI magnetic resonance image/imaging

nfvPPA nonfluent/agrammatic variant PPA

PET positron emission tomography

PPA primary progressive aphasia

PrP prion protein

ROI region of interest

RS regular spiking (excitatory neuron)

rsfMRI resting-state functional MRI

SSG synaptic strength gradient

svPPA semantic variant PPA

T1w T1-weighted (MRI acquisition)

TTNB time to network breakdown

Mathematical notation

θ brain scale and multiscale work, set of simulation parameters

$\theta^{\star}$ brain scale and multiscale work, set of optimal simulation parameters

θ^{AD} multiscale work, optimal parameter set for Alzheimer's disease

$\theta^{C9orf72}$ multiscale work, optimal parameter set for C9orf72 mutation related frontotemporal dementia

θ^{dis} multiscale work, optimal parameter set for neurodegenerative disease dis

θ^{GRN} multiscale work, optimal parameter set for GRN mutation related frontotemporal dementia

θ^{MAPT} multiscale work, optimal parameter set for MAPT mutation related frontotemporal dementia

$\mu_{\text{Txc}}(t)$ neuronal scale work, mean toxicity among neurons at timestep t

$\rho_r(t)$ brain scale and multiscale work, radius of brain region r at timestep t

σ_{ED} brain scale and multiscale work, extracellular diffusion speed (standard deviation of a normal distribution)

σ_{ID} multiscale work, intracellular diffusion speed (standard deviation of a normal distribution)

$\sigma_{\text{ND|E}}$ brain scale work, standard deviation of normal distribution for diffusion of effective connectivity related network-mediated diffusion, used to control the speed of diffusion

$\sigma_{\text{ND|F}}$ brain scale work, standard deviation of normal distribution for diffusion of functional connectivity related network-mediated diffusion, used to control the speed of diffusion

$\sigma_{\text{ND|S}}$ brain scale work, standard deviation of normal distribution for diffusion of structural connectivity related network-mediated diffusion, used to control the speed of diffusion

σ_{NND} neuronal scale and multiscale work, neuronal network diffusion speed (standard deviation of a normal distribution)

$\sigma_{\text{Txc}}(t)$ neuronal scale work, standard deviation of toxicity among neurons at timestep t

$\Phi(x|\mu,\sigma)$ cumulative distribution function of the normal distribution, with mean μ, and standard deviation σ

$\mathbf{ACT}_{i,j\leftarrow\bar{i},\bar{j}}(t)$ neuronal scale work, probability of protein spreading via active transport from neuron $\bar{i}$, compartment $\bar{j}$ to neuron i, compartment j at timestep t

$\mathbf{ACT}_{i,j|r\leftarrow\bar{i},\bar{j}|r}(t)$ multiscale work, probability of protein spreading via active transport from compartment $\bar{j}$ of neuron $\bar{i}$ from brain region r to compartment j of neuron i from brain region r at timestep t

$\text{Alive}_r(t)$ multiscale work, set of alive neurons from brain region r at timestep t

$\text{Area}_{i,j}$ neuronal scale work, base area of the neuronal compartment j of neuron i

$\text{Area}_{i,j|r}$ multiscale work, base area of compartment j of neuron i from brain region r

$A_r(t)$ brain scale and multiscale work, atrophy of brain region r at timestep t

ASY neuronal scale work, overall asymmetry of neuronal toxicity during a simulation

AThr brain scale work, minimum protien concentration threshold for any atrophy to occur

$\mathbf{BSS}_{i,j|r\leftarrow\bar{i},\bar{j}|\bar{r}}(t)$ multiscale work, probability of protein spreading via all brain scale spread mechanisms from compartment $\bar{j}$ of neuron $\bar{i}$ from brain region $\bar{r}$ to compartment j of neuron i from brain region r at timestep t

$\mathbf{BSS}(t)$ brain scale work, matrix combining all of the matrices related to spread mechanisms at timestep t

$\mathbf{CA}_{i,j|r\leftarrow\bar{i},\bar{j}|\bar{r}}(t)$ multiscale work, indicates whether there is a connection from compartment $\bar{j}$ of neuron $\bar{i}$ from brain region $\bar{r}$ to compartment j of neuron i from brain region r at timestep t

$\text{C}|\text{dis}(\theta)$ multiscale work, cost function

Cmin multiscale work, minimum concentration required to cause an increase in the toxicity level of a neuron

$\text{CnClear}_{i,j|r}(t)$ multiscale work, non-pathogenic protein cleared at compartment j of neuron i from brain region r at timestep t

$\text{CnClear}_{i,j}(t)$ neuronal scale work, concentration of non-pathogenic protein cleared in compartment j of neuron i at timestep t

$\text{CnClear}_r(t)$ brain scale work, non-pathogenic protein concentration cleared at brain region r at timestep t

CnHealth all work, healthy concentration level for non-pathogenic protein

$\text{Cn}_{i,j|r}(t)$ multiscale work, non-pathogenic protein concentration at compartment j of neuron i from brain region r at timestep t

$\text{Cn}_{i,j}(t)$ neuronal scale work, concentration of non-pathogenic protein in compartment j of neuron i at timestep t

$\text{CnMis}_{i,j|r}(t)$ multiscale work, concentration of non-pathogenic protein which misfolded and converted to pathogenic at compartment j of neuron i from brain region r at timestep t

$\text{CnMis}_{i,j}(t)$ neuronal scale work, concentration of non-pathogenic protein which misfolded and converted to pathogenic in compartment j of neuron i at timestep t

$\text{CnMis}_r(t)$ brain scale work, concentration of non-pathogenic protein which misfolded and converted to pathogenic at brain region r at timestep t

$\text{CnProd}_{i,j|r}(t)$ multiscale work, non-pathogenic protein produced at compartment j of neuron i from brain region r at timestep t

$\text{CnProd}_{i,j}(t)$ neuronal scale work, concentration of non-pathogenic protein produced via transcription and translation in compartment j of neuron i at timestep t

$\text{CnProd}_r(t)$ brain scale work, non-pathogenic protein concentration produced at brain region r at timestep t

$\text{Cn}_r(t)$ brain scale work, non-pathogenic protein concentration at brain region r at timestep t

Col_i neuronal scale work, the column that neuron i belonged to

$\text{Col}_{i|r}$ multiscale work, cortical column that neuron i from brain region r belonged to

$\mathbf{CONV}_{par1,par2}$ neuronal scale work, mean time to convergence between all simulations in set H_{par1} against all simulations in set H_{par2}

ConvThr neuronal scale work, time to convergence threshold

$\mathbf{Coor}_r$ brain scale and multiscale work, 3D coordinates of brain region r

$\text{CpClear}_{i,j|r}(t)$ multiscale work, pathogenic protein cleared at compartment j of neuron i from brain region r at timestep t

$\text{CpClear}_{i,j}(t)$ neuronal scale work, concentration of pathogenic protein cleared in compartment j of neuron i at timestep t

$\text{CpClear}_r(t)$ brain scale work, pathogenic protein concentration cleared at brain region r at timestep t

CpHealth all work, healthy concentration level for pathogenic protein

$\text{Cp}_{i,j|r}(t)$ multiscale work, pathogenic protein concentration at compartment j of neuron i from brain region r at timestep t

$\text{Cp}_{i,j}(t)$ neuronal scale work, concentration of pathogenic protein in compartment j of neuron i at timestep t

$\text{CpMis}_{i,j|r}(t)$ multiscale work, concentration of newly converted/misfolded pathogenic protein at compartment j of neuron i from brain region r at timestep t

$\text{CpMis}_{i,j}(t)$ neuronal scale work, concentration of newly converted/misfolded pathogenic protein in compartment j of neuron i at timestep t

$\text{CpMis}_r(t)$ brain scale work, concentration of newly converted/misfolded pathogenic protein at brain region r at timestep t

$\text{CpProd}_{i,j|r}(t)$ multiscale work, pathogenic protein produced at compartment j of neuron i from brain region r at timestep t

$\text{CpProd}_{i,j}(t)$ neuronal scale work, concentration of pathogenic protein produced via transcription and translation in compartment j of neuron i at timestep t

$\text{CpProd}_r(t)$ brain scale work, pathogenic protein concentration produced at brain region r at timestep t

$\mathrm{Cp}_r(t)$ brain scale work, pathogenic protein concentration at brain region r at timestep t

CpSeed brain scale and multiscale work, pathogenic protein seed concentration

$\mathrm{Dead}_r(t)$ multiscale work, set of dead neurons from brain region r at timestep t

$\mathbf{DF}|\mathbf{E}_{i,j|r\leftarrow\bar{i},\bar{j}|\bar{r}}(t)$ multiscale work, probability of protein spreading via effective connectivity related diffusive frequency related spread from compartment $\bar{j}$ of neuron $\bar{i}$ from brain region $\bar{r}$ to compartment j of neuron i from brain region r at timestep t

$\mathbf{DF}|\mathbf{F}_{i,j|r\leftarrow\bar{i},\bar{j}|\bar{r}}(t)$ multiscale work, probability of protein spreading via functional connectivity related diffusive frequency related spread from compartment $\bar{j}$ of neuron $\bar{i}$ from brain region $\bar{r}$ to compartment j of neuron i from brain region r at timestep t

$\mathbf{DF}|\mathbf{S}_{i,j|r\leftarrow\bar{i},\bar{j}|\bar{r}}(t)$ multiscale work, probability of protein spreading via structural connectivity related diffusive frequency related spread from compartment $\bar{j}$ of neuron $\bar{i}$ from brain region $\bar{r}$ to compartment j of neuron i from brain region r at timestep t

$\mathrm{Diam}_{i,j}$ neuronal scale work, diameter of the neuronal compartment j of neuron i

$\mathrm{Diam}_{i,j|r}$ multiscale work, diameter of compartment j of neuron i from brain region r

$\mathrm{Dice}_{s,\bar{s}}(n)$ neuronal scale work, Dice coefficient between sets $G_s(n)$ and $G_{\bar{s}}(n)$

$\mathbb{D}^n$ space of discrete numbered vector of dimension n

$\mathbf{D}_{r\leftarrow\bar{r}}$ brain scale and multiscale work, Euclidean distance between brain region r and $\bar{r}$

dt neuronal scale work, individual timestep interval

$\mathbf{DW}|\mathbf{E}_{i,j|r\leftarrow\bar{i},\bar{j}|\bar{r}}(t)$ multiscale work, probability of protein spreading via effective connectivity related diffusive spread from compartment $\bar{j}$ of neuron $\bar{i}$ from brain region $\bar{r}$ to compartment j of neuron i from brain region r at timestep t

$\mathbf{DW|F}_{i,j|r\leftarrow\bar{i},\bar{j}|\bar{r}}(t)$ multiscale work, probability of protein spreading via functional connectivity related diffusive spread from compartment $\bar{j}$ of neuron $\bar{i}$ from brain region $\bar{r}$ to compartment j of neuron i from brain region r at timestep t

$\mathbf{DW|S}_{i,j|r\leftarrow\bar{i},\bar{j}|\bar{r}}(t)$ multiscale work, probability of protein spreading via structural connectivity related diffusive spread from compartment $\bar{j}$ of neuron $\bar{i}$ from brain region $\bar{r}$ to compartment j of neuron i from brain region r at timestep t

$\mathbf{ED}_{i,j|r\leftarrow\bar{i},\bar{j}|\bar{r}}(t)$ multiscale work, probability of protein spreading via extracellular diffusion from compartment $\bar{j}$ of neuron $\bar{i}$ from brain region $\bar{r}$ to compartment j of neuron i from brain region r at timestep t

$\mathbf{ED}_{r\leftarrow\bar{r}}(t)$ brain scale work, probability of protein spreading via extracellular diffusion from brain region $\bar{r}$ to brain region r at timestep t

$\mathbf{Ent}_{i,j\leftarrow\bar{i},\bar{j}}$ neuronal scale work, probability of protein managing to pass through the entrance from neuron $\bar{i}$, compartment $\bar{j}$ to neuron i, compartment j

$\mathbf{Ent}_{i,j|r\leftarrow\bar{i},\bar{j}|r}$ multiscale work, probability of protein managing to pass through the entrance from compartment $\bar{j}$ of neuron $\bar{i}$ from brain region r to compartment j of neuron i from brain region r

$\mathbf{E}_{r\leftarrow\bar{r}}$ brain scale and multiscale work, effective connectivity from brain region $\bar{r}$ to brain region r

f_{ACT} neuronal scale and multiscale work, intrinsic probability of protein spreading via active transport

$f_{\mathrm{DF|F}}$ multiscale work, intrinsic probability of protein spreading via functional connectivity related diffusive frequency related spread

$f_{\mathrm{DF|S}}$ multiscale work, intrinsic probability of protein spreading via structural connectivity related diffusive frequency related spread

$f_{\mathrm{DF|E}}$ multiscale work, intrinsic probability of protein spreading via effective connectivity related diffusive frequency related spread

$f_{\mathrm{DW|E}}$ multiscale work, intrinsic probability of protein spreading via effective connectivity related diffusive spread

$f_{\mathrm{DW|F}}$ multiscale work, intrinsic probability of protein spreading via functional connectivity related diffusive spread

$f_{\mathrm{DW|S}}$ multiscale work, intrinsic probability of protein spreading via structural connectivity related diffusive spread

f_{ED} multiscale work, intrinsic probability of protein spreading via extracellular diffusion

$\mathbf{FF|E}_{i,j|r\leftarrow\bar{i},\bar{j}|\bar{r}}(t)$ multiscale work, probability of protein spreading via effective connectivity related fast frequency related spread from compartment $\bar{j}$ of neuron $\bar{i}$ from brain region $\bar{r}$ to compartment j of neuron i from brain region r at timestep t

$f_{\mathrm{FF|E}}$ multiscale work, intrinsic probability of protein spreading via effective connectivity related fast frequency related spread

$f_{\mathrm{FF|F}}$ multiscale work, intrinsic probability of protein spreading via functional connectivity related fast frequency related spread

$\mathbf{FF|F}_{i,j|r\leftarrow\bar{i},\bar{j}|\bar{r}}(t)$ multiscale work, probability of protein spreading via functional connectivity related fast frequency related spread from compartment $\bar{j}$ of neuron $\bar{i}$ from brain region $\bar{r}$ to compartment j of neuron i from brain region r at timestep t

$f_{\mathrm{FF|S}}$ multiscale work, intrinsic probability of protein spreading via structural connectivity related fast frequency related spread

$\mathbf{FF|S}_{i,j|r\leftarrow\bar{i},\bar{j}|\bar{r}}(t)$ multiscale work, probability of protein spreading via structural connectivity related fast frequency related spread from compartment $\bar{j}$ of neuron $\bar{i}$ from brain region $\bar{r}$ to compartment j of neuron i from brain region r at timestep t

$f_{\mathrm{FW|E}}$ multiscale work, intrinsic probability of protein spreading via effective connectivity related fast spread

$f_{\mathrm{FW|F}}$ multiscale work, intrinsic probability of protein spreading via functional connectivity related fast spread

$f_{\mathrm{FW|S}}$ multiscale work, intrinsic probability of protein spreading via structural connectivity related fast spread

f_{NFS} multiscale work, intrinsic probability of protein spreading via neuronal frequency related spread

f_{NND} neuronal scale and multiscale work, intrinsic probability of protein spreading via neuronal network diffusion

FReffect multiscale work, refers to the toxic effect, specifically whether it was an increase or a decrease of firing frequencies

$\mathrm{freq}_r(t)$ brain scale work, firing frequency of brain region r at timestep t

$\mathrm{fr}_{i|r}(t)$ multiscale work, firing frequency of neuron i from brain region r at timestep t

$\mathbf{F}_{r\leftarrow\bar{r}}$ brain scale and multiscale work, functional connectivity between brain regions r and $\bar{r}$

$\mathbf{FS}|\mathbf{E}_{r\leftarrow\bar{r}}(t)$ brain scale work, probability of protein spreading via effective connectivity related firing frequency related spread from brain region $\bar{r}$ to brain region r at timestep t

$\mathbf{FS}|\mathbf{F}_{r\leftarrow\bar{r}}(t)$ brain scale work, probability of protein spreading via functional connectivity related firing frequency related spread from brain region $\bar{r}$ to brain region r at timestep t

$\mathbf{FS}|\mathbf{S}_{r\leftarrow\bar{r}}(t)$ brain scale work, probability of protein spreading via structural connectivity related firing frequency related spread from brain region $\bar{r}$ to brain region r at timestep t

f_{SYN} neuronal scale work, intrinsic probability of protein spreading via synaptic transfer

$\mathbf{FW}|\mathbf{E}_{i,j|r\leftarrow\bar{i},\bar{j}|\bar{r}}(t)$ multiscale work, probability of protein spreading via effective connectivity related fast spread from compartment $\bar{j}$ of neuron $\bar{i}$ from brain region $\bar{r}$ to compartment j of neuron i from brain region r at timestep t

$\mathbf{FW}|\mathbf{F}_{i,j|r\leftarrow\bar{i},\bar{j}|\bar{r}}(t)$ multiscale work, probability of protein spreading via functional connectivity related fast spread from compartment $\bar{j}$ of neuron $\bar{i}$ from brain region $\bar{r}$ to compartment j of neuron i from brain region r at timestep t

$\mathbf{FW}|\mathbf{S}_{i,j|r\leftarrow\bar{i},\bar{j}|\bar{r}}(t)$ multiscale work, probability of protein spreading via structural connectivity related fast spread from compartment $\bar{j}$ of neuron $\bar{i}$ from brain region $\bar{r}$ to compartment j of neuron i from brain region r at timestep t

GDS_i neuronal scale work, geodesic distance from neuron i to the seed of the simulation

$G_s(n)$ neuronal scale work, set of the first n neurons to reach neuronal death in a simulation s

H_{par} neuronal scale work, set of all simulations where the parameter *par* was the same among them (but other parameters may have varied)

i refers to a single neuron

$i,j|r$ multiscale work, refers to compartment j of neuron i from brain region r

$\mathrm{InAl}_r(t)$ multiscale work, intersection between set of alive neurons and set of input neurons from brain region r at timestep t

In_r multiscale work, set of input neurons of brain region r

$i|r$ multiscale work, refers to a single neuron from brain region r

j refers to a single neuronal compartment (1 for dendrites, 2 for soma, 3 for axon)

Lay_i neuronal scale work, the layer of neuron i

$\mathrm{Lay}_{i|r}$ multiscale work, cortical column layer that neuron i from brain region r belonged to

$\mathrm{Len}_{i,j}$ neuronal scale work, length of the neuronal compartment j of neuron i

$\mathrm{Len}_{i,j|r}$ multiscale work, length of compartment j of neuron i from brain region r

$\mathbf{NAE}_{r\leftarrow\bar{r}}(t)$ brain scale and multiscale work, normalised absolute values of effective connectivity from brain region $\bar{r}$ to brain region r at timestep t

$\mathbf{NAF}_{r\leftarrow\bar{r}}(t)$ brain scale and multiscale work, normalised absolute values of functional connectivity between brain regions $\bar{r}$ and r at timestep t

$\mathbf{NAS}_{r\leftarrow\bar{r}}(t)$ brain scale and multiscale work, normalised absolute values of structural connectivity between brain regions $\bar{r}$ and r at timestep t

NCol neuronal scale work, number of cortical columns

NCol_r multiscale work, number of cortical columns representing brain region r

$\mathbf{ND}|\mathbf{E}_{r\leftarrow\bar{r}}(t)$ brain scale work, probability of protein spreading via effective connectivity related network-mediated diffusion from brain region $\bar{r}$ to brain region r at timestep t

$\mathbf{ND}|\mathbf{F}_{r\leftarrow\bar{r}}(t)$ brain scale work, probability of protein spreading via functional connectivity related network-mediated diffusion from brain region $\bar{r}$ to brain region r at timestep t

$\mathrm{NDout}|\mathrm{E}_{\bar{r}}$ brain scale work, probability of protein spreading out of brain region $\bar{r}$ from effective connectivity related network-mediated diffusion

$\mathrm{NDout}|\mathrm{F}_{\bar{r}}$ brain scale work, probability of protein spreading out of brain region $\bar{r}$ from functional connectivity related network-mediated diffusion

$\mathrm{NDout}|\mathrm{S}_{\bar{r}}$ brain scale work, probability of protein spreading out of brain region $\bar{r}$ from structural connectivity related network-mediated diffusion

$\mathbf{ND}|\mathbf{S}_{r\leftarrow\bar{r}}(t)$ brain scale work, probability of protein spreading via structural connectivity related network-mediated diffusion from brain region $\bar{r}$ to brain region r at timestep t

$\mathbf{NFS}_{i,j|r\leftarrow\bar{i},\bar{j}|r}(t)$ multiscale work, probability of protein spreading via neuronal frequency related spread from compartment $\bar{j}$ of neuron $\bar{i}$ from brain region r to compartment j of neuron i from brain region r at timestep t

$\mathbf{NNDF}_{i,j\leftarrow\bar{i},\bar{j}}(t)$ neuronal scale work, (final) probability of protein spreading via neuronal network diffusion from neuron $\bar{i}$, compartment $\bar{j}$ to neuron i, compartment j at timestep t

$\mathbf{NND}_{i,j\leftarrow\bar{i},\bar{j}}(t)$ neuronal scale work, probability of protein spreading via neuronal network diffusion from neuron $\bar{i}$, compartment $\bar{j}$ to a neighbouring neuron i, compartment j at timestep t

$\mathbf{NND}_{i,j|r\leftarrow\bar{i},\bar{j}|r}(t)$ multiscale work, probability of protein spreading via neuronal network diffusion from compartment $\bar{j}$ of neuron $\bar{i}$ from brain region r to compartment j of neuron i from brain region r at timestep t

$textNND_{\text{thr}}$ neuronal scale work, minimum concentration threshold below which protein would not spread via neuronal network diffusion

NNeu neuronal scale work, number of total neurons

NNeu_r multiscale work, number of neurons within brain region r

NReg brain scale and multiscale work, number of brain regions

OS_r brain scale work, event position that brain region r became abnormal during a simulation

$\text{OutAl}_r(t)$ multiscale work, intersection between set of alive neurons and set of output neurons from brain region r at timestep t

Out_r multiscale work, set of output neurons of brain region r

$\text{QnAcc}_{i,j|r}(t)$ multiscale work, net change of non-pathogenic protein quantity from production, clearance, and misfolding at compartment j of neuron i from brain region r at timestep t

$\text{QnAcc}_{i,j}(t)$ neuronal scale work, net change in protein quantity from production, clearance, and misfolding for non-pathogenic protein at neuron i, compartment j, timestep t

$\text{QnAcc}_r(t)$ brain scale work, net change of non-pathogenic protein quantity from production, clearance, and misfolding, for brain region r at timestep t

$\text{QnBSSadd}_{i,j|r}(t)$ multiscale work, non-pathogenic protein quantity that spread via brain scale spread mechanisms into compartment j of neuron i from brain region r at timestep t

$\mathrm{QnBSS}_{i,j|r}(t)$ multiscale work, net change in non-pathogenic protein quantity from brain scale spread mechanisms at compartment j of neuron i from brain region r at timestep t

$\mathrm{QnBSSrem}_{i,j|r}(t)$ multiscale work, non-pathogenic protein quantity that spread via brain scale spread mechanisms out of compartment j of neuron i from brain region r at timestep t

$\mathrm{Qn}_{i,j|r}(t)$ multiscale work, non-pathogenic protein quantity at compartment j of neuron i from brain region r at timestep t

$\mathrm{Qn}_{i,j}(t)$ neuronal scale work, quantity of non-pathogenic protein in compartment j of neuron i at timestep t

$\mathrm{QnNSS}_{i,j|r}(t)$ multiscale work, net change of non-pathogenic protein quantity from neuronal scale spread mechanisms at compartment j of neuron i from brain region r at timestep t

$\mathrm{QnNSS}_{i,j}(t)$ neuronal scale work, net change in protein quantity from spread mechanisms for non-pathogenic protein at neuron i, compartment j, timestep t

$\mathrm{Qn}_{r}(t)$ brain scale work, non-pathogenic protein quantity at brain region r at timestep t

$\mathrm{QpAcc}_{i,j|r}(t)$ multiscale work, net change of pathogenic protein quantity from production, clearance, and misfolding at compartment j of neuron i from brain region r at timestep t

$\mathrm{QpAcc}_{i,j}(t)$ neuronal scale work, net change in protein quantity from production, clearance, and misfolding for pathogenic protein at neuron i, compartment j, timestep t

$\mathrm{QpAcc}_{r}(t)$ brain scale work, net change of pathogenic protein quantity from production, clearance, and misfolding, for brain region r at timestep t

$\mathrm{QpBSSadd}_{i,j|r}(t)$ multiscale work, pathogenic protein quantity that spread via brain scale spread mechanisms into compartment j of neuron i from brain region r at timestep t

$\text{QpBSS}_{i,j|r}(t)$ multiscale work, net change in pathogenic protein quantity from brain scale spread mechanisms at compartment j of neuron i from brain region r at timestep t

$\text{QpBSSrem}_{i,j|r}(t)$ multiscale work, pathogenic protein quantity that spread via brain scale spread mechanisms out of compartment j of neuron i from brain region r at timestep t

$\text{Qp}_{i,j|r}(t)$ multiscale work, pathogenic protein quantity at compartment j of neuron i from brain region r at timestep t

$\text{Qp}_{i,j}(t)$ neuronal scale work, quantity of pathogenic protein in compartment j of neuron i at timestep t

$\text{QpNSS}_{i,j|r}(t)$ multiscale work, net change of pathogenic protein quantity from neuronal scale spread mechanisms at compartment j of neuron i from brain region r at timestep t

$\text{QpNSS}_{i,j}(t)$ neuronal scale work, net change in protein quantity from spread mechanisms for pathogenic protein at neuron i, compartment j, timestep t

$\text{Qp}_r(t)$ brain scale work, pathogenic protein quantity at brain region r at timestep t

r refers to a single brain region

R_A brain scale work, rate of atrophy

$R_{\text{FS|E}}$ brain scale work, strength of effective connectivity related firing frequency related spread

$R_{\text{FS|F}}$ brain scale work, strength of functional connectivity related firing frequency related spread

$R_{\text{FS|S}}$ brain scale work, strength of structural connectivity related firing frequency related spread

R_{Mis} all work, misfolding/templating rate

$\mathbb{R}^n$ space of real numbered vectors of dimension n

R_{nClear} all work, rate of non-pathogenic protein clearance

R_{nProd} all work, rate of non-pathogenic protein production

R_{pClear} all work, rate of pathogenic protein clearance

R_{pProd} all work, rate of pathogenic protein production

R_{Txc} neuronal scale and multiscale work, toxicity rate

SeedLoc multiscale work, refers to the brain region that had the pathogenic protein seed

$\mathbf{SEL}_{i,j\leftarrow\bar{i},\bar{j}}$ neuronal scale work, intrinsic tendency of protein to spread selectively from neuron $\bar{i}$, compartment $\bar{j}$ to neuron i, compartment j

$\mathbf{Sig}_r$ brain scale work, population regional synaptic signals for brain region r

$\text{SO}_r(\theta)$ multiscale work, event order position that brain region r became abnormal during a simulation with parameter set θ

$\mathbf{S}_{r\leftarrow\bar{r}}$ brain scale and multiscale work, structural connectivity between brain regions r and $\bar{r}$

$\mathbf{SS}_{i,j|r\leftarrow\bar{i},\bar{j}|r}$ multiscale work, strength of a synapse connecting compartment $\bar{j}$ of neuron $\bar{i}$ from brain region r to compartment j of neuron i from brain region r

$\mathbf{SS}_{i,j\leftarrow\bar{i},\bar{j}}$ neuronal scale work, synaptic strength from neuron $\bar{i}$, compartment $\bar{j}$ to neuron i, compartment j

SSG_i neuronal scale work, synaptic strength gradient of neuron i

$\mathbf{SYN}_{i,j\leftarrow\bar{i},\bar{j}}(t)$ neuronal scale work, probability of protein spreading via synaptic transfer from neuron $\bar{i}$, compartment $\bar{j}$ to neuron i, compartment j at timestep t

t simulation timestep

$\text{Tatr}_r(\theta)$ multiscale work, timestep that brain region r first showed abnormal amount of atrophy in a simulation with parameter set θ

$\text{tConv}_{s,\bar{s}}$ neuronal scale work, time to convergence between simulations s and $\bar{s}$

tdeath_i neuronal scale work, timestep that neuron i died

$\mathrm{Txc}_{i|r}(t)$ multiscale work, toxicity level of neuron i from brain region r at timestep t

$\mathrm{Txc}_{i}(t)$ neuronal scale work, toxicity level of neuron i, at timestep t

Type_{i} neuronal scale work, the type of neuron i

$\mathrm{Type}_{i|r}$ multiscale work, neuronal type of neuron i from brain region r

$\mathbf{UM}|\mathbf{dis}_{r,o}$ multiscale work, probability of region r being o-th in the order of brain regional volumes becoming abnormal based on an event based model

$\mathbf{UM}_{r,i}$ brain scale work, uncertainty matrix of an event based model of some neurodegenerative disease, indicating the probability of brain region r showing atrophy right after $i-1$ regions show atrophy before it (i.e., showing atrophy i-ith in the sequence of brain regions showing atrophy)

$\mathrm{Vol}_{i,j}$ neuronal scale work, volume of the neuronal compartment j of neuron i

$\mathrm{Vol}_{i,j|r}$ multiscale work, volume of compartment j of neuron i from brain region r

$V_r(t)$ brain scale and multiscale work, volume of brain region r at timestep t

$\mathrm{Vth}_{i|r}(t)$ multiscale work, voltage threshold for an action potential for neuron i from brain region r at timestep t

$\mathrm{Vth}_{i}(t)$ neuronal scale work, voltage threshold for an action potential for neuron i at timestep t

Vthres_{r} brain scale work, threshold for abnormal volume for brain region r

$\mathbf{WNND}_{i,j\leftarrow\bar{i},\bar{j}}$ neuronal scale work, neuronal network diffusion weight from neuron $\bar{i}$, compartment $\bar{j}$ to neuron i, compartment j

$\mathbf{WNND}_{i,j|r\leftarrow\bar{i},\bar{j}|r}$ multiscale work, neuronal network diffusion weight from compartment $\bar{j}$ of neuron $\bar{i}$ from brain region r to compartment j of neuron i from brain region r

Chapter 1

Introduction

Neurodegenerative diseases, such as Alzheimer's disease (AD), describe a family of pathologies that are caused by pathogenic proteins, which accumulate and spread in neural networks, causing a progressive loss of neuronal function and of structural integrity, and eventually neuronal death. Most neurodegenerative diseases affect brain neurons, leading to what is known as brain atrophy (Figure 1.1) and eventual patient death. These diseases manifest symptoms, most of which fall under the category of dementia, e.g., impairments in memory, linguistic ability, cognition, etc.

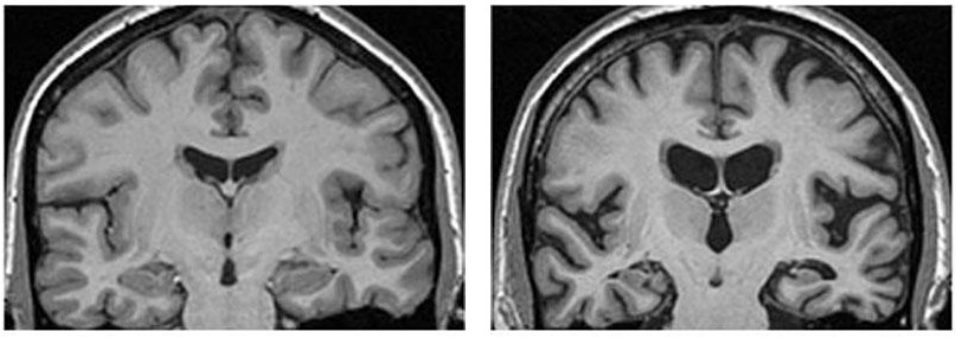

Figure 1.1: Magnetic resonance images (MRIs) showcasing the atrophy occurring in neurodegenerative diseases. Left: healthy control. Right: AD patient. Figure from https://institute.progress.im/en/content/brain-imaging-psychiatrists-part-2-structural-static-measures.

1.1 Clinical motivation

Neurodegenerative diseases are currently incurable, with therapies being able to only temporarily ameliorate symptoms [1, 2]. This fact, coupled with the type of symptoms that manifest in neurodegenerative diseases limits patient care to be predominantly home care and nursing, requiring high financial and human resources for every patient. Around 25 million people globally had dementia in 2005 [3], and that number grew to around 50 million in 2018 [4], with the number expected to continue growing due to the increasing life expectancy, especially in developing countries. Worldwide, it has been estimated that the annual cost of care was 1 trillion dollars in 2018 [4], while in the United Kingdom it was 17 billion GBP in 2007 [5], much higher than the 9 billion GBP total cost of care for patients with heart disease, stroke, and cancer. All of these issues motivate the scientific and clinical community to discover better therapeutic interventions.

Neurodegenerative diseases are caused by pathogenic protein accumulation, thus it stands to reason that future research into therapies will focus on developing therapies which aim at modifying these proteins in some manner, e.g., by removing them, or by reducing the effectiveness of the mechanisms by which they accumulate. The mechanisms that govern pathogenic proteins make an obvious choice as potential targets for therapeutic intervention [6, 7]. A better understanding of pathogenic proteins and the neurobiological mechanisms that govern their behaviour (hereinafter referred to as simply ‘mechanisms’), as well as how they would be affected in the event of a therapeutic intervention, would provide useful information for the drug designing process [8].

Noticeable symptoms of cognitive decline manifest decades after pathogenesis [9], making early diagnosis rare and difficult. However, early diagnosis is of great interest, as the effectiveness of many current therapies is increased the earlier the treatment begins [2, 10], and this could also be the case with future therapies. How and where pathogenesis occurs remains to some extent a mystery, which, if solved, would assist in the development of biomarkers for earlier diagnosis. Improved prognosis in individuals could also be beneficial for treatment planning [11].

A better understanding of the mechanisms could lead to learning the equations that describe them, thus being able to predict their behaviour and assist in the development of new prognostic tools.

There are still many facts about pathogenic proteins which have yet to be elucidated [12–15]. For example, it is still unknown by which mechanisms they spread throughout the brain. Neuroscientists and neurobiologists have come up with many, sometimes conflicting hypotheses regarding the nature of these mechanisms [16–20]. However, testing and validating every hypothesis can be difficult and resource intensive. Therefore, neurobiological research could be prioritised to focus on those hypotheses whose likelihood of being true is higher. As such, any evidence that can suggest which hypotheses are more or less likely to be true would assist in this endeavour.

In conclusion, it appears that a better understanding of the mechanisms would be useful for prognosis, earlier diagnosis, drug development, and for guiding future neurobiological research.

1.2 The 'molecular nexopathies' paradigm

Neurodegenerative diseases have been observed clinically to produce spatiotemporal patterns of atrophy and protein deposition in histopathological, in-vivo, and in-vitro studies [21–28]. The existence of patterns leads us to hypothesise that they must be the product of the interaction between pathogenic proteins and certain mechanisms. Researchers have also observed that each neurodegenerative disease has its own spatiotemporal pattern of protein deposition and of brain atrophy. In addition, the degree of heterogeneity of these patterns among patients inflicted with the same disease varies depending on the disease [28] (see Section 2.2), e.g., the pattern in AD is more homogeneous among patients (although there are variants) compared to frontotemporal dementias, where it is more heterogeneous among patients. This leads us to two conclusions: (a) neurodegenerative diseases are primarily governed by the same or similar mechanisms, which lead to the similarities between them (i.e., following pathogenesis, pathogenic proteins accumulate into

aggregates, cause neuronal dysfunction and death, brain atrophy in a pattern, clinical symptoms, and finally patient death [29]), and (b) there must be some variations in the mechanisms, which account for the phenotypic variation. These mechanism variations could explain the perceived "randomness" of neurodegenerative disease propagation, for example, if the instigating event in one disease occurs in one specific brain region, whereas in another disease it could occur in any of a number of brain regions, after which the spread follows anatomical connections, this would lead to higher heterogeneity of progression patterns in the latter case.

In general, there are many common characteristics among neurodegenerative diseases, as well as a lot of variation in other aspects (a theme that will become more evident in Chapter 2). Two major commonalities among neurodegenerative diseases is that they are caused by pathogenic proteins, and that the spatiotemporal patterns of protein accumulation and of brain atrophy coincide with the neural network's connectivity. There are many pathogenic proteins which are linked to neurodegenerative diseases [30], such as tau, amyloid-beta, etc. Additionally, for each of these proteins, there are many variants that are pathogenic [30, 31]. Therefore, a natural conclusion is to hypothesise that the spatiotemporal disease progression patterns are, at least partially, determined by the specific pathogenic protein variant. This hypothesis implies that each variant produces a different pattern [32–35], which would explain the pattern diversity.

Additionally, the spatiotemporal patterns of protein accumulation and brain atrophy follow different parts of the neural network of the brain in each neurodegenerative disease, and the patterns show a variety of characteristics in each disease [17, 35, 36], such as left-right brain asymmetry, distributed or clustered spread, fast or slow atrophy progression, etc. This variety indicates a differential degree of vulnerability for different parts of the brain network depending on the specific neurodegenerative disease, or the specific pathogenic protein variant. Therefore, the elements, characteristics, and connections of the brain neural network are hypothesised to also play a role in determining the form of the spatiotemporal patterns of protein accumulation and brain atrophy [17, 37–39].

The ‘molecular nexopathies’ paradigm [36] combines the previous two hypotheses, suggesting that network disintegration phenotypes can be predicted based on the specific pathogenic protein variant and the neural network’s characteristics. There is a large amount of evidence that supports the ‘molecular nexopathies’ hypothesis, including animal inoculation studies that show different patterns of protein spread for different proteins, and the fairly distinctive patterns of genetic dementias [17, 30, 34, 35]. There are many articles in the literature that state similar hypotheses, suggesting that exploring this paradigm would be of interest to the scientific community [37–41]. The validity of this paradigm can be better tested by first gaining a better understanding of the mechanisms, their interactions with different proteins and protein variants, the interactions of pathogenic proteins with the brain neural network, and a validation methodology that makes use of the network disintegration phenotypes.

1.3 Previous approaches

Thus far, most research into mechanisms has focused on observing protein behaviour under different conditions [42–47]. Animal inoculation and in-vitro research is undoubtedly useful, as it is able to assess hypotheses, such as the ‘molecular nexopathies’ hypothesis. However, they provide mostly observational information of the end result, without much new information regarding the causal mechanisms themselves. The primary factors limiting the rate of progress of neurodegenerative disease research is the complexity of the brain, as well as the limitations of the techniques employed for ethically acceptable in-vivo studies (the invasive nature that is typical of in-vivo studies would result in the death of subjects). These limitations force researchers and clinicians to more indirect avenues of research, such as brain imaging studies [48–51], post-mortem histopathological examinations [26, 52–54], in-vivo animal studies [55–59], and in-vitro studies [60–62]. However, such lab research is expensive and can take a long time. Computational research can complement biological research, and by comparison, it has the ability to test many hypotheses much faster, more inexpensively, and more easily, but at

the price of being further removed from the "ground truth".

There has been a lot of computational research in diagnosis, prognosis, and other areas related to neurodegenerative diseases [63, 64]. However, such techniques and studies are not as well suited for gaining a better understanding of the mechanisms, as their models are not easily interpretable from a neurobiological standpoint. There have been quite a few studies in computational and mathematical modelling of many aspects of neurodegenerative diseases [12, 28, 33, 65, 66], which model and study the behaviour of mechanisms. However, most of them use a systems biology approach, which models mechanisms in a very abstract manner, typically modelling one or two neurons and the interactions between them without taking into account 3D geometry. Such approaches do not model the brain neural network and the specific connections among neurons or brain regions, which appear crucial to predicting disease progression and thus understanding the mechanisms governing neurodegenerative diseases. There has been little work in modelling mechanisms in conjunction with neural networks of the brain and the interaction between them, and only a few studies have modelled neural networks at the brain scale [37, 41, 67–70], or at the neuronal scale [71, 72], or combining the two scales [73]. Chapter 3 provides a more detailed review of the related literature.

1.4 Proposed approach

In this thesis, I propose a multi-compartmental (e.g., in Chapter 4, one compartment can represent the dendrites or the soma or the axon of a single neuron, and there are multiple neurons) computational modelling (see Section 2.4) approach to better understand pathogenic proteins, the mechanisms governing them, and their spread patterns within the brain neural network. Computational modelling approaches are commonly used for better understanding of a system, and prediction of system output. By modelling mechanisms, neural networks, and their interactions, one is able to study them under different conditions, as well as make predictions using simulations. A sufficiently accurate model would enable the possibility of earlier diagnosis [37, 67, 69] and improved prognosis [37, 41, 67–70]. Computa-

tional modelling approaches have also been previously used in the pharmaceutical industry for drug discovery and development, improving the quality, efficiency, and cost-effectiveness [66, 74].

Mechanisms of protein accumulation, spread, and toxic effects were modelled based on neurobiological and neuroscientific knowledge and evidence, in addition to rational hypotheses in cases where no evidence was available. Accumulation comprised of three models: (a) protein production, (b) clearance, and (c) misfolding (normal protein gets transformed into pathogenic), which are three mechanisms commonly considered as fundamental for accurate modelling of pathogenic proteins. There is less consensus regarding the mechanisms that spread protein, but they can be categorised on certain criteria: (a) if the mechanism spreads protein intracellularly, intercellularly, or extracellularly, (b) if the mechanism is passively diffusing protein, or if it spreads protein fast and targeted towards elements with specific characteristics, and (c) if the quantity of protein a mechanism spreads is a function of synaptic activity (this list is not necessarily exhaustive). In this thesis, I used combinations of the aforementioned criteria to create models of protein spread. Lastly, I modelled toxicity, which is the net negative impact of protein concentration within a neuron, and which eventually leads to neuronal death.

In the first part of the work of this thesis (Chapter 4), I simulated a small artificial neural network. In the second part of the work of this thesis (Chapter 5), I simulated the brain neural network where "nodes" represented grey matter brain regions and "edges" were based on functional, structural, or effective connectivity (see Section 2.1.3). However, the neurobiological mechanisms generally function at the neuronal scale, whereas network disintegration empirical data that can be used for validation are acquired only at the brain scale. In order to link the mechanisms occurring at the neuronal scale with empirical data acquired at the brain scale, in the last part of the work of this thesis (Chapter 6), I combined the previous two approaches, modelling each grey matter brain region as a small artificial neural network and connecting them based on functional, structural, or effective connectivity.

The most promising validation methodology is to evaluate the predictive abil-

ity of the constructed models against available evidence of network disintegration phenotypes. Aiming to replicate and predict the behaviour of pathogenic proteins as it is observed in in-vitro or in-vivo studies is very difficult; for example, in-vitro studies could only be used for this purpose if the neural network that is created in the Petri dish could also be copied to in-silico format, which is currently infeasible. The network created in the Petri dish would need to be imaged thoroughly and longitudinally and then parcellated and recreated in-silico, which has not been done to this day, although that is an emerging field of research [75]. As such, there was no validation methodology for the work presented in Chapter 4. At the brain scale, one way to perform validation is to gather longitudinal MRIs of patients with a specific neurodegenerative disease, and then evaluate how well a set of constructed models can predict atrophy progression as observed in the images [41] (Figure 1.2). This manner of validation is intuitive, and MRIs suitable for this task are easily accessible. Longitudinal positron emission tomography (PET) tracer imaging for protein concentration could be used instead of atrophy [69], or in conjunction with atrophy; however, it is still not regarded as accurate as MR atrophy quantification [76].

Such a simple approach is suitable for validation of predictive power. However, longitudinal scans are rare, whereas there are far more cross-sectional scans, but how to implement a validation scheme that uses cross-sectional scans correctly is not obvious, as well as beyond the scope of this thesis. In order to simplify the process, I evaluated how well atrophy progression prediction given by the modelled mechanisms matched the atrophy progression prediction given by an event based model (EBM) for different neurodegenerative diseases [64, 77]. An EBM describes how atrophy is likely to progress spatiotemporally on a population-basis for a neurodegenerative disease, and has already solved the problem of how to combine cross-sectional MRIs. Its output is the probabilities for each brain region (given a brain parcellation) to show signs of atrophy in a specific order, e.g., the probability that the hippocampus shows atrophy fifth, meaning that four other brain regions have shown atrophy before the hippocampus. Using the EBM for validation will allow us to find the mechanisms that govern each disease without (or with reduced)

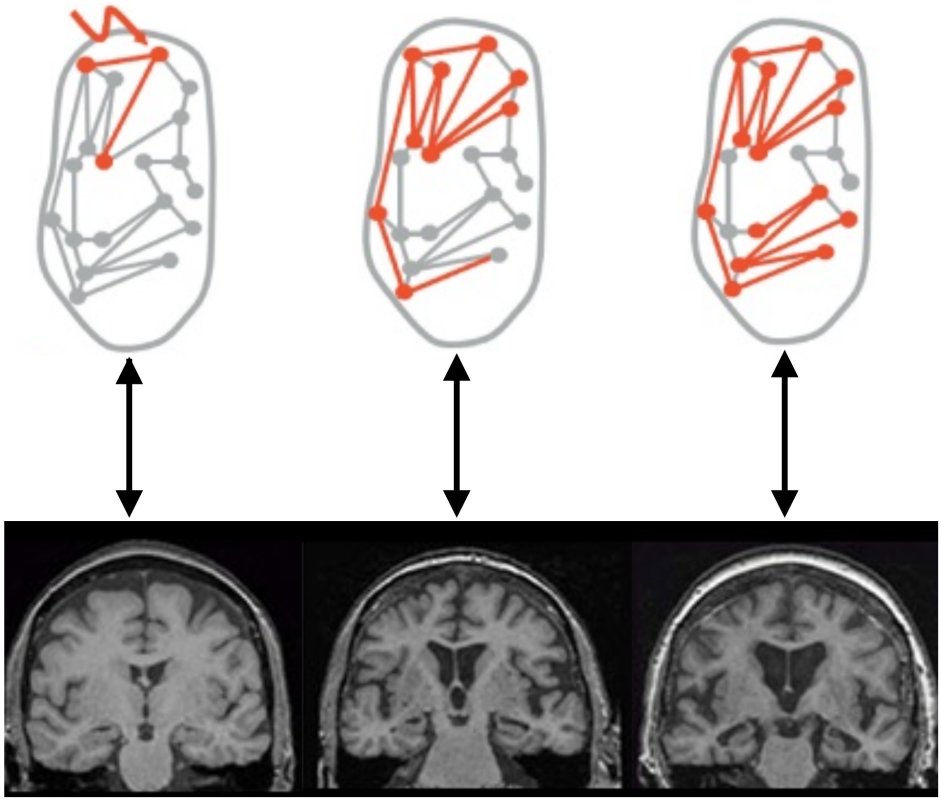

Figure 1.2: An illustration of the validation methodology, where predicted atrophy in a simulation is compared against atrophy observed in patient longitudinal MR images. Top part of the figure from the work of Warren et al. [36] (modified) and bottom part of the figure from https://www.mayo.edu/research/labs/aging-dementia-imaging/overview.

individual patient noise, however individual patient prognosis is not possible.

1.5 Thesis contributions

This thesis aimed at developing and validating computational models of mechanisms, which were constructed based on neurobiological evidence and common hypotheses made in the scientific literature. These models can improve our understanding of neurodegenerative diseases, inform the design of therapeutic interventions, and be used as a prognostic tool. Being a fairly new field within neurodegenerative disease research, there were many ways to make novel contributions. The contributions I made with this thesis include the following:

- In Chapter 4, neurobiologically plausible models were constructed for the mechanisms of transcription and translation, clearance, 'prion-like' mis-

folding, intraneuronal and interneuronal passive diffusion, active transport, synaptic transfer, and neuronal toxicity and death. Then, I ran simulations within an artificial neuronal scale network of cortical columns. Some of these mechanisms have been previously modelled in a similar manner, but not within the context of a small artificial neural network. This work resulted in a journal abstract publication and a conference poster [78], presented in the 10th International Conference on Frontotemporal Dementias, as well as a journal publication [79].

- In Chapter 5, computational models were constructed for protein production, clearance, misfolding, extracellular diffusion, functional connectivity related spread, structural connectivity related spread, effective connectivity related spread, as well as firing frequency related spread. Simulations were ran on a brain network, where model parameters were optimised to fit the EBM for ApoE 4 positive AD. Existing similar work has only modelled extracellular diffusion and structural connectivity related spread, whereas I modelled additional mechanisms of protein spread. Additionally, the validation methodology used by similar work has been qualitative or individual patient based, whereas I used a population based validation methodology. Results agreed with previous evidence that fibre tract connectivity and extracellular diffusion are the primary drivers of protein spread in AD, providing evidence against other mechanisms of spread. This work resulted in a conference paper publication and a poster [80], presented in the 21st International Conference on Medical Image Computing and Computer Assisted Intervention.

- In Chapter 6, I combined my previous two approaches, linking the neuronal scale mechanisms with validation using network disintegration phenotypes acquired at the brain scale, using the neural networks at both scales. No previous work has combined the two scales. Model parameters that best fitted atrophy progression of ApoE 4 positive AD and three genetic variants of frontotemporal dementia (FTD) were found and a comparison study among them was performed. A sensitivity analysis was performed to study the effect of al-

tering each model's parameter values, and potential therapeutic targets were found, most notably, increasing the firing frequency of neurons. This work is under submission to be published as a journal article [81] in the near future. At the time of writing (February 2020), this work has been submitted to PLoS Computational Biology and is undergoing the review/rebuttal phase.

1.6 Thesis organisation

This chapter presented the clinical and scientific motivation, the goals, a brief review of related work, my proposed approach, how my approach can achieve the previously stated goals, and contributions compared to related work. In Chapter 2, I present the relevant neurobiological and computational background. Chapter 3 has a more detailed review of the relevant state-of-the-art work, while also noting how my approach differs. Chapter 4 presents my first work, where computational models for pathogenic protein mechanisms are developed within an artificial neural network of cortical columns. A sensitivity analysis is performed, exploring how changing the parameters of the models can affect the results of the simulations. Chapter 5 presents the brain scale framework, the constructed models and the result of fitting the model parameters to atrophy progression of ApoE 4 positive AD data. Chapter 6 presents the link between neuronal and brain scales. Some new models are constructed and some are adjusted from the previous two chapters. A comparison study among four neurodegenerative diseases is performed. Conclusions and a number of ideas for potential future work are presented in Chapter 7.

Chapter 2

Neurodegenerative diseases and computational modelling background

In this chapter, the scientific background necessary for this thesis is presented. In Section 2.1, I provide a brief description of the brain, its structures and functions, the connectivity between regions, various brain imaging modalities, as well as information about neurons. Section 2.2 provides general information about a variety of neurodegenerative diseases, such as what are the pathogenic proteins that cause them, their atrophy patterns, epidemiology, clinical symptoms, neuropathology, etc. In Section 2.3, the neurobiological background that is relevant for the modelled mechanisms, as well as various hypotheses regarding the mechanisms are presented. Section 2.4 is an introduction to computational modelling, as well as to simulation optimisation.

2.1 Brain and neurons

The human brain is the most complex organ of the body. It consists of approximately 86 billion neurons, which are the basic units of calculation in the brain. Their function and health are supported by glial and astrocytic cells. Neurons are made up of dendrites, which receive the output signal of other neurons, a cell body (also called a 'soma'), where the cell nucleus also exists, and a single axon, which transmits electrical impulses to other neurons. Axons can be myelinated; myelin has the effect of speeding up the transmission of the electrical impulse. Neurons

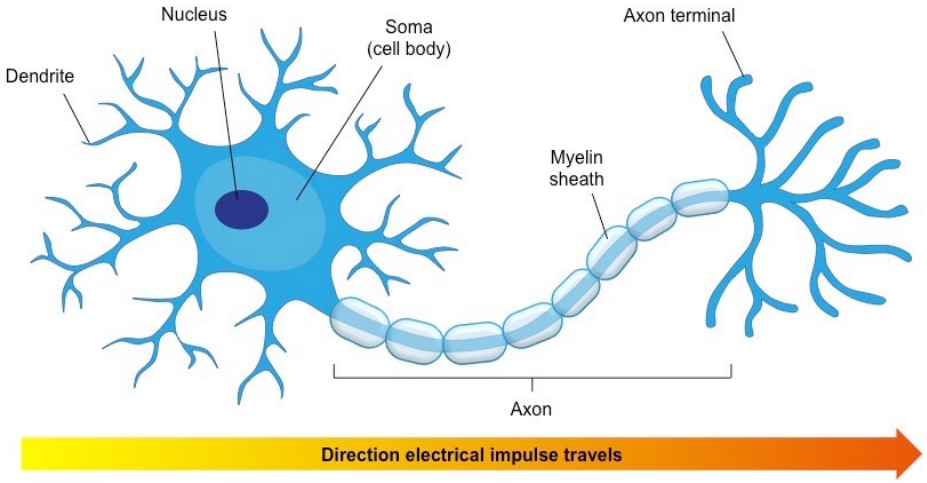

Figure 2.1: An illustration of a neuron and its structures. Figure from https://socratic.org/questions/how-is-a-neuron-adapted-to-perform-its-function.

connect to one another via synapses which typically exist at the small gaps between a neuron's axon terminal and another neuron's dendrites (Figure 2.1). Electrical impulses transmit from a presynaptic neuron to postsynaptic neurons via neurochemical transduction every time an action potential occurs in the presynaptic neuron. Neuron's membranes maintain a voltage difference between the exterior and interior of the cell, called the membrane potential. A typical voltage across the cell membrane is -70mV, meaning that the interior of the cell has a negative voltage relative to the exterior. Voltage fluctuations, which take the form of a rapid upward spike followed by a rapid fall, are called action potentials. Synaptic connections vary in strength; the strength determines how much an action potential occurring at the presynaptic neuron will affect the postsynaptic neuron's voltage potential. Neurons can be categorised as excitatory or inhibitory. Whenever excitatory neurons have an action potential (or "fire"), they affect the postsynaptic neuron's voltage potential towards it also having an action potential. Inhibitory neurons have the opposite effect.

Neurons are similar to computer transistors to some extent. Their ability to "fire" only under specific circumstances, specifically whether the voltage potential is below a certain threshold or not, allows for mathematical logic to occur, as is the

case with transistors. This fact makes it possible that when many neurons connect in a logical manner, they are able to perform complex tasks and calculations. In the brain, billions of neurons connect to each other in a number of 'functional neural networks' in order to perform specific functions. In addition, it is worth noting that although neurons typically do not change or reproduce (one of the reasons that neurodegenerative diseases exist in the first place) over their lifetime, synaptic strengths of neuronal connections can change. This phenomenon is called synaptic plasticity and is generally thought to contribute to learning and memory.

2.1.1 Brain structures, anatomy, and functions

Structurally, the brain consists of grey matter, white matter, and cerebrospinal fluid (Figure 2.4). Grey matter consists primarily of neurons. White matter consists primarily of bundles of long-range, myelinated axons, which connect different grey matter regions of the brain. Cerebrospinal fluid is a fluid that protects the brain among other functions.

Anatomically, the brain consists of the cerebrum, the brain stem, and the cerebellum. The cerebrum is the largest part of the brain. The grey matter of the cerebrum makes up the cerebral cortex, which is located in the outer part of the cerebrum, while the inner part is comprised mostly of white matter. The cerebral cortex is further divided into the neocortex and the allocortex. Most notably for the purposes of this thesis, the neocortex comprises roughly 75% of the entire brain [82], and is a common target of neurodegenerative diseases. Another common anatomical division for the cerebral cortex is to divide it into the four lobes: frontal, parietal, temporal, and occipital. Figure 2.2 illustrates the anatomical regions defining the main four brain lobes, the brain stem, and the cerebellum, and lists a number of functions they each serve.

2.1.2 Cortical columns

The cortex is comprised of hundreds of thousands of cortical columns, which are groups of highly interconnected neurons with a relatively consistent configuration and connectivity profile [83]. The neocortex consists of neocortical columns, each

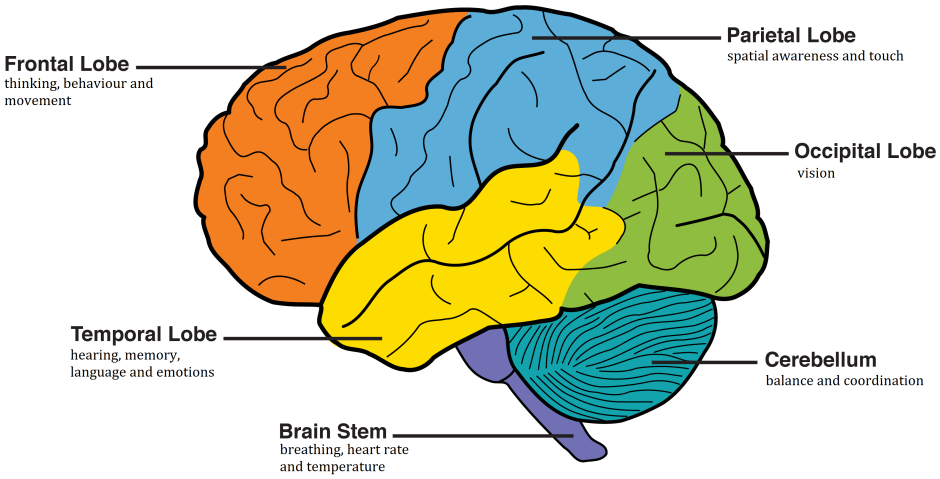

Figure 2.2: An illustration of the main anatomical parts of the brain and some of their functions. Figure from https://www.theayurveda.org/ayurveda/5-foods-to-fight-dementia-and-boost-brain-health (modified).

of which is comprised of many minicolumns. While the numbers are disputed, one commonly cited study by Mountcastle [84] claims that the neocortex contains approximately 3×10^{10} neurons, organised in minicolumns, with each minicolumn in primates consisting of approximately 100 neurons.

Each cortical column consists of six layers (typically denoted with latin numbers, i.e., layer I to layer VI), with layer I being the most superficial, and layer VI the deepest. Each layer performs a different function and has different types of neurons [85] and a different connectivity pattern [86]. Layer I primarily contains dendrites and axons from deeper-lying neurons, as well as a few inhibitory neurons [82]. Layer II contains mostly granular cells, small pyramidal neurons, and dendrites from neurons of layers V and VI [82]. Layer III contains a variety of cells, most of which are small pyramidal neurons [82]. Layer IV has mostly inhibitory interneurons and spiny stellate cells [82]. Layer V consists mostly of large pyramidal neurons, dendrites of layer III and IV neurons, and axons and dendrites of non-spiny bipolar neurons [82]. Layer VI contains neurons that blend with white matter, and dendrites from layer III and IV neurons [82].

The afferent and efferent connectivity from neocortical columns to other brain regions, and vice versa, is somewhat disputed [87]. Layers II and III supply the majority of corticocortical outputs [88]. Layer V projects outputs to the basal ganglia,

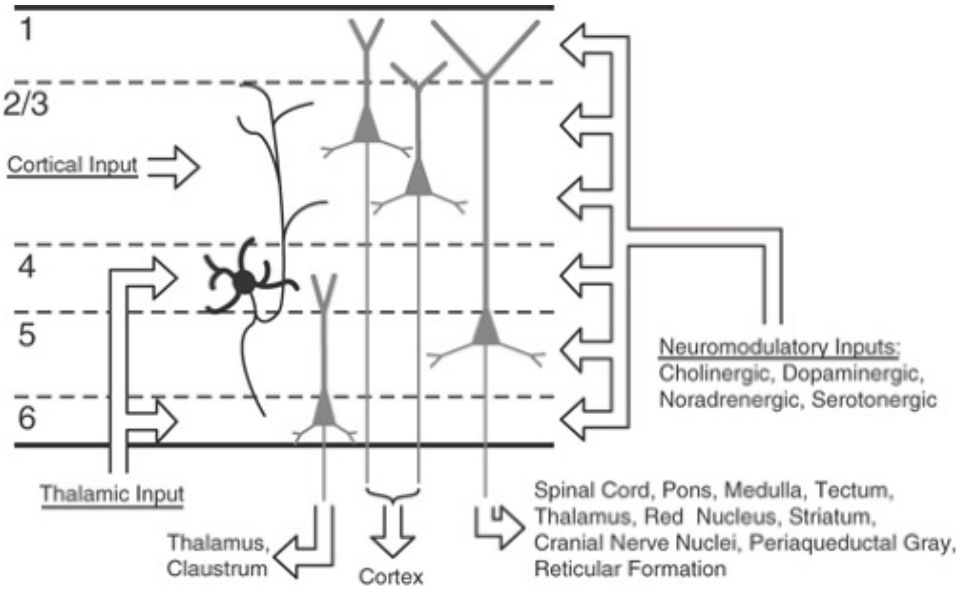

Figure 2.3: Typical cortical column connectivity. Figure from Richardson et al. [90]

the brain stem, and the spinal cord [88]. Layer VI projects outputs to the thalamus [88]. More than 99% of white matter fibres are corticocortical projections, and the majority of them are reciprocal, i.e., layer II and III neurons of one cortical region both project to and receive input from another cortical region, and that region's layer II and III neurons project to and receive input from the first cortical region [82, 89]. The thalamus projects outputs mostly towards layers IV and VI [82, 89]. Figure 2.3 illustrates the afferent and efferent connectivity of neocortical columns.

2.1.3 Brain imaging and connectivity

There are many brain imaging modalities, such as magnetic resonance imaging (MRI), positron emission tomography (PET), computed tomography (CT), etc. For the purposes of this thesis, the most relevant imaging techniques are T1-weighted (T1w) MRI, functional MRI (fMRI) and resting-state functional MRI (rsfMRI), and diffusion weighted MRI. These imaging techniques are the ones most used for determining brain connectivity profiles; specifically, functional connectivity, structural connectivity, and effective connectivity. Functional connectivity is related to synaptic activity correlations, structural connectivity is related to fibre tract connections, and effective connectivity is related to causal interactions of directed synaptic

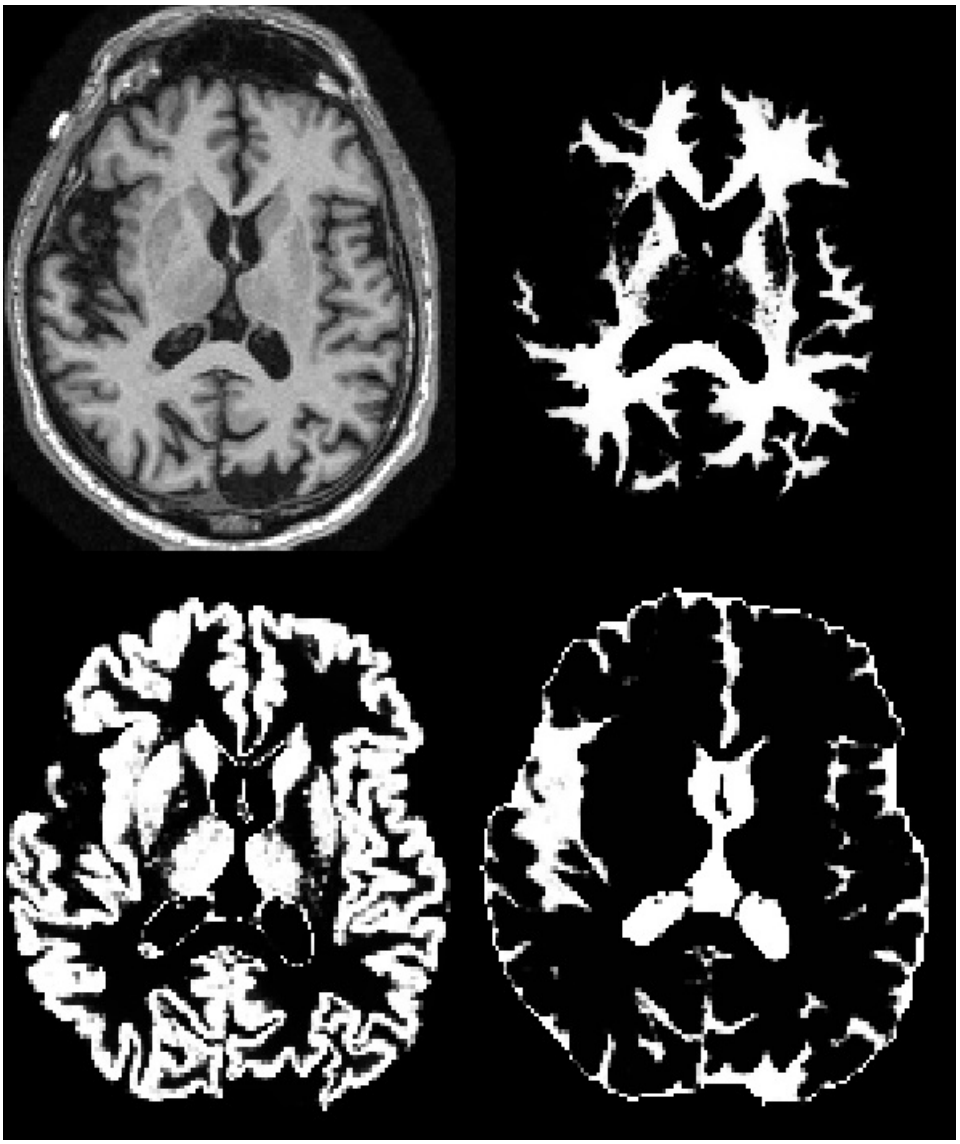

Figure 2.4: Segmentations of the three main brain tissues. Top left: T1w MRI. Top right: white matter. Bottom left: grey matter. Bottom right: cerebrospinal fluid. Figure from the thesis of Cardoso [91].

activity between brain regions.

T1w MRI is the most widely used imaging acquisition for a general structural brain scan as it provides good contrast for visualisation of anatomical structures (Figure 2.4). In addition, parcellating the brain into anatomical regions is typically performed using T1w MRIs (Figure 2.5).

Diffusion tensor MRI is computed from diffusion weighted MR acquisitions. It measures the diffusion of water in tissue. For each voxel, the rate of diffusion, as

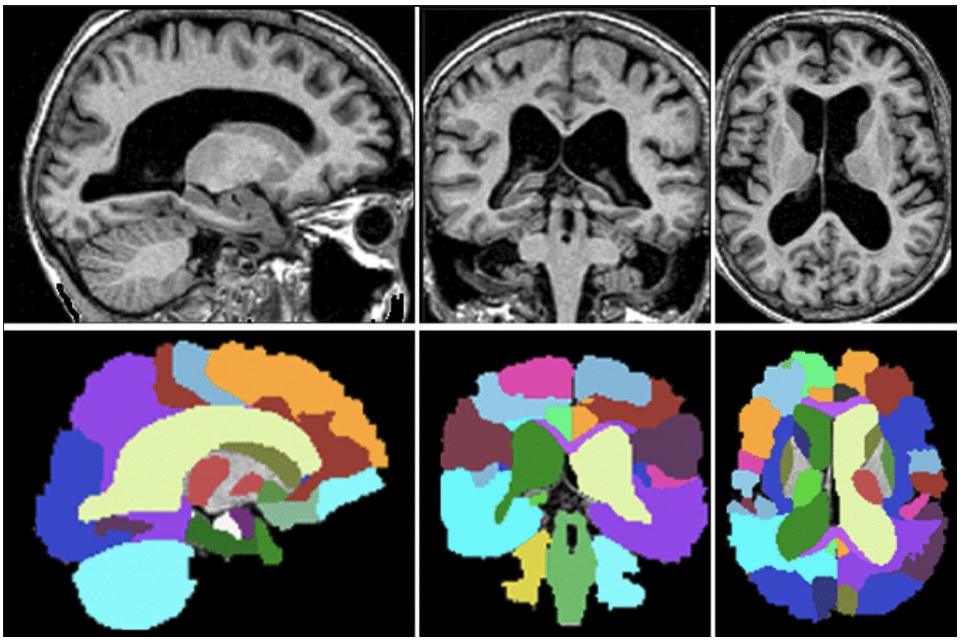

Figure 2.5: Brain parcellation example. Top: T1w MRIs. Bottom: views of the parcellation of the brain into different brain regions, with each colour representing a different region of interest (ROI). Figure from the work of Cardoso et al. [92]

well as the direction of diffusion, is calculated, which allows for the computation of neuronal fibre tract pathways, a process called tractography [93] (Figure 2.6). Using the result of tractography, one can estimate the structural connectivity of the brain, which is a matrix with its elements indicating the probability of a fibre tract structural connection between the two respective brain regions.

Functional MRI measures changes associated with blood flow, specifically, the blood-oxygen-level dependent (BOLD) signal. When the neuronal activity of a region of the brain increases, blood flow to that area will also increase as a consequence, although after a short time delay [94]. During the image acquisition in typical fMRI studies, the subject is either exposed to a stimulus, or not, at different periods of this process. The change in signal observed between the different periods at each voxel is related to that brain region's response to the stimulus (Figure 2.7). Resting-state fMRI on the other hand is concerned with what neuronal activity occurs in the brain in the absense of any stimulus [95]. A common processing procedure in fMRI studies is to compute the functional correlations between brain regions, which is simply the Pearson's correlation coefficient computed for each

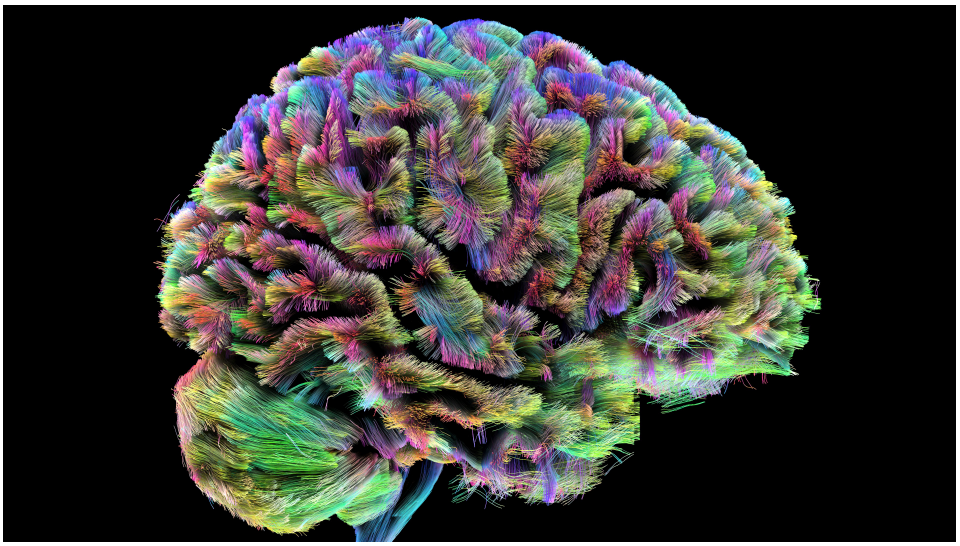

Figure 2.6: An example of 3D visualisation of the result of tractography (called a 'tractogram'). Figure from https://resource.loni.usc.edu/research/gallery/.

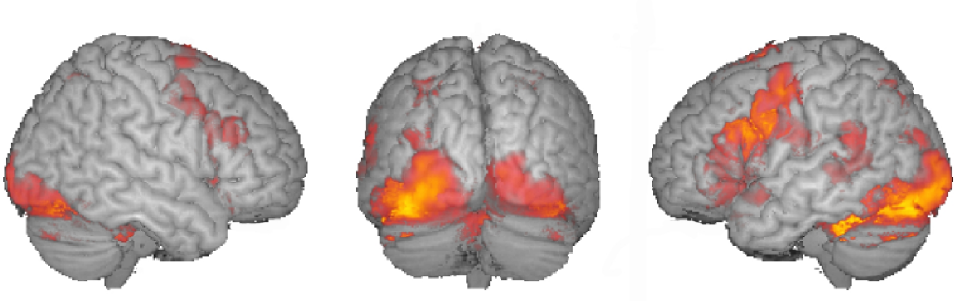

Figure 2.7: Typical images for visualisation of the brain for an fMRI study. Areas highlighted by yellow/orange are brain regions which were statistically significantly active during a task or stimulus. Figure from https://med.nyu.edu/thesenlab/research-0/research-functional-magnetic-resonance-imaging-fmri/.

pair of brain regions BOLD signals over time. The computed matrix represents the brain's functional connectivity. A common hypothesis is that a high correlation coefficient for two brain regions' BOLD signals indicates that their synaptic activity patterns are also similar.

There also exists the concept of effective connectivity between brain regions, which is meant to measure the strength of the directional neuronal connections between brain regions, or the influence one neural system exerts over another. It can also be seen as the union of structural and functional connectivity [96] (Figure 2.8). While effective connectivity models can be quite complex, the simplest one ex-

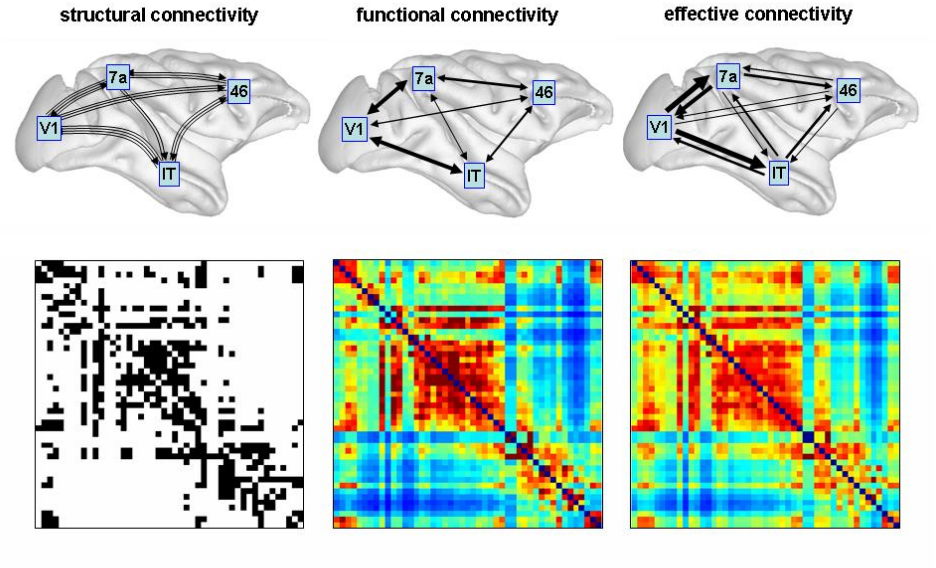

Figure 2.8: Illustration of structural connectivity, functional connectivity, and effective connectivity. Top: figures illustrating the differences between the concepts of structural connectivity, functional connectivity, and effective connectivity. Structural connectivity measures the quantity of fibre tracts connecting two regions, functional connectivity measures correlation between BOLD signals, and effective connectivity is an estimate the directed causal relation of synaptic strength between two regions. Bottom: the related connectivity matrices [97]. Figure from slide 11 of https://www.slideshare.net/emilielommers/connectome.

presses the hemodynamic change at one voxel as a weighted sum of changes in other voxels, which requires the use of the hemodynamic response equation. Friston [96] introduces the concept and the basic maths underlying effective connectivity.

2.2 Neurodegenerative diseases

Neurodegenerative diseases follow a similar general pattern of pathogenesis and progression [21, 22]. It is still unknown what the instigating event is that causes pathogenesis. One common hypothesis is that this instigating event somehow causes proteins to misfold and become pathogenic. After pathogenesis, pathogenic proteins (prion, amyloid-beta, tau, etc.) aggregate in inclusions, tangles, plaques, etc., which are less soluble or completely insoluble structures, and these proteins

begin accumulating and spreading in the brain, causing neuronal toxicity [29], although there are also soluble pathogenic proteins which can cause toxicity. The cumulative result of the toxic effects is that neurons and other cells gradually malfunction and subsequently die, resulting in brain atrophy, then clinical symptoms, and eventually patient death.

Despite the common general pattern of neurodegeneration among diseases, diseases also vary vastly in other aspects [98], such as what the underlying pathogenic protein variant is, their atrophy patterns, epidemiology, clinical symptoms, neuropathology, etc. In this section, I provide a summary review of these aspects for a few neurodegenerative diseases: Creutzfeldt-Jakob disease (CJD), Alzheimer's disease, and frontotemporal dementia (in general, as well as some variants of frontotemporal dementia). CJD is the most common disease caused by the prion protein, and prion diseases are important due to the 'prion-like' hypothesis, which is explained in Section 2.3.3. AD and FTD are presented, as they are two of the most common neurodegenerative diseases, and I focused on these diseases for this thesis. AD is a more homogeneous disease, while FTD is much more heterogeneous among patients. A more detailed review of many neurodegenerative diseases, including AD and FTD, was recently written by Erkkinen et al. [98] All of these diseases have both sporadic variants, as well as genetic variants.

2.2.1 Creutzfeldt-Jakob disease

- Pathogenic proteins: Misfolded prion protein (PrP) accumulating in intracellular plaques.
- Neuropathology: Brain vacuolation, neuronal loss, and astrocytosis [99].
- Spread pattern: CJD commonly involves the insula, the cingulate gyrus, the superior frontal gyrus, the precuneus, and the paracentral lobe [100].
- Epidemiology: Unlike other neurodegenerative diseases, diseases related to prion protein are transmissible [99], with recorded cases of occurrence through cannibalism, contaminated medical instruments, as well as through contaminated beef (the notoriously named 'mad cow' disease). Despite its

ability to transmit itself, CJD incidence rate is only 1 in 1,000,000 people [99]. Age of onset can vary from 16 to 82 years [99]. Disease progression is very fast, with most patients dying 4 to 6 months after diagnosis [101].

- Genetics: Inherited CJD is caused by mutations in the PrP gene. Individuals who are heterozygous (methionine-valine) at codon 129 of the prion protein gene are at lower risk [101].

- Clinical symptoms: Patients with CJD show symptoms of extremely rapid dementia compared to other neurodegenerative diseases as disease duration is typically four to six months [101]. Symptoms include ataxia, myoclonus and visual hallucinations [101].

- Treatment: There are presently no effective treatments, with certain drugs able to alleviate symptoms, such as clonazepam or levetiracetam for myoclonus, donepezil for visual hallucinations, and risperidone for agitation [101].

2.2.2 Alzheimer's disease

- Pathogenic proteins: (a) Amyloid-beta 42, which is a cleavage product of the amyloid precursor protein (APP), accumulates in extracellular plaques, and (b) hyperphosphorylated microtubule-associated protein tau (MAPT), which accumulates in intracellular neurofibrillary tangles [40]. It is unclear what the importance, interaction, and relative roles of the two proteins are.

- Neuropathology: Neurofibrillary tangles are first noticeable in the entorhinal cortex, followed by the hippocampus, basal forebrain nuclei, amygdala, and anterodorsal thalamic nuclei, then in the mesial temporal and parietal isocortex, and in prefrontal areas, and lastly in primary motor, sensory and visual areas [24]. By comparison, the longitudinal distribution of amyloid plaques varies a lot more among patients. Plaques first form in the basal frontal, temporal, and occipital lobes, followed by the association cortices, and lastly in

the primary sensorimotor areas and the striatum, thalamus, and hypothalamus [24].

- Spread pattern: Atrophy has been shown to start in the medial temporal lobes and fusiform gyrus at least 3 years before subjects reach a diagnosis of AD, and then spread to the posterior temporal lobes and parietal lobes, and then eventually the frontal lobes [102].

- Epidemiology: AD is the most common neurodegenerative disease. Between 60% to 80% of dementia patients have AD, and it was estimated that around 50 million people worldwide were afflicted with AD in 2018 [4]. Risk factors include age, which shows the strongest correlation with AD prevalence [103], cerebrovascular disease, smoking, diabetes, obesity, and family history [104].

- Genetics: Genetic risk factors include mutations in genes presenilin 1, presenilin 2, or APP [98]. Genetic forms of AD have a much earlier onset compared to sporadic AD [105]. Another risk factor for AD is the presence of the Apolipoprotein E (ApoE) $\varepsilon 4$ allele [106]. Patients who genetically possess this allele are called ApoE 4 positive.

- Clinical symptoms: Typically, there is a gradual progression of event related memory loss, as well as deterioration of visuospatial and executive functions [98].

- Treatment: Acetylcholinesterase inhibitors and memantine can ameliorate cognitive symptoms and enhance cognitive abilities of patients [107, 108], but they are unable to slow down the underlying degeneration.

2.2.3 Frontotemporal dementia

- Variants: Behavioural variant frontotemporal dementia (bvFTD), primary progressive aphasia (PPA), which in turn has three variants: semantic (svPPA), nonfluent/agrammatic (nfvPPA), and logopenic (lvPPA).

- Pathogenic proteins: BvFTD can be associated with tau, TDP-43 (transactive response DNA binding protein 43kDa), or FUS (fused in sarcoma), which

accumulate in aggregates or inclusions in neurons and glia [109]. There are different subtypes of TDP-43 and isoforms of tau which have been defined on histochemical and morphological grounds, which have distinct neuroimaging signatures [109].

- Neuropathology: Neuronal death, microvascuolisation, swollen neurons, white matter myelin loss, and gliosis [110]. SvPPA is generally associated with TDP-C [111], whereas nfvPPA is associated with tau [112]. In lvPPA, neurofibrillary tangles are distributed asymmetrically, with more of them located in the left hemisphere. Progranulin (GRN) mutations are associated with TDP-43 type A pathology, MAPT mutations with tau inclusions, and expansions in chromosome 9 open reading frame 72 (C9orf72) with type A or type B TDP-43 pathology [113].

- Spread pattern: Initial mild atrophy occurs in the orbital and superior medial frontal cortices and hippocampus, then progresses to involve the other anterior frontal regions, temporal cortices, and basal ganglia, then involves all remaining tissue in these coronal slices, until very marked atrophy is observed in all areas [114]. Early in bvFTD, the frontal, anterior insular, and anterior temporal cortices show atrophy [115]. Compared to AD, bvFTD shows more anterior temporal, frontal, and subcortical atrophy [116]; svPPA shows predominantly left sided anterior temporal lobe atrophy, especially in the fusiform and inferior temporal gyrus [117]; nfvPPA shows predominantly left frontoinsular atrophy [118]; lvPPA shows predominantly left temporoparietal junction atrophy [119]. Patients with GRN mutations show asymmetric frontal, temporal and parietal lobe atrophy, whereas patients with MAPT show anterior and medial temporal lobe atrophy, and patients with C9orf72 mutations show highly variable atrophy patterns on an individual level, but in group studies showing symmetric grey matter atrophy involving the thalamus and the cerebellum is common [49]. Atrophy patterns can be quite left-right brain hemisphere asymmetric or symmetric, depending on the specific pathogenic protein variant [48].

- Epidemiology: The incidence of FTD is on the scale of 10 in 100,000 people [120]. It typically has a relatively early onset, with the average age being between 50 and 60 years old, and median survival from onset being over 10 years [120]. BvFTD is approximately two times more common than nfvPPA or svPPA [121]. SvPPA diagnosis age averages around 65 years old, and median survival from symptom onset is 10 to 13 years, which is longer than other forms of FTD [121]. NfvPPA accounts for 15% of FTD cases, with the average age of onset being 67, and survival after onset being 8 to 12 years [121].

- Genetics: Mutations in the MAPT, C9orf72, or GRN genes are the major contributors of genetic cases of FTD [109] (along with other, less commonly implicated genes), each having distinct patterns of atrophy [122].

- Clinical symptoms: BvFTD symptoms include behavioural disinhibition, apathy, lack of sympathy, compulsive behaviour, and dietary changes. The earliest symptoms of PPA are language deficits [123]. More specifically, patients with svPPA show deterioration in vocabulary [123]; nfvPPA patients show deterioration in speech sound production and grammatical expression [118]; lvPPA patients have problems with word retrieval and sentence repetition [123].

- Treatment: Dopamine blockade [124], trazodone [125], and other drugs relieve symptoms, but do not deal with the pathology itself. Speech therapy and other supportive interventions are recommended for patients with PPA variants of FTD.

2.3 Pathogenic protein neurobiological mechanisms

In this section, I present some of the most important neurobiological mechanisms that are hypothesised to govern pathogenic proteins, as well as some of the evidence and hypotheses regarding their interactions with pathogenic proteins in neurodegenerative diseases. Unfortunately, empirical data on these mechanisms remains limited. The mechanisms presented include transcription and translation, clearance

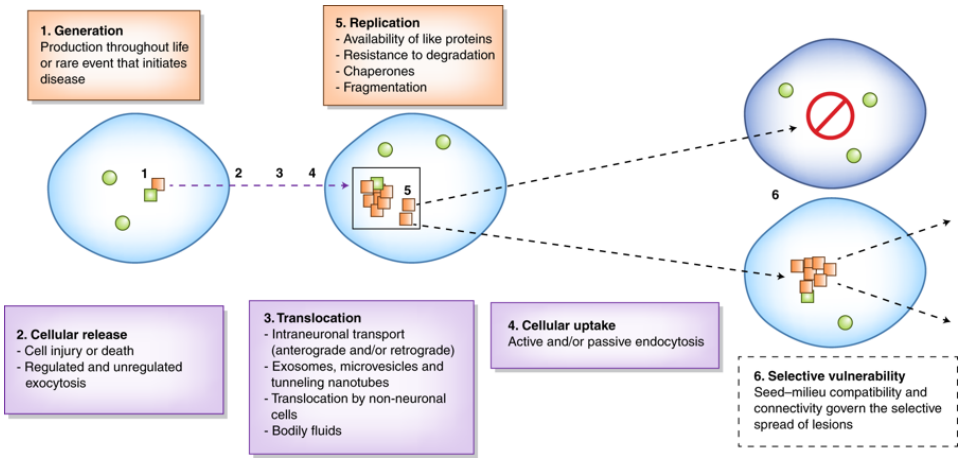

Figure 2.9: An illustration of how pathogenic proteins accumulate and spread in the brain. Figure from the work of Jucker and Walker [32].

mechanisms, the 'prion-like' hypothesis and 'prion-like' misfolding and templating, various mechanisms of protein spread, and toxic effects caused by protein accumulation on neurons and the brain. Although I attempt to separate these mechanisms to some extent, it is quite likely that disease spread patterns are produced as a result of the interplay between multiple neurobiological mechanisms [32, 33]. Thus, it is important to understand and model all of the mechanisms that play an important role, as the mismodelling of even one of these mechanisms might be enough to make the overall model inaccurate [66]. Additionally, this also implies that a potential treatment that targets just one of these mechanisms may not have the desired effect, as the interplay between them all might end in a different and unexpected result. A general idea of how proteins accumulate and spread is presented in Figure 2.9.

2.3.1 Transcription and translation

Protein is normally produced via the process of transcription and translation (see Figure 2.10 for a short description), which occurs at the somas of cells. It might be the case that some pathogenic variants of protein are also produced via transcription and translation, but not necessarily [35, 126, 127]. Chaperones assure the proper folding of proteins during the translation procedure, but their activity declines with age [128, 129], which might cause the systemic production of pathogenic proteins.

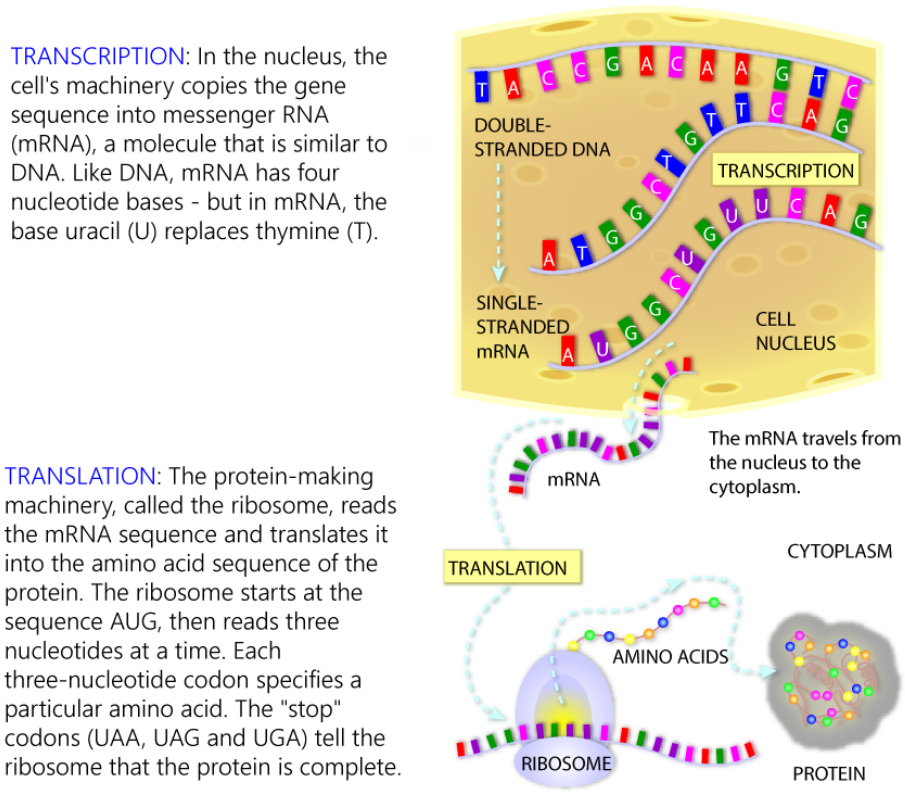

Figure 2.10: Visual representation of transcription and translation with a summarised description of these biological processes. Figure from https://learn.genetics.utah.edu/content/basics/transcribe/.

2.3.2 Clearance

Protein clearance refers to the proteolytic neurobiological mechanisms that break down and remove proteins from cells. Proteins which are clearable are called soluble, while those which cannot be cleared are called insoluble. There is evidence that some pathogenic proteins are soluble and some are insoluble [46, 130]. While there are many proteolytic mechanisms, pathogenic proteins are primarily cleared through the ubiquitin-proteasome system or the autophagy-lysosome system [131]. In the ubiquitin–proteasome system, proteins are targeted for degradation by the ubiquitination mechanism, and then recognised, unfolded and proteolysed by the proteasome [132], whereas in the autophagy-lysosome system, proteins are degraded by the lysosome [133]. For more details regarding these clearance mechanisms, the reader is referred to the review by Vilchez et al. [133] Protein can also be

cleared with enzymes, such as insulin-degrading enzymes, neprilysin, endothelin-converting enzymes, angiotensin converting enzymes, plasmin, and matrix metalloproteinases enzymes [134].

Autophagy is starting to be considered as a selective mechanism for misfolded or aggregated proteins degradation [135], including aggregates of tau, alpha-synuclein and polyglutamine-expanded proteins [136]. One hypothesis is that protein aggregation may occur all the time, but in most individuals clearance mechanisms are able to remove small soluble aggregates, thus preventing the formation of large insoluble aggregates [137]. However, even if this hypothesis is true, the effectiveness of the autophagic-lysosomal mechanism declines with age [138, 139], impairing clearance of autophagosomes, thus accumulating undigested cargos that reside inside the lysosome [140], and allowing the formation of the larger insoluble aggregates. Misfolded proteins that are aggregate-prone pose a continual challenge to degradative pathways, forcing neurons to heavily rely on autophagy for proteostasis [16].

The aggregates of Alzheimer's disease, Parkinson's disease, Huntington's disease and amyotrophic lateral sclerosis contain abnormal amounts of ubiquitin, suggesting a link between them, and ineffective proteasome and autophagy [131, 135]. In AD, the maturation and transport of autophagosomes are impaired, resulting in the accumulation of autophagosomes containing amyloid [141, 142]. The aggregated form of huntingtin has been found to be ubiquitinated, suggesting an impairment of the proteasome's ability to degrade it [143]. Neurons may direct amyloidogenic proteins to the autophagy pathway to promote their intracellular degradation, but also to enable the cell to eliminate them by the process of secretion via exocytosis, which occurs when the capacity for lysosomal degradation is exceeded [16]. Inflammatory phagocytic cells may modulate neurodegenerative pathology as they have been speculated to be involved in the clearance of amyloid-beta from the central nervous system [16]. A study by Dolan and Johnson [144] showed evidence that different tau protein variants are cleared by different mechanisms.

2.3.3 'Prion-like' hypothesis and protein misfolding/templating

The folding or conformation of a protein refers to its 3D architecture. Correctly folded proteins serve certain useful biological functions, while misfolded proteins can be inactive, dysfunctional, or pathogenic. A protein initially is a chain of amino acids, and this chain needs to be folded correctly. The process of folding is achieved with hydrophobic interactions or molecular chaperones. Misfolded proteins are produced as a result of mutations or due to disruptions of the folding process.

Prion is named after 'proteinaceous infectious particle', which received its name due to it being a misfolded protein that caused transmissible neurodegenerative diseases called spongiform encephalopathies (with CJD being one of them). The misfolded prion is able to template its misfolded state onto other non-pathogenic prion molecules and aggregate as shown in Figure 2.11. In addition, after misfolding, these proteins become more resistant to clearance mechanisms, or entirely insoluble [145], and they spread in the brain via various mechanisms. With these two properties, they are able to find non-pathogenic prion in other brain areas and continue to template, spread, and accumulate.

The 'prion-like' hypothesis is that misfolded pathogenic proteins of non-prion related neurodegenerative diseases share the same templating and aggregating mechanisms as prion (albeit at a much slower rate), and spread through the brain network [30, 36, 146, 147]. This concept has been shown to be true for prion, but despite the evidence in favour of this hypothesis, it remains a controversial hypothesis, as spread patterns could also be explained by selective tissue vulnerability [148]. Key commonalities between prion and non-prion neurodegenerative diseases include: disease starts with pathogenesis, which usually occurs for unknown reasons, but it is followed by an inevitable, long period of pre-symptomatic incubation of protein accumulation, followed by a shorter period of brain atrophy, clinical symptoms, and eventually death [146, 149]; the incubation duration depends on the protein, the specific variant of the protein, the initial seeding concentration, and the misfolding rate [146, 149]; there is great phenotypic diversity among diseases [30]; pathology spreads from one neuron to another [30]. Prion

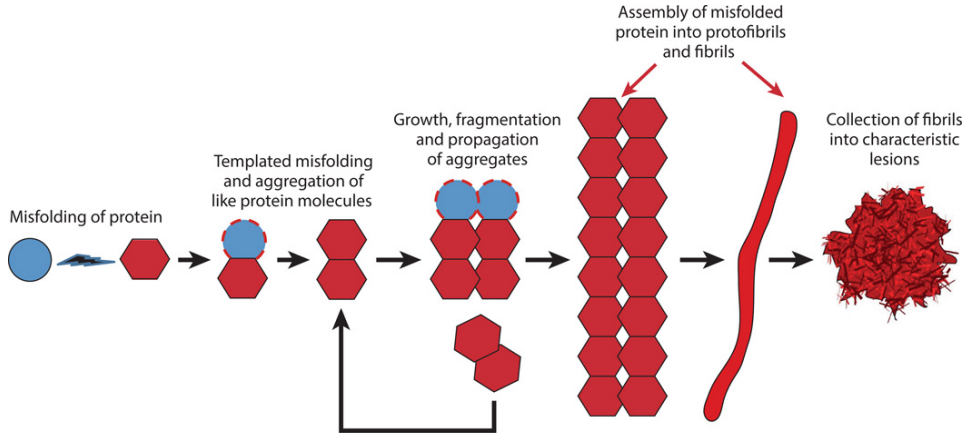

Figure 2.11: The prion paradigm of seeded protein aggregation. A schematic diagram shows the hypothetical series of events leading from the misfolding and self aggregation of protein molecules to the formation of characteristic lesions. The assemblies that act as seeds for the templated misfolding of other molecules can vary in size from small oligomers to large polymers. These seeds initiate and sustain the disease process and may be the agents by which the aggregates proliferate and spread within the nervous system. In addition, small, oligomeric assemblies have been identified as cytotoxic agents in several instances. The lesions that result from the seeding cascade can occur as intracellular inclusions (such as neurofibrillary tangles or Lewy bodies) or extracellular masses (such as amyloid plaques). Figure from the work of Walker and Jucker [146]

protein shows conformational diversity [150, 151], templating [152], and transcellular spread in in-vitro culture studies [153–155]. Similarly, amyloid-beta, tau, and alpha-synuclein show conformational diversity [156–158], templating and aggregating in in-vivo experiments [44, 57, 159–161], and transcellular spread in in-vitro culture studies [147, 153, 162].

2.3.4 Proteostasis

Proteostasis refers to the competing biological mechanisms that control folding, concentration, cellular localisation, and interactions of proteins from their synthesis till their eventual degradation [7, 163]. In healthy individuals, these mechanisms are at a steady-state equilibrium that preserves the concentration, function, and localisation of proteins at a certain desired status in order to maintain healthy cellular function. However, the effectiveness of these mechanisms is reduced with age, and this equilibrium is lost [133].

In individuals afflicted with a neurodegenerative disease, these mechanisms

become ineffective, and thus the proteins cannot be maintained at healthy concentration levels, resulting in protein accumulation. Both proteasome functionality and autophagic-lysosomal potential decline during the ageing process, and this failure contributes to the development of age related diseases [131, 164]. Proteasome dysfunction during ageing can manifest in various ways, such as decreased expression, alteration and/or replacement of proteasome subunits [165–167], disassembly of proteasomes [168] or inactivation by interacting with protein aggregates [169, 170]. The latter mechanism could induce a catastrophic proteostasis feedback during ageing, since inhibition of proteostasis itself can induce the accumulation of protein inclusions, which in turn can obstruct and further inhibit proteasome activity [169].

Therefore, a common hypothesis for the cause of overall protein accumulation is an imbalance between whole brain protein production and protein clearance [171]. This could be due to three mutually compatible scenarios: (a) proteostasis mechanisms generally remain healthy, but an instigating event introduces insoluble pathogenic proteins into the brain, which proteostasis mechanisms cannot clear, (b) clearance mechanisms remain healthy, but are overwhelmed by extreme accumulation of protein due to other mechanisms [172] (e.g., targeted network spread, templating, etc.), or (c) clearance mechanisms weaken with ageing, resulting in reduced clearance rates [133, 134, 173].

2.3.5 Protein spread mechanisms

While there is a lot of evidence supporting the idea that pathogenic proteins spread, elucidating the mechanisms by which they do so is difficult to determine experimentally. This has led to a lot of hypotheses being presented [16, 30, 36, 42–45, 174, 175]. A few hypotheses and illustrations can be seen in Figure 2.12 and Figure 2.13. Non-pathogenic and pathogenic variants of a protein can spread in the brain via the same spread mechanisms [137, 176], although that is not necessarily always the case. In the rest of this section, I present various mechanisms of spread, hypotheses and evidence regarding them, as well as whether pathogenic proteins spread through these mechanisms.

Diffusive intercellular, possibly trans-synaptic, spread of pathogenic proteins

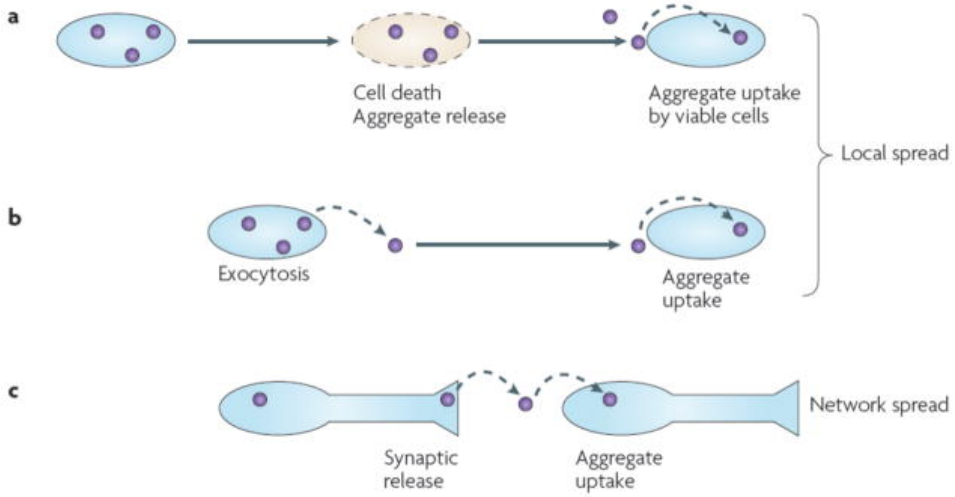

Figure 2.12: Illustration of various hypotheses of possible transcellular spread mechanisms. (a) Intracellular protein aggregation leads to cell death. This results in the release of protein aggregates into the extracellular space, which are subsequently taken up by other cells. (b) As part of the physiology of a living cell, protein aggregates may be released, potentially via exosomes or exocytosis. This results in protein aggregates in the extracellular space that may be taken up by adjacent cells. These last two hypothesised mechanisms can account for local propagation of misfolded proteins. (c) Aggregates might cross synapses. Release could be due to local degeneration of a synapse, normal synaptic physiology, or as part of an exocytic process as in (b). This mechanism can explain network (or non-local) degeneration in neurodegenerative diseases. Figure from the work of Frost and Diamond [30].

holds promise as a general mechanism for the evolution of the neurodegenerative process in a wide range of diseases [30, 36, 37, 177], including prion, amyloid-beta, tau, [147], alpha-synuclein [175, 178], TDP-43, and superoxide dismutase 1 [36]. In-vitro seeding and animal inoculation studies suggest that tau protein spread co-opts neural circuitry [44, 147]. Proteins spread primarily through the neural network [47, 179], in either anterograde or retrograde fashion [47].

Axonal transport refers to the mechanisms that transport proteins and other molecules through the cytoplasm of its axon [180]. This generally occurs at a fast rate, as opposed to, for example, passive diffusion. Axonal transport is generally occurring more often in the anterograde direction, which refers to movement of molecules from the neuron's soma towards the axon's synapses, as opposed to retrograde, which refers to the opposite direction of movement. There is evidence for axonal transport of tau [43, 47, 47, 181, 182] and prion [183, 184]. Certain

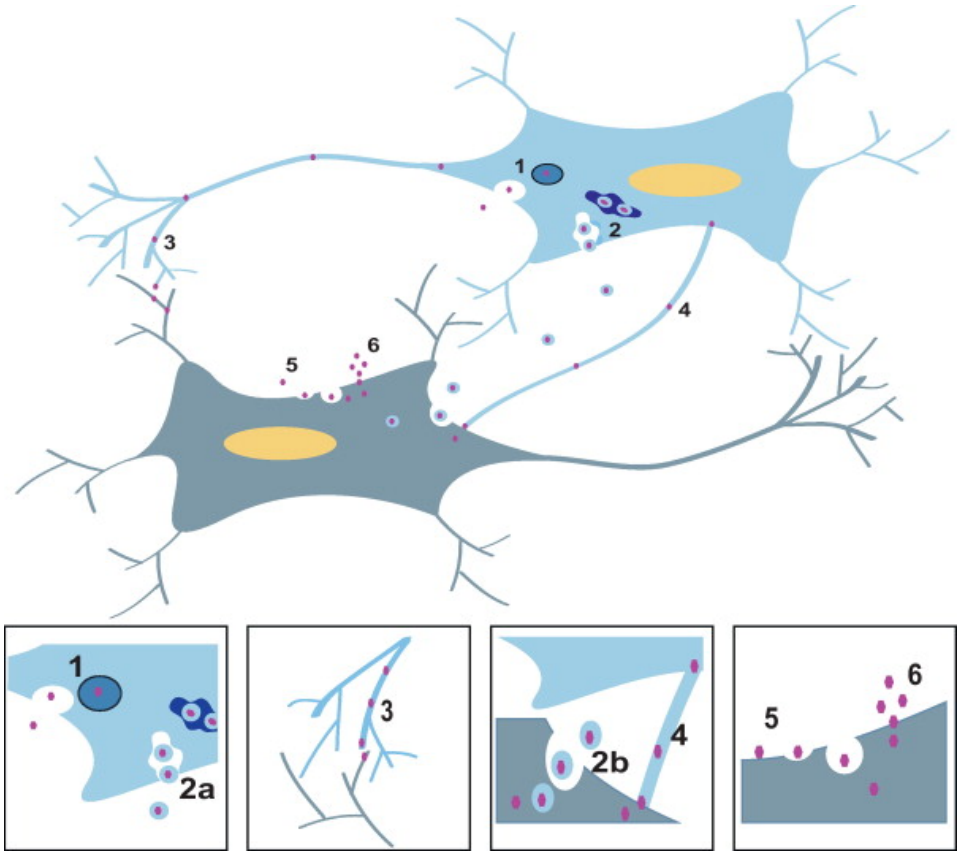

Figure 2.13: Illustration of various hypotheses of possible transcellular spread mechanisms. Protein might spread out of cells through exocytotic vesicles (1), or exosomes (2a and 2b). Direct cell-to-cell transmission is proposed to occur trans-synaptically (3) or through tunneling nanotubes (4), which have been shown to transfer prion from one cell to another. Pathogenic proteins could be taken up by cells using endocytosis (5) or passive diffusion (6). Figure from the work of Dunning et al. [175]

pathogenic tau variants show reduced transport rates [45, 182, 185].

Another mechanism that could affect protein spread is synaptic activity within a neuron. There is evidence that more tau (250% increase [176]) and amyloid-beta are released from neurons when those neurons are actively neurostimulated [176, 179]. This implies that neuronal activity (or the lack thereof) within a neuron could significantly affect the rate of protein spread. However, in later chapters, I will note that spread of protein due to electrical activity is, perhaps unexpectedly, neuroprotective and delays disease progression despite the higher volume of protein spread.

Yet another mechanism of intercellular spread is through tunneling nanotubes,

which are transient, long, actin-rich projections that connect cells [16]. There are cell culture studies showing evidence for prion spreading through tunneling nanotubes [155].

It is also possible for proteins to show preferential spread based on certain structural characteristics. One primary network feature that could affect the vulnerability of specific neurons to specific pathogenic proteins is the type of synaptic connection. Shorter-range or clustered dendritic and interneuronal connections appear particularly vulnerable to some tauopathies, whereas longer-range, more widely distributed axonal projections may be relatively more vulnerable to other molecular insults, such as toxic oligomers derived from amyloid precursor protein [36].

Endocytosis and exocytosis are the processes that occur when molecules enter or exit a cell through the membrane using vesicles called endosomes and exosomes. Lipid raft-mediated endocytosis has been proposed to occur with amyloid-beta and alpha-synuclein [186, 187]. Studies have found evidence of packaging of alpha-synuclein [188], prion [189], and amyloid-beta aggregates [190] into exosomes for intercellular spread. Exocytosis has been shown to be involved in transporting alpha-synuclein out of cells [191] of SH-SY5Y human neuroblastoma cells that were overexpressing alpha-synuclein. Alpha-synuclein has been detected both in exosomes and in the membrane and lumen of endosomes [188].

Protein molecules can spread in the extracellular space [176]. Exocytotic vesicles carrying alpha-synuclein have been shown to release it into the extracellular space [192]. Cellular entry of extracellular alpha-synuclein monomers occurred via passive diffusion [193–195], whereas the ability to enter was dependent on the structural folding for oligomers and fibrillar species [196], with some species being unable to enter.

The aforementioned mechanisms concerned themselves with spread at the molecular scale. At the brain scale, atrophy has been shown to follow neural network functional connectivity [37–39], and structural connectivity [38, 69, 197], with diseases afflicting different networks [27], such as the posterior default mode network in AD, and the anterior salience network in bvFTD [198]. Raj et al. [41]

modelled the spread of AD and FTD based on graph heat diffusion using the fibre tract structural connectivity and were able to improve atrophy prediction compared to previous similar models [41]. Zhou et al. [37] found that shorter graph paths (graph edges were based on functional connectivity derived from rsfMRI) to the epicentres of various neurodegenerative diseases coincided with greater disease vulnerability [37].

2.3.6 Toxic effects

Another aspect of pathogenic proteins that causes much speculation is the toxic effects on neurons and other cells in the brain caused by pathogenic proteins. Due to the complexity and interdependence of cellular pathways, it is difficult to discern the direct effects of pathogenic protein aggregation using empirical evidence that could be influenced by many confounding elements. In general, there can be toxic gain of function and toxic loss of function effects [17]. Pathogenic protein effects would exploit intrinsic network vulnerabilities [36], potentially causing different toxic effects at different brain areas or different types of neurons, depending on their individual vulnerability. In the rest of this section, I present examples of pathogenic protein adverse effects, but the list is by no means exhaustive.

Amyloid-beta can cause synaptic deficits [17]. Tau can cause synaptic deficits and impairment of axonal transport [17]. Prion can cause synaptic deficits, neurotoxic signaling, impairment of proteasomal and lysosomal degradation, and increased vulnerability to stress [17]. Alpha-synuclein can cause impairment of proteasomal and lysosomal degradation, pore formation, defective cellular trafficking, and impairment of synaptic dynamics [17]. Progranulin can cause loss of trophic support [17].

Pathogenic proteins can affect neuronal electric activity and synaptic function. Amyloid-beta may cause hyperexcitability [176, 179], whereas tau causes synaptic loss, reducing neuronal activity [179]. It is thus possible that neurons with high concentration of amyloid will spread tau out of them and tau will thus have higher probability of "targeting" neurons with low amyloid concentration, causing snyaptic loss. Glutamate excitotoxicity has been proposed to contribute to neurodegeneration

in amyotrophic lateral sclerosis and Huntington's disease [199].

Neuronal dysfunction can develop from loss of afferent input or postsynaptic targets, and defects in the molecular machinery at the synapse that disrupt neurotransmission and plasticity, which frequently precede structural and anatomic alterations [16]. Presynaptic inputs influence the function and health of their target neurons through the delivery of neurotrophic factors. The loss of these neurotrophic factors has been hypothesised to contribute to the pathogenesis of several neurodegenerative disorders, such as nerve growth factor in AD, glial-derived neurotrophic factor in Parkinson's disease, and both insulin-like growth factor-1 and vascular endothelial growth factor in amyotrophic lateral sclerosis [200–204].

2.4 Computational modelling

Computational modelling refers to using a mix of mathematical modelling and computer simulations to study the behaviour of complex systems that cannot be studied by using only analytical forms of equations [205, 206]. The mathematical equations of these models typically have many parameters and variables, interact with each other, and are non-linear. All of these properties make it extremely difficult or impossible to provide an analytical solution to questions of such complex systems, thus requiring the use of simulations. Computational modelling has been used in many research fields, including neurobiology, pharmacology, and medicine [207–209], as well as physics and other engineering fields [210].

There are many ways in which computational modelling approaches are useful for research. They can provide a better understanding of the underlying system being modelled, find optimal parameters so that the system achieves some desired outcome, perform sensitivity analysis to estimate how robust system outcome and behaviour is under different conditions, perform hypothesis testing, suggest future "real-world" experiments, predict system outcome for given inputs, etc. Studies using computational modelling adjust the parameters of the computational models and observe changes to the overall system output to gain a better understanding of it, as well as for hypothesis testing. Using simulation optimisation and an optimi-

sation function, optimal models and parameters can be found. The sensitivity of a system's outcomes to a change in a single parameter or multiple parameters can be determined by systematically varying their values and observing if there were any changes to the outcome. If a system has been sufficiently accurately modelled, then simulations of the modelled system can provide predictions of the behaviour of the "real-world" system.

Construction of computational models requires a few steps. A decision has to be made regarding what scale (or scales) the model will be based at. Using the topic of this thesis as an example, one could model pathogenic proteins at the individual molecule scale with elaborate models of neurons and proteins, or at the brain scale where proteins would be modelled in a more abstract manner as concentrations. Similarly, it is important to know which mechanisms are necessary, and thus should be modelled (and which ones might play a less significant role) so that the model can produce outcomes which are sufficiently close to what the outcome of a "real-world" experiment would be. For example, there are many proteins and many interactions between proteins and other neurobiological mechanisms that could affect pathogenic protein behaviour; modelling all of them increases computational complexity and requires more effort. Therefore, simplifications and assumptions need to be made. Making the correct simplifications and assumptions is perhaps the most difficult part of computational modelling. One approach would be to start with a model that is as abstract, simple, and general as possible and then continually refine with more complex models within a model selection framework. After assumptions are made, mathematical equations for each mechanism of the modelled system need to be created, based on existing knowledge, rational assumptions, complementary experiments or simulations, and empirical evidence.

The main limitation of computational modelling approaches is that since they are virtual, they are further removed from the "ground truth", whereas real-world experiments present more substantial evidence in favour or against a hypothesis. If real-world experiments could be done at zero cost and required no time, then one would vary the input parameters with all possible permutations and learn the

behaviour of the system. However, real-world experiments can require intensive effort, time and money. Computational models can help narrow down the "parameter space" of the inputs and "model space" of model hypotheses so that fewer real-world experiments need to be performed.

2.4.1 Simulation optimisation

Computational modelling optimisation is typically a very difficult problem due to the complexity of the objective function, as it can be linear or non-linear, convex or non-convex, differentiable or non-differentiable, deterministic or have uncertainty, and can have a single, multiple, or even infinite inputs [211]. In addition, the function will typically not have an algebraic form. The optimisation literature and methodologies available depend on the objective function. Deterministic objective functions with an algebraic model available are the most common problems in engineering and use linear, integer, and non-linear optimisation. Objective functions with an algebraic model available, but with uncertainty use stochastic and robust optimisation. However, objective functions of simulations do not generally have algebraic forms available. Deterministic objective functions of simulations use derivative-free optimisation, whereas those with uncertainty use 'simulation optimisation', which are the same techniques as in derivative-free optimisation, but taking into account uncertainty.

The general objective function for a simulation optimisation problem can be represented by:

$$\begin{aligned} \min \quad & \mathbb{E}_{\omega}[f(x,y,\omega)] \\ \text{s.t.} \quad & \mathbb{E}_{\omega}[g(x,y,\omega)] \leq 0 \\ & h(x,y) \leq 0 \\ & x_l \leq x \leq x_u \\ & x \in \mathbb{R}^n, y \in \mathbb{D}^m \end{aligned}$$

The function f can be evaluated through simulation for a particular instance of

the continuous inputs x, discrete inputs y, and a realisation of the random variables ω (which may or may not be a function of the inputs, x and y). Similarly, the constraints defined by the vector valued function g are also evaluated with each simulation run. In this formulation, expected values for these stochastic functions are used. There may be other constraints (represented by h) that do not involve random variables, as well as bound constraints on the decision variables.

In my thesis, I deliberately chose not to include uncertainty in the modelled mechanisms, in order to simplify the modelling and hasten the optimisation convergence. This comes at the cost of being less able to test how robustly a specific set of modelled mechanisms produce similar results. For example, if there is uncertainty in the way that a spread mechanism works, it could be that in one iteration a specific brain area atrophies first before another one because more protein spread to the first one, whereas in another iteration it could be the other way around.

Thus, in my work there is no uncertainty in the optimisation function, there are multiple parameters as inputs, the objective function is non-linear, non-smooth, non-convex, and non-differentiable with only function evaluations available after each simulation. This complexity required the use of optimisation techniques from the derivative-free literature.

A review of derivative-free optimisation algorithms and software implementations was written by Rios and Sahinidis [212]. A common technique used by some algorithms is to create a surrogate model of the objective function; in essence a function that is an approximation of the objective function, except it has properties such as smoothness, differentiable, potentially convex, etc. Direct local search methods, such as the Nelder-Mead [213], the generalised pattern search [214] and the generating set search [215] algorithms converge to a single local optimum, without very sophisticated algorithms to attempt to find the global optimum. Model based local search, such as trust-region methods [216] and implicit filtering [217] build a surrogate model and use its gradient as information to guide the search while continually refining the surrogate model. Lipschitzian based partitioning global search techniques [218] construct and optimise a function that underestimates the

objective function, but allows for search of the global minimum. Multilevel coordinate search [219] attempts to find the global optimum by partitioning the parameter space in boxes and searching each box. Response surface methods, such as efficient global optimisation [220], radial basis functions [221] and sequential design for optimisation [222] use a surrogate model where any error between the surrogate and the objective functions is assumed to be model error rather than noise in experimental measurements. Surrogate management framework [223] is a generalised pattern search method combined with a surrogate model to help guide the search. Optimisation by branch-and-fit [224] combines surrogate models and randomisation. Stochastic global search algorithms include hit-and-run algorithms, which include randomness in the direction and step size of the search, simulated annealing [225], which simulate a process of temperature gradual reduction, genetic algorithms [226], which resemble natural selection with mutations and reproduction, and particle swarm algorithms [227], which simulate animal and insect behaviour.

The review by Rios and Sahinidis [212] also included evaluation of various software implementations of 22 derivative-free optimisation algorithms, where the objective functions of the tests could have been convex and smooth, convex and non-smooth, non-convex and smooth, and non-convex and non-smooth. Since the objective function used in my thesis was non-smooth and non-convex, I focused my attention primarily to how well the algorithms performed with these tests. There were 18 non-smooth and non-convex tests, 4 of which had 1-2 input variables, 11 had 3-9 input variables, and 3 had 10-30 input variables. Also, 11 of them had no bounds, 4 had only lower bounds, and 3 had lower and upper bounds on the values that the input variables could take. Figure 2.14 shows the performance of the algorithms.

The first two algorithms (TOMLAB/MULTIMIN and TOMLAB/LGO) are part of a commercial software. I instead chose to download and try the PSWARM and MCS algorithms, which performed well in the tests. In addition, since my code was written in MATLAB, I used MATLAB's own generalised pattern search, particle swarm, and simulated annealing functions (*patternsearch, particleswarm,*

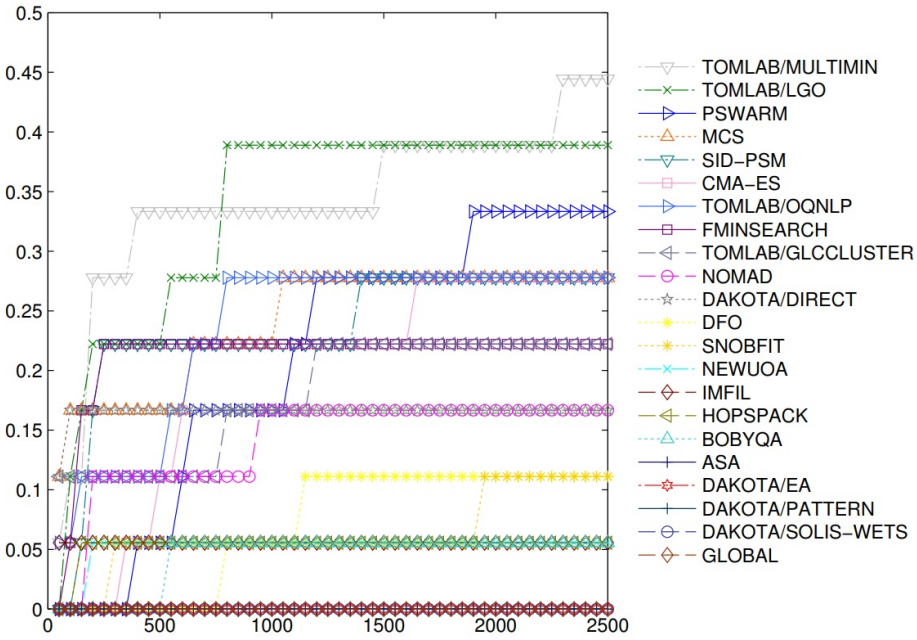

Figure 2.14: Comparison of derivative-free optimisation algorithms. Fraction of non-convex and non-smooth problems solved as a function of allowable number of function evaluations. Figure from the work of Rios and Sahinidis [212].

simulannealbnd), as they were easy to include in my implementation. MATLAB's particle swarm software consistently optimised and converged faster than the other four algorithms, although it is impossible to know if it converged to the global optimum, or if another algorithm would overtake it and perform better in the long-run.

2.4.2 Simulation optimisation parameter space sampling

An important aspect when using such optimisation algorithms is that they search the parameter space assuming that the optimum parameter value is uniformly distributed, but this assumption does not always hold. In order to address this, one can force the optimising software to search uniformly/linearly in the normalised bounded space between 0 and 1 for each parameter. Following the software's search, the appropriate transformation function must be applied to the parameter values given by the optimising software, with the goal being to change the sampling distribution from uniform to a desired one, but keeping the range of the sampling distribution between 0 and 1. This is best explained with an example:

Assume that a parameter's acceptable values are between 10^{-4} and 10. The

order of magnitude that the global optimum exists in is not known, but it is assumed that it has equal probability of existing in any order of magnitude between 10^{-4} and 10 (e.g., equal probability of existing in the range 10^{-4} to 10^{-3} or in the range 10^{-2} to 10^{-1}). If one lets the optimising software to simply sample uniformly between 10^{-4} and 10, then with 90% probability, it would sample in the 1 to 10 range and would undersample lower values. To sample the 'orders of magnitude space' instead in a uniform fashion, this translates to an exponential sampling of the space of real numbers. If, for example, the optimising software can only sample uniformly between 0 and 1, and the variable sampled for is x, then a function that has 1/5th probability of sampling in the 10^{-5} to 10^{-4} range, 1/5th in the 10^{-4} to 10^{-3} range, 1/5th in the 10^{-3} to 10^{-2} range, 1/5th in the 10^{-2} to 10^{-1} range, and 1/5th in the 10^{-1} to 1 range is desired. In the limit of such logarithmic subdivisions this is done with the function:

$$y = \frac{e^{1+(a-1)x}}{e^{a}} \tag{2.1}$$

The constant a can be calculated as such:

$$\frac{e^{1}}{e^{a}} = 10^{-5}$$

After some calculations, a becomes equal to:

$$a = 1 + 5\log(10) \approx 12.5129$$

Eq. 2.1 with $a = 1 + 5\log(10)$ samples the parameter space exponentially, as opposed to uniformly. Multiplying y by 10 gets the desired parameter value.

Chapter 3

State of the art

The most important research in neurodegenerative diseases are in-vivo and in-vitro studies, as any evidence from such research is closer to the underlying truth of what happens in the human brain, and thus has more merit compared to in-silico research. There have been many in-vivo [42–47, 174] and in-vitro studies [127, 144, 147, 182, 185] showing that after injection of pathogenic proteins into healthy animal brains or cell cultures, they will aggregate, template, and spread. Each study provides evidence that increases our understanding of these mechanisms, as well as demonstrates the variations in the interactions between these mechanisms and different pathogenic protein variants. However, these studies are limited by how time and resource intensive they are, and thus are unable to test many hypotheses quickly and efficiently. Computational research on the other hand, is on the opposite side of the spectrum, where many hypotheses can be tested quickly and inexpensively, but all the mechanisms have to be modelled.

Many computational and mathematical models that fall under the umbrella term of systems biology have been developed for neurodegenerative disease mechanisms. A few review articles [12, 28, 33, 65, 66, 228] on systems biology contain references to previous relevant work, in addition to discussing the importance of computational modelling as a complementary tool to in-vivo and in-vitro studies in neurodegenerative disease and drug development research. Many of these models can be found at 'Biomodels' (https://www.ebi.ac.uk/biomodels/), a website where many mathematical and computational models regarding biological mech-

anisms, including neurodegenerative diseases are published [228]. These models have heavily focused on elucidating the mechanisms of protein aggregation and protein clearance, as they are two fundamental mechanisms of neurodegenerative diseases. Other mechanisms that have been studied in systems biology [66] include protein misfolding, genetics, tauopathy, ion homeostasis, blood brain barrier transport, microtubule based transport, intercellular signaling, synaptic transmission, oxidative stress, apoptosis, amyloid protein precursor breakdown, energy metabolism, inflammatory response, etc.

Following are some examples of computational modelling systems biology approaches. Büchel et al. [229] modelled a nerve cell, dopamine metabolism and transport, oxidative stress, aggregation of alpha-synuclein, lysosomal and proteasomal clearance, and mitophagy. Their simulations showed that increased levels of alpha-synuclein induce apoptosis, followed by an increase of alpha-synuclein in the extracellular space. Proctor et al. [74] studied the aggregation of amyloid-beta and tau in AD, their toxicity to neurons, and they evaluated what impact a candidate therapeutic intervention, amyloid-beta immunisation, would have. They found that immunotherapy reduced plaques, but not soluble amyloid-beta or tau (which are hypothesised to be the more toxic protein molecules in AD). Edelstein-Keshet and Spiros [8] modelled amyloid-beta proteins and their production, aggregation, and removal, as well as neurons, microglia, astrocytes, inflammation, secreted cytokines, and the stress, recovery, health, and death of neuronal tissue within the setting of a small square slice of neural tissue. A variety of hypotheses regarding the causes of stress and death of neurons were explored. Peptides spread via rapid diffusion, whereas cells moved via slower diffusion, based on a 2D diffusion equation expressed in flux based form. Amyloid-beta was seeded and produced at the centre of a region of healthy neuronal tissue from where it started diffusing. Puri and Li [230] modelled AD pathogenesis using differential rate equations that represent cross-talks among microglia, astroglia, neurons, and amyloid-beta. From their results, they suggested that future therapies attempt to inhibit microglia. Winter, Bludszuweit-Philipp, and Wolkenhauer [231] modelled the BOLD signal, as well

as the effect that AD has on it, and found that AD had an impact on peak height, peak timing, and full width at half maximum. Qosa et al. [232] modelled the contribution of the blood brain barrier and of degradation mechanisms to amyloid-beta clearance, concluding that transport of amyloid-beta across the blood brain barrier contributes twice as much to amyloid-beta clearance as the degradation pathway. Lockwood, Ewy, Hermann, and Holford [233], and Masel and Jansen [234] modelled the aggregation of pathogenic proteins and multiple hypothetical drugs to combat AD, and compared their simulated performance, demonstrating the value of computational modelling in drug design. Morris, Watzky, Agar, and Finke [235], in addition to providing a review of protein aggregation modelling literature, they also modelled it using nucleation and growth rate parameters, which they found to fit extremely well with data of many different studies. Clarke et al. [236] modelled the probability of neuronal death over lifetime based on empirical data, including Huntington's and Parkinson's disease data. Their findings suggested that there is no increasing risk of neuronal death as time goes forward, but rather that a random (single) event initiates the disease process, and afterwards, protein accumulation and spread occurs. Kuznetsov and Kuznetsov [237] modelled prion protein spread through tunnelling nanotubes.

However, these works have focused more on pathogenesis, aggregation, and other proteostatic mechanisms, while little work has been done on spread of pathogenic protein [33, 238], and even less on modelling all of these mechanisms within a single unified framework [12]. In addition, most systems biology work occurs at an abstract, "systems level", whereas little work is done specifically with interconnected neural networks or at the brain scale. While there has been other work related to spread of pathogenic proteins [238, 239], the most recent work that is similar to mine is the work of Kerr et al. [71], who modelled mechanisms of neurodegenerative diseases in small artificial neural networks, the work of Rowan et al. [72], who also modelled mechanisms of neurodegenerative diseases in small artificial neural networks, the work of Zhou et al. [37] and the follow-up work of Mandelli et al. [68] who studied functional connectivity in neurodegenerative dis-

eases, the work of Raj et al. [41, 177] and the follow-up work of Pandya et al. [67], who modelled disease progression in AD, FTD, and progressive supranuclear palsy using a graph network heat diffusion model, the work of Iturria et al. [69] who modelled amyloid-beta spatiotemporal spread in AD, the recent work of Weickenmeier et al. [70], who modelled mechanisms of protein production, protein misfolding, protein clearance, structural connectivity related spread, and extracellular diffusion in order to replicate the disease progression of amyloid-beta and tau in AD, alpha-synuclein in Parkinson's disease, and TDP-43 in amyotrophic lateral sclerosis, and the recent work of Bertsch et al. [73], who attempted to link the microscale and the macroscale, modelling aggregation of monomers into polymers and fibrils, production, clearance, diffusive spread, and toxic effects of soluble amyloid-beta 42 in AD.

Simulations using NEURON (see Section 4.1) and small artificial neural networks aimed at answering questions regarding neurodegenerative diseases have been done before by Kerr et al. [71] and Rowan et al. [72], but their work was concerned with questions regarding different aspects of neurodegenerative diseases. Kerr et al. [71] attempted to answer how the influence of the basal ganglia on cortical information becomes pathological in Parkinson's disease. Rowan et al. [72] performed a study of the effects of synaptic scaling driven progression of AD and how directed brain electrostimulation could slow down disease progression.

In the work of Zhou et al. [37] and in the follow-up work of Mandelli et al. [68] the authors proposed four competing hypotheses for the underlying mechanism that is responsible for the atrophy patterns: nodal stress (regions subject to heavy network traffic, i.e., hubs, undergo activity related "wear and tear" that gives rise to or worsens disease), transneuronal spread (i.e., 'prion-like' spread), trophic failure (in which, network connectivity disruption undermines interneuronal trophic factor support, accelerating disease within neurons lacking collateral trophic sources, i.e., more isolated neurons), and shared vulnerability (regions that feature a common gene or protein expression signature that confers disease vulnerability). They used rsfMRI to derive the healthy intrinsic connectivity patterns seeded by the spe-

cific brain regions which are vulnerable to five distinct neurodegenerative diseases. They then investigated if intrinsic connectivity in health can predict which regions are vulnerable to disease [37]. For each disease, specific regions emerged as seed regions whose normal connectivity profiles most resembled the atrophy pattern [37]. Performing graph theoretical analyses in healthy subjects revealed that regions with higher total 'connectional flow' (hubs) and, more consistently, shorter functional paths to the seed regions, showed greater vulnerability [37]. The authors believe that these findings best fit a transneuronal spread model of network based vulnerability [37]. However, while these works explored functional connectivity and its role as a spread mechanism, the authors did not model any mechanisms of proteostasis.

Raj et al. [177] mathematically modelled trans-synaptic diffusive spread of protein via the brain's structural connectivity, which was obtained from 14 healthy brain MRIs. Subsequently, they derived a graph and computed the eigenvectors of the Laplacian matrix of the graph, and then they used a heat kernel to model trans-synaptic diffusion. The authors discovered a correlation between the second eigenvector and AD subjects' atrophy regions, and between the third eigenvector and FTD subjects' atrophy regions [177]. In the follow-up work of Raj et al. [41], the authors attempted to develop their model into a clinically useful computational biomarker with the ability to predict future patterns of atrophy in individual patients. Given initial concentrations of the pathogenic proteins in each brain region, they used regression to learn the diffusion parameter for each individual subject, and then they were able to predict atrophy for that subject [41]. Their predicted results had a high correlation (Pearson's R between baseline atrophy and predicted atrophy was 0.96 when using their model as opposed to 0.89 when correlating the baseline atrophy to follow-up atrophy with p-values below 0.01) with the atrophy observed in longitudinal images, which shows strong support in favour of a hypothesis that pathogenic proteins spread using a simple diffusive mechanism via the neural network [41]. In a more recent follow-up work by Pandya et al. [67], the authors used the network diffusion model of their previous work to predict progressive supranuclear palsy progression, adding directionality to the model, based on an

adaptation of mouse tracer studies to the human brain. They concluded that their updated model was a better predictor of disease progression than the non-directional model. Additionally, they found that the hypothalamus was the brain region that, when considered as a seed, their model was able to best predict disease progression. However, this network diffusion model only spread protein, assuming that it was all gathered at the start of the simulation within a single seed region, rather than modelling a build-up of protein starting from a small seed, which is the more likely hypothesis. This is a consequence of the lack of modelling of protein production, templating, or clearance, which I modelled for the work of this thesis. In addition, I also modelled functional and effective connectivity, as well as synaptic activity related spread, and I used a population based validation.

Iturria et al. [69] modelled the spatiotemporal spread of amyloid-beta concentration using an epidemic spread model. Simulations would initialise with a healthy brain where amyloid-beta is seeded to, and thereafter amyloid-beta would accumulate and spread based on the modelled mechanisms. They compared their results against empirical data of amyloid-beta concentration PET imaging of 733 subjects from the Alzheimer's Disease Neuroimaging Initiative (ADNI). They parcellated the healthy brain into 78 grey matter regions, and modelled that each region has a concentration of amyloid-beta. They modelled amyloid-beta production, templating, and clearance, as well as spread based on a linear model of the structural connectivity (structural connectivity of the young healthy brain was derived using 60 young healthy subjects from the CMU-60 DSI Template) that also took into account the Euclidean distance between brain regions. The model had four parameters, one controlling the production and templating strength, one controlling the clearance strength, the set of seed regions (which were up to a maximum of 6 grey matter brain regions), and one controlling the variance of normally distributed noise, which hypothetically accounted for other factors that were not modelled. For each subject of the ADNI data set, the authors found the optimal parameters, as well as the optimal time point at which the simulated amyloid-beta concentration pattern best matched the amyloid-beta concentration pattern of the subject's PET image.

The optimal set of seed regions were selected based on the best fit across the entire subject dataset. Results found that the posterior and anterior cingulate cortices were the most probable seed regions, structural connectivity played a crucial role in the spread of amyloid-beta, hub regions were more vulnerable to amyloid-beta spread, clearance rates were lower for AD patients versus controls, and, in general, their prediction of amyloid-beta deposition matched well against the amyloid-beta deposition shown in empirical data. In contrast, I additionally modelled non-pathogenic protein concentration, brain regional volume and atrophy, and more mechanisms of spread. I also compared my results among four different diseases.

The work of Weickenmeier et al. [70] is the most similar to the work of this thesis, especially to the work presented in Chapter 5. The authors computationally modelled pathogenic protein mechanisms, based on the Fisher-Kolmogorov equation for population dynamics, with an anisotropic diffusion model. They also modelled pathogenic and non-pathogenic protein, protein transcription and translation, and protein misfolding (identically to my model in Chapter 5), while they had a simpler model for clearance. Protein spread was modelled based on fast spread via fibre tracts derived from structural connectivity, and slower spread via extracellular diffusion. They modelled the brain using a finite element approximation to represent regions, each with its own concentration of pathogenic and non-pathogenic protein. They ran simulations at the whole brain scale, attempting to replicate the disease progression of amyloid-beta and tau in AD, alpha-synuclein in Parkinson's disease, and TDP-43 in amyotrophic lateral sclerosis. However, their results were evaluated only visually, where their ground truth consisted of histopathological literature regarding disease progression, as opposed to a quantitative method. By contrast, I modelled additional mechanisms of spread, including functional and effective connectivity related spread and synaptic activity related spread, my ground truth was based on an event based model of patient MRI scans (and thus my evaluation was quantitative), and lastly, I modelled the brain as regions based on a brain parcellation of functional and structural grey matter areas.

In the work of Bertsch et al. [73], the authors attempted to bridge the gap

between the microscopic and the macroscopic scales, modelling aggregation of monomers into polymers and fibrils, production, clearance, diffusive spread, and toxic effects of soluble amyloid-beta 42 in AD. They use a jump process to instigate the seeding event of the disease and Smoluchowski equations to model the change in amyloid concentration over a 2D uniformly sampled grid that represents a transversal section of the brain. The equation for the toxicity of neurons at the macroscopic scale was derived starting from the microscopic setting. They compare their simulation results of global concentration of amyloid fibrils against PIB-PET (Pittsburgh Compound-B positron emission tomography) data, occipital region concentration of amyloid polymers against CSF (cerebrospinal fluid) measurements of amyloid, and global atrophy against MRI data. Although their results broadly agree with clinical evidence, their comparison is qualitative, whereas ours is quantitative, attempting to capture the entire atrophy progression. Additionally, the authors used a simple 2D slice of the brain as a lattice, whereas we model the brain using specific grey matter regions, as well as functional, structural, and effective connectivity, and we model a larger variety of spread mechanisms.

Chapter 4

Computational modelling at the neuronal scale

The 'molecular nexopathies' paradigm (see Section 1.2) hypothesises that structural features of neural circuits confer vulnerability to particular pathogenic proteins [36]. It predicts that protein mechanisms and network properties together can determine disease effects. In this chapter, I explored the 'molecular nexopathies' hypothesis with a computational modelling approach using the NEURON simulator for neural network simulations.

Previous similar work in computational modelling of pathogenic protein mechanisms has not focused on an artificial neuronal scale neural network. An example is the work of Proctor et al., which was a study of the aggregation of amyloid-beta and tau in AD, and an evaluation of therapeutic interventions [74]. Although the work was focused at the neuronal scale, this was at a more abstract layer, rather than an explicit neural network with graph elements or compartments. There has also been work that modelled pathogenic protein mechanisms focused at the brain scale, such as the work of Raj et al. [41] and the work of Weickenmeier et al. [70]. Simulations using NEURON and small artificial neural networks to answer questions regarding neurodegenerative diseases have been done before by Kerr et al. [71] and Rowan et al. [72], but they focused on questions regarding different aspects of neurodegenerative diseases. Kerr et al. [71] attempted to answer how the influence of the basal ganglia on cortical information becomes pathological in Parkinson's disease.

Rowan et al. [72] performed a study of the effects of the synaptic scaling driven progression of AD and how directed brain electrostimulation could slow down disease progression. Therefore, to my knowledge this chapter presents the first work of computational modelling of neurobiological mechanisms of pathogenic proteins within a compartment based small artificial neural network.

To construct my computational modelling framework, I first developed mathematical models for mechanisms of protein accumulation, spread, and toxic effects. Using the NEURON simulator software [240], I simulated an artificial neural network comprised of cortical columns [241], which are a representative and frequent target of neurodegenerative diseases (see Section 2.1.2). I then ran simulations, systematically varying protein and network parameters in an analysis to observe how variations affect the disease progression. I defined metrics that related these parameter variations to the protein spread and the network damage pattern.

There are both soluble and insoluble pathogenic proteins and potentially certain diseases are caused by soluble proteins and others by insoluble proteins. Discovering the mechanisms that play an important role with each of them would help in understanding their behaviour. I hypothesised that soluble pathogenic protein spread would be determined more by the neural network connectivity, whereas for insoluble by the initial seed.

Although modifying certain mechanisms, such as enhancing clearance in the case of soluble pathogenic protein, are almost certain to delay disease progression, for most mechanisms it is not immediately clear. To that end, I assessed how modifying model parameters affected the overall network survival, in order to find potential neuroprotective cases.

Spatiotemporal patterns of progression can converge among patients with the same disease, but different seeds. Atrophy could initially present itself in different brain regions, but eventually converge and progress similarly in two different patients afterwards. Discovering which mechanisms are more prone to cause convergence of spatiotemporal spread patterns of differently seeded cases could help in understanding what mechanisms drive diseases whose atrophy patterns show strong

convergence.

4.1 NEURON simulator

In order to model the neuronal scale and run simulations, I required a simulator that models and simulates the neurobiological processes and structures present in neural networks. Due to my lack of neuroscientific knowledge and the wide range of already available simulators, I decided to find an already well-established one that is appropriate for the aims of this thesis. A review and comparison of certain simulators was written in 2007 [242]. I chose the NEURON [240] neural network simulator, as it has been the most used software for neural network simulations for many years. NEURON provides a powerful and flexible environment for implementing biologically realistic models of electrical and chemical signaling in neurons and networks of neurons. It uses the Hodgkin-Huxley equations, but greatly refined over the years. The basic computational task is to solve numerically the cable equation, which describes the relationship between current and voltage in a one-dimensional cable:

$$\frac{\partial V}{\partial t} + I(V,t) \quad = \quad \frac{\partial^2 V}{\partial x^2} \tag{4.1}$$

The application of cable theory to the study of electrical signaling in neurons has a long history, which is briefly summarised by Rall [243]. Within NEURON, dendrites, somas, and axons are represented by 'compartments', in a branched architecture that is typical of most neurons.

4.1.1 Neocortical column artificial neural network

I chose to perform my analysis on an artificial neural network of neocortical columns (see Section 2.1.2). They are the most common structure in the brain, making them an interesting target to analyse.

There are already many available models of neurons and neuronal networks for NEURON at ModelDB [244]. I used the network described by Neymotin, Ja-

cobs, Fenton, and Lytton [241]. This network consisted of a number of cortical columns NCol each consisting of 470 neurons, for a total of $\text{NNeu} = 470 \times \text{NCol}$ neurons. Although in reality they are arranged in two dimensions, in this simulated network, columns were arranged in a single dimension, e.g., column 5 would neighbour column 4 and column 6. I believe this simplification will not have a significant impact on results due to the similar definition of the columns and the high number of connections between columns. Each neuron $i \in \{1,...,\text{NNeu}\}$ belonged to a cortical column $\text{Col}_i \in \{1,...,\text{NCol}\}$, to a layer $\text{Lay}_i \in \{2,4,5,6\}$ (layers 2 and 3 were combined as they contain similar neurons, and layer 1 was not simulated as it contains only axons and dendrites of deeper neurons), and had a type, which could have been excitatory Regular Spiking (RS), excitatory Intrinsically Bursting (IB), inhibitory Fast Spiking (FS), or inhibitory Low-Threshold Spiking (LTS), $\text{Type}_i \in \{\text{RS},\text{IB},\text{FS},\text{LTS}\}$. The amount of neurons of each type within each cortical column is shown in Figure 4.1.

Each neuron consisted of three cylindrical compartments; one represented its dendrites ($j = 1$), one represented its soma ($j = 2$), and one represented its axon ($j = 3$). Many neuronal properties and the neural network's connectivity were defined by Neymotin et al. [241]. For the purposes of this thesis, I defined the diameter $\text{Diam}_{i,j}$, length $\text{Len}_{i,j}$, base area $\text{Area}_{i,j} = \pi(\text{Diam}_{i,j}/2)^2$, and volume $\text{Vol}_{i,j} = \text{Len}_{i,j} \times \text{Area}_{i,j}$ of each compartment. I also defined the synaptic strength $\mathbf{SS}_{i,j\leftarrow\bar{i},\bar{j}}$ of a synapse starting from neuron $\bar{i}$, compartment $\bar{j}$ connecting to the postsynaptic neuron i, compartment j. If there was no synaptic connection, then $\mathbf{SS}_{i,j\leftarrow\bar{i},\bar{j}} = 0$. Neurons were randomly connected depending on their type and layer according to the connection densities shown in Figure 4.3 for connections between neurons of the same column, and the connection densities shown in Figure 4.5 for connections between neurons of neighbouring columns. The authors state that the connections densities had to be several times higher than in real neuronal networks, claiming it was necessary sustain activity due to the small scale of the model. The synaptic strengths $\mathbf{SS}_{i,j\leftarrow\bar{i},\bar{j}}$ were derived from Figure 4.4 and Figure 4.6 for same column and neighbouring column connections, respectively. In order for a neuron to

Type	L2RS	L2IB	L2LTS	L2FS	L4RS	L4LTS	L4FS	L5RS	L5IB	L5LTS	L5FS	L6RS	L6LTS	L6FS
Count	142	8	13	25	30	14	20	65	17	13	25	60	13	25

L4RS represents regular spiking (RS) excitatory cells in layer 4

Figure 4.1: The number of neurons of each type within a cortical column. Figure from Neymotin et al. [241].

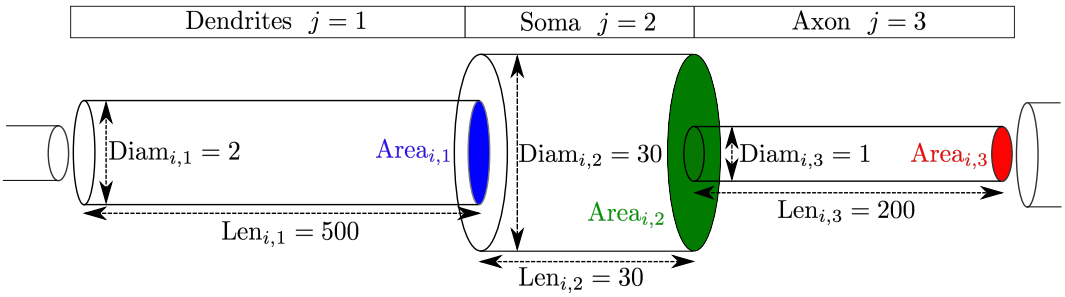

Figure 4.2: A visual representation of a simulated neuron and its cylindrical compartment parameters.

have an action potential, the voltage potential had to exceed a threshold, which was predefined as $\text{Vth}_i(t)$. This threshold was $-40mV$ for regular spiking, intrinsically bursting, and fast spiking neurons, and $-47mV$ for low-threshold spiking neurons. Figure 4.2 is a schematic representation of a simulated neuron. The reader can find more information about the network in the work of Neymotin et al. [241]

From ↓	To →													
	L2RS	L2IB	L2LTS	L2FS	L4RS	L4LTS	L4FS	L5RS	L5IB	L5LTS	L5FS	L6RS	L6LTS	L6FS
L2RS	0.187	0.187	0.51	0.43	0.024	-	-	0.057	0.024	-	-	-	-	-
L2IB	0.187	0.187	0.51	0.43	0.024	-	-	0.057	0.024	-	-	-	-	-
L2LTS	0.35	0.35	0.09	0.53	-	-	-	0.35	0.5	-	0.53	0.25	-	0.53
L2FS	0.44	0.44	0.34	0.62	-	-	-	-	-	-	-	-	-	-
L4RS	0.145	-	-	-	0.243	0.51	0.43	0.116	0.122	-	-	0.032	-	-
L4LTS	-	-	-	-	0.35	0.09	0.53	-	-	-	-	-	-	-
L4FS	-	-	-	-	0.44	0.34	0.62	-	-	-	-	-	-	-
L5RS	0.022	-	-	-	0.007	-	-	0.191	0.08	0.51	0.43	0.032	-	-
L5IB	0.018	-	-	-	0.007	-	-	0.017	0.07	0.51	0.43	0.07	-	-
L5LTS	0.35	-	-	0.53	-	-	-	0.35	0.35	0.09	0.53	0.25	-	0.53
L5FS	-	-	-	-	-	-	-	0.44	0.44	0.34	0.62	-	-	-
L6RS	-	-	-	-	-	-	-	0.006	0.028	-	-	0.028	0.51	0.43
L6LTS	0.35	-	-	0.53	-	-	-	0.25	0.25	-	0.53	0.35	0.09	0.53
L6FS	-	-	-	-	-	-	-	-	-	-	-	0.44	0.34	0.62

Figure 4.3: Connection probabilities for intracolumnar connections. Figure from Neymotin et al. [241].

From ↓	To →													
	L2RS	L2IB	L2LTS	L2FS	L4RS	L4LTS	L4FS	L5RS	L5IB	L5LTS	L5FS	L6RS	L6LTS	L6FS
L2RS	0.78	0.78	0.23	0.23	0.36	-	-	0.93	0.36	-	-	-	-	-
L2IB	0.78	0.78	0.23	0.23	0.36	-	-	0.93	0.36	-	-	-	-	-
L2LTS	0.83	0.83	1.5	1.5	-	-	-	0.83	0.83	-	0.83	0.83	-	0.83
L2FS	1.5	1.5	1.5	1.5	-	-	-	-	-	-	-	-	-	-
L4RS	0.58	-	-	-	0.95	0.23	0.23	0.54	1.01	-	-	2.27	-	-
L4LTS	-	-	-	-	0.83	1.5	1.5	-	-	-	-	-	-	-
L4FS	-	-	-	-	1.5	1.5	1.5	-	-	-	-	-	-	-
L5RS	0.67	-	-	-	0.48	-	-	0.66	0.88	0.23	0.23	0.28	-	-
L5IB	0.26	-	-	-	0.17	-	-	0.24	0.71	0.23	0.23	0.49	-	-
L5LTS	0.83	-	-	0.83	-	-	-	0.83	0.83	1.5	1.5	0.83	-	0.83
L5FS	-	-	-	-	-	-	-	1.5	1.5	1.5	1.5	-	-	-
L6RS	-	-	-	-	-	-	-	0.08	0.53	-	-	0.53	0.23	0.23
L6LTS	0.83	-	-	0.83	-	-	-	0.83	0.83	-	0.83	0.83	1.5	1.5
L6FS	-	-	-	-	-	-	-	-	-	-	-	1.5	1.5	1.5

Figure 4.4: Synaptic strengths for intracolumnar connections. Figure from Neymotin et al. [241].

From ↓	To →													
	L2RS	L2IB	L2LTS	L2FS	L4RS	L4LTS	L4FS	L5RS	L5IB	L5LTS	L5FS	L6RS	L6LTS	L6FS
L2RS	0.14	-	-	0.14	-	-	-	-	-	-	-	-	-	-
L2IB	-	-	-	-	-	-	-	-	-	-	-	-	-	-
L2LTS	-	-	-	-	-	-	-	-	-	-	-	-	-	-
L2FS	-	-	-	-	-	-	-	-	-	-	-	-	-	-
L4RS	-	-	-	-	-	-	0.14	-	-	-	-	-	-	-
L4LTS	-	-	-	-	-	-	-	-	-	-	-	-	-	-
L4FS	-	-	-	-	-	-	-	-	-	-	-	-	-	-
L5RS	-	-	-	-	-	-	-	0.14	0.25	-	0.14	-	-	-
L5IB	0.25	-	0.14	-	-	-	-	0.25	0.25	0.14	0.14	-	-	-
L5LTS	-	-	-	-	-	-	-	-	-	-	-	-	-	-
L5FS	-	-	-	-	-	-	-	-	-	-	-	-	-	-
L6RS	-	-	-	-	-	-	-	-	-	-	-	-	-	-
L6LTS	-	-	-	-	-	-	-	-	-	-	-	-	-	-
L6FS	-	-	-	-	-	-	-	-	-	-	-	-	-	0.14

Figure 4.5: Connection probabilities for intercolumnar connections to adjacent column. Figure from Neymotin et al. [241].

4.2 Neuronal scale modelling

There are many different proteins present in the brain under normal conditions, and some neurodegenerative diseases are caused by a combination of multiple pathogenic proteins (e.g., AD is caused by amyloid-beta and tau). However, modelling all of these proteins and their interactions is beyond the scope of this thesis, but should be considered for future work as they could be very important, especially in diseases with multiple proteins interacting with each other, such as amyloid-beta and tau in AD. Instead, I simply modelled an abstract non-pathogenic (normal/healthy) protein and an abstract pathogenic (misfolded) protein.

From ↓	To →													
	L2RS	L2IB	L2LTS	L2FS	L4RS	L4LTS	L4FS	L5RS	L5IB	L5LTS	L5FS	L6RS	L6LTS	L6FS
L2RS	0.47	-	-	1.5	-	-	-	-	-	-	-	-	-	-
L2IB	-	-	-	-	-	-	-	-	-	-	-	-	-	-
L2LTS	-	-	-	-	-	-	-	-	-	-	-	-	-	-
L2FS	-	-	-	-	-	-	-	-	-	-	-	-	-	-
L4RS	-	-	-	-	-	-	1.5	-	-	-	-	-	-	-
L4LTS	-	-	-	-	-	-	-	-	-	-	-	-	-	-
L4FS	-	-	-	-	-	-	-	-	-	-	-	-	-	-
L5RS	-	-	-	-	-	-	-	0.47	0.47	-	1.5	-	-	-
L5IB	0.47	-	1.5	-	-	-	-	0.47	0.47	1.5	1.5	-	-	-
L5LTS	-	-	-	-	-	-	-	-	-	-	-	-	-	-
L5FS	-	-	-	-	-	-	-	-	-	-	-	-	-	-
L6RS	-	-	-	-	-	-	-	-	-	-	-	-	-	1.5
L6LTS	-	-	-	-	-	-	-	-	-	-	-	-	-	-
L6FS	-	-	-	-	-	-	-	-	-	-	-	-	-	-

Figure 4.6: Synaptic strengths for intercolumnar connections to adjacent column. Figure from Neymotin et al. [241].

A concentration of non-pathogenic protein $\mathrm{Cn}_{i,j}(t)$ and pathogenic protein $\mathrm{Cp}_{i,j}(t)$ existed within each compartment at each timestep t. These concentrations could easily be converted to quantities $\mathrm{Qn}_{i,j}(t) = \mathrm{Cn}_{i,j}(t) \times \mathrm{Vol}_{i,j}$ and $\mathrm{Qp}_{i,j}(t) = \mathrm{Cp}_{i,j}(t) \times \mathrm{Vol}_{i,j}$. Naturally, there is a limited number of protein molecules that can physically exist within a compartment. As I had no information on the dimensions of these pathogenic proteins, I set an arbitrary limit to them so that their sum could not exceed one, i.e., $\mathrm{Cn}_{i,j}(t) + \mathrm{Cp}_{i,j}(t) \leq 1$. Thus theoretically a concentration of 1 would mean that the respective compartment is physically full of protein molecules.

I modelled mechanisms of protein accumulation, spread, and toxic effects. More specifically, production, clearance, and misfolding accounted for protein accumulation. Neuronal network diffusion, active transport, and synaptic transfer accounted for protein spread. Toxic effects included a change on the voltage thresholds required for an action potential at neurons, neuronal toxicity, and neuronal death.

I chose to model mechanisms that are widely considered as crucial to the neurodegenerative process, such as production, clearance, misfolding, toxic effects and neuronal death. Additionally, I modelled a small number, but of varied types of spread mechanisms which are commonly hypothesised to potentially be of relevance: one for slow, passive diffusion, one for fast spread intracellularly and one for electrical-activity based spread. The model equations were based on neuro-

biological literature where possible, but due to the limitations of neurobiological knowledge, many simple and rational assumptions had to be made.

4.2.1 Production

Protein production modelled the biological processes of transcription and translation (see Section 2.3.1). I defined non-pathogenic $\text{CnProd}_{i,j}(t)$, and pathogenic $\text{CpProd}_{i,j}(t)$ protein production (Eq. 4.2). I assumed that protein was produced based on predefined rates of protein concentration per unit of time ($R_{\text{nProd}}, R_{\text{pProd}}$), which remained constant during simulations until neuronal death. While realistically this rate will vary a bit over time (which could be modelled as an extra random noise element), it is reasonable to assume that under healthy normal conditions and the long time scale that I am modelling, the rate is constant and instead it is the clearance rates that "needs" to adapt in order to have equilibrium in a neuron.

$$\begin{aligned} \text{CnProd}_{i,j}(t) &= \begin{cases} R_{\text{nProd}}, \text{ if } j = 2 \\ 0, \text{ otherwise} \end{cases} \\ \text{CpProd}_{i,j}(t) &= \begin{cases} R_{\text{pProd}}, \text{ if } j = 2 \\ 0, \text{ otherwise} \end{cases} \end{aligned} \tag{4.2}$$

4.2.2 Clearance

I modelled protein clearance (see Section 2.3.2) such that in a healthy individual it would compensate for protein production in order to achieve proteostasis (see Section 2.3.4). When protein levels were below or above 'healthy concentration levels' $\text{CnHealth}, \text{CpHealth}$, production rates remained constant, thus clearance rates had to adaptively decrease or increase, respectively. Given clearance rates $R_{\text{nClear}}, R_{\text{pClear}}$ (typically $R_{\text{nClear}} = R_{\text{nProd}}, R_{\text{pClear}} = R_{\text{pProd}}$), I defined $\text{CnClear}_{i,j}(t), \text{CpClear}_{i,j}(t)$ as clearance terms (Eq. 4.3). Although my choice of a logarithmic function was arbitrary, it had the property of adapting to the current timestep's concentration levels and it was sub-linear, which I believed to be a biologically plausible assumption. While self-degradation is a clearance mechanism that scales linearly with the con-

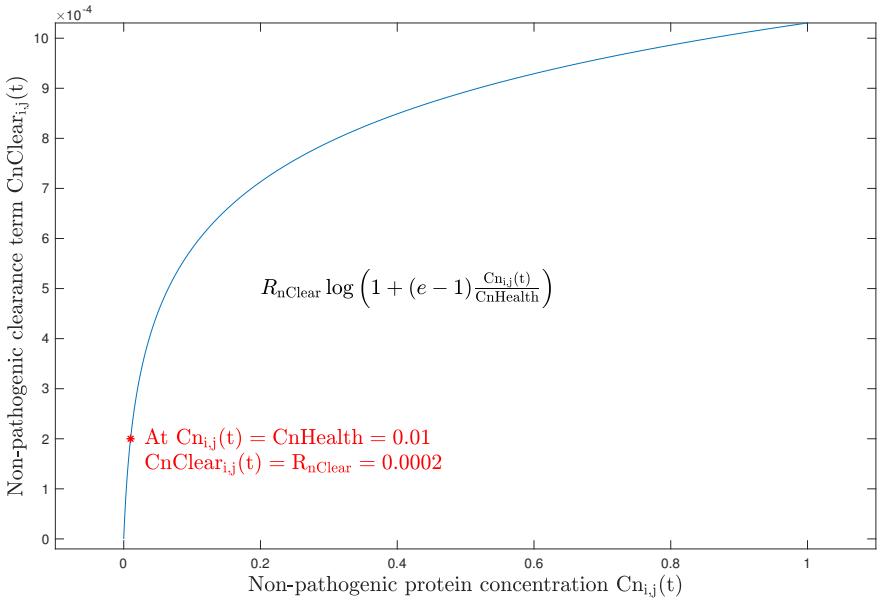

Figure 4.7: An example of the clearance mechanism for non-pathogenic protein. Parameters were set $R_{\text{nClear}} = 0.0002$ and $\text{CnHealth} = 0.01$.

centration, other clearance systems have limited molecules which "roam around" in the cell finding proteins to clear, thus while they will find more proteins when concentration is increased, since these clearance molecules are occupied with clearing that specific molecule for a certain period of time, it is reasonable to assume a sublinear relationship. Figure 4.7 plots an example of this function.

$$\begin{aligned} \text{CnClear}_{i,j}(t) &= -R_{\text{nClear}} \log\left(1 + (e-1)\frac{\text{Cn}_{i,j}(t)}{\text{CnHealth}}\right) \\ \text{CpClear}_{i,j}(t) &= -R_{\text{pClear}} \log\left(1 + (e-1)\frac{\text{Cp}_{i,j}(t)}{\text{CpHealth}}\right) \end{aligned} \tag{4.3}$$

4.2.3 Misfolding

In order to derive a model for misfolding (see Section 2.3.3), I simulated a cube volume within which I added non-pathogenic and pathogenic protein molecules (simulated as points), and randomly initialised their positions, and movement directions (based on uniform distributions), and let them diffuse in 3D space for a predefined number of timesteps. Whenever a non-pathogenic and pathogenic pro-

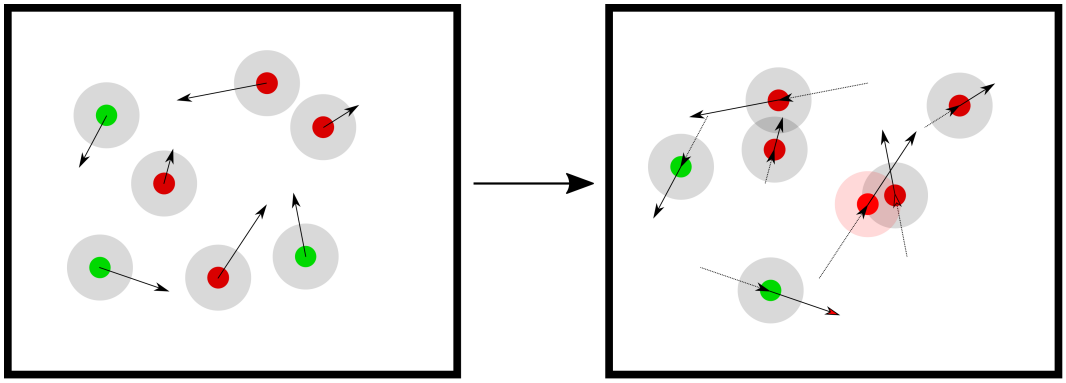

Figure 4.8: A representation of the misfolding simulations portraying two timesteps in a 2D environment. The green circles represent non-pathogenic protein molecules, whereas the red circles represent pathogenic protein molecules. The grey wider circles represent the range over which pathogenic protein molecules were able to template their fold onto non-pathogenic protein molecules. Their directions and velocities are represented by arrows. On the right part of this figure, a non-pathogenic protein was misfolded, because it was in close proximity to a pathogenic protein.

tein molecule came in close proximity of each other during the simulation, then the non-pathogenic protein molecule would misfold and become pathogenic. At the end of the simulation, I calculated the number of molecules that had transformed to a pathogenic state. I repeated this simulation for many variations of the initial number of non-pathogenic and pathogenic molecules. Figure 4.8 shows an example of two steps of such a simulation. Figure 4.9 shows the simulation results and my proposed model, which were in close agreement. Although the assumption that non-pathogenic and pathogenic protein in close proximity always would cause misfolding is unlikely to be true and there is an additional random element to this process, this would not affect the resulting relationship of multiplying the two concentrations. Given a misfolding rate R_{Mis}, I define $\text{CnMis}_{i,j}(t), \text{CpMis}_{i,j}(t)$ as the misfolding terms (Eq. 4.4).

$$\begin{aligned} \text{CnMis}_{i,j}(t) &= -R_{\text{Mis}}\text{Cn}_{i,j}(t)\text{Cp}_{i,j}(t) \\ \text{CpMis}_{i,j}(t) &= R_{\text{Mis}}\text{Cn}_{i,j}(t)\text{Cp}_{i,j}(t) \end{aligned} \tag{4.4}$$

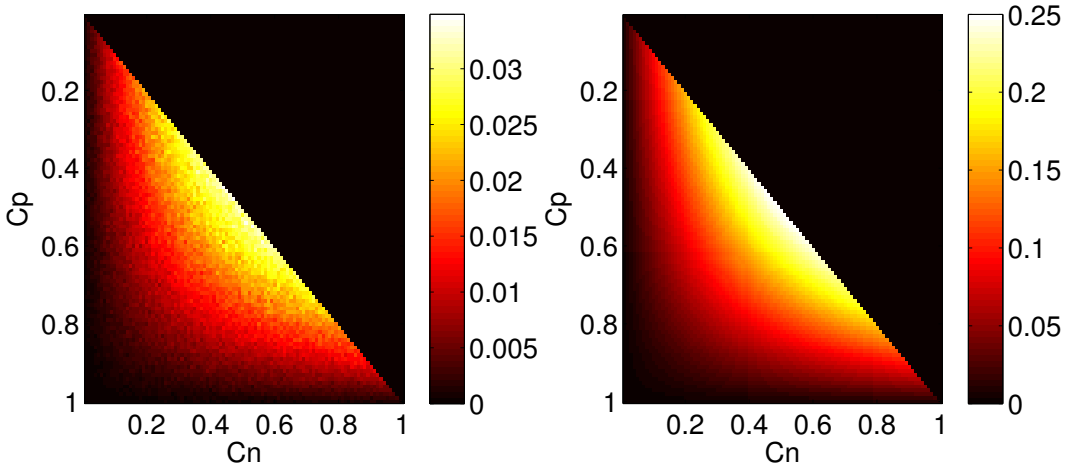

Figure 4.9: Simulation results and proposed model for misfolding. Left: concentration of non-pathogenic protein converted to pathogenic based on simulations. Right: output of the proposed model for the concentration of non-pathogenic protein converted. Suggested model: $R_{\text{Mis}} * \text{Cn} * \text{Cp}$, where $R_{\text{Mis}} = 1$; adjusting R_{Mis} can negate the scaling difference.

4.2.4 Protein spread

There are many hypotheses regarding the spread of pathogenic proteins (see Section 2.3.5). I modelled intracellular and intercellular neuronal network diffusion based on Brownian motion, intracellular active transport, and intercellular synaptic transfer. No extracellular spread was modelled, as the cortical column network did not have 3D coordinates information for neuronal compartments (although it is possible to have 3D coordinates in NEURON, this specific network was only considered as a graph, which is a limitation). I modelled that both normal and pathogenic protein can spread via the same mechanisms in the same manner. I defined f_{NND}, f_{ACT}, and f_{SYN} as the probability of protein spreading with each respective mechanism. These variables took non-negative values, while their sum had to be lower or equal to one. I also defined $\mathbf{SEL}_{i,j \leftarrow \bar{i},\bar{j}}$ as the intrinsic tendency of protein to spread selectively via intercolumnar synaptic connections.

4.2.5 Neuronal network diffusion

I modelled neuronal network diffusion as Brownian motion, which was restricted to the cylindrical shape of compartments for intracellular spread, and to the synaptic connections and their synaptic strengths for intercellular spread. The cumulative

distribution function of the normal distribution $\Phi(x|\mu,\sigma)$ modelled Brownian motion and for $x = -\text{Len}_{\bar{i},\bar{j}}/2, \mu = 0$, and a neuronal network diffusion speed σ_{NND}, it calculated the probability of protein diffusing past the boundary of compartment $\bar{i},\bar{j}$, thus entering neighbouring compartments. I defined $\mathbf{Ent}_{i,j\leftarrow\bar{i},\bar{j}}$ as the proportion of protein managing to pass through the entrance from $\bar{i},\bar{j}$ to i,j (Eq. 4.6). Neuronal network diffusion weights $\mathbf{WNND}_{i,j\leftarrow\bar{i},\bar{j}}$ modelled the intrinsic propensity of protein diffusing intracellularly (note the value of 20 was chosen fairly arbitrarily, but I chose a much higher value than the values given by $\mathbf{SS}_{i,j\leftarrow\bar{i},\bar{j}}$ as I assumed that protein would passively diffuse much more freely within neurons than being transported to a postsynaptic neuron), and the synaptic strengths when diffusing intercellularly, as well as their intrinsic tendency to spread via intercolumnar synaptic connections (Eq. 4.5). I defined $\mathbf{NND}_{i,j\leftarrow\bar{i},\bar{j}}(t)$ (Eq. 4.7) as the probability of protein spreading from compartment $\bar{i},\bar{j}$ to a neighbouring compartment i,j via neuronal network diffusion.

$$\mathbf{WNND}_{i,j\leftarrow\bar{i},\bar{j}} = \begin{cases} 20, \text{ if } i=\bar{i}, \text{ and } \bar{i},\bar{j} \text{ neighbour of } i,j \\ \mathbf{SS}_{i,j\leftarrow\bar{i},\bar{j}}\mathbf{SEL}_{i,j\leftarrow\bar{i},\bar{j}}, \text{ if } i\neq\bar{i}, \text{ and } \bar{i},\bar{j} \text{ neighbour of } i,j \\ 0, \text{ if } \bar{i},\bar{j} \text{ not a neighbour of } i,j \end{cases} \quad (4.5)$$

$$\mathbf{Ent}_{i,j\leftarrow\bar{i},\bar{j}} = \frac{\min(\text{Area}_{i,j},\text{Area}_{\bar{i},\bar{j}})}{\text{Area}_{\bar{i},\bar{j}}} \quad (4.6)$$

$$\mathbf{NND}_{i,j\leftarrow\bar{i},\bar{j}}(t) = \mathbf{WNND}_{i,j\leftarrow\bar{i},\bar{j}}\mathbf{Ent}_{i,j\leftarrow\bar{i},\bar{j}}\Phi\left(-\text{Len}_{\bar{i},\bar{j}}/2|0,\sigma_{\text{NND}}\right) \quad (4.7)$$

Figure 4.10 illustrates the neuronal network diffusion from an axon to a soma.

This model could diffuse protein to neighbouring compartments only over a single timestep, and not to every geodesically nearby compartment, which is the more biologically plausible case. I defined $\mathbf{NNDF}_{i,j\leftarrow\bar{i},\bar{j}}(t)$ as the probability of protein diffusing from compartment $\bar{i},\bar{j}$ to compartment i,j using the following approach: choose a source compartment $\bar{i},\bar{j}$ and calculate what fraction of protein will diffuse to its neighbour compartments based on $\mathbf{NND}_{i,j\leftarrow\bar{i},\bar{j}}(t)$. Then, iterate the following: if the fraction of protein that a neighbour compartment receives is above

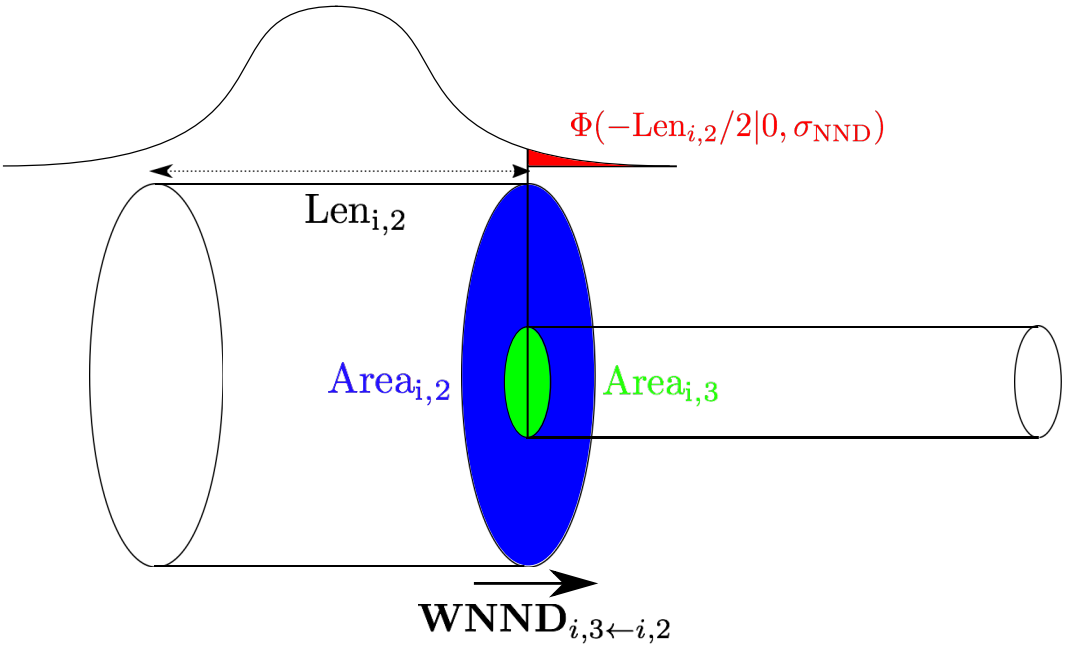

Figure 4.10: An illustration of neuronal network diffusion from a soma to a neighbouring axon: $\mathbf{NND}_{i,3\leftarrow i,2}(t) = \mathbf{WNND}_{i,3\leftarrow i,2}\frac{\text{Area}_{i,3}}{\text{Area}_{i,2}}\Phi\left(-\text{Len}_{i,2}/2|0,\sigma_{\text{NND}}\right)$

a threshold NND_{thr}, repeat the process for every such compartment as a source, spreading the fraction of protein those compartments receive, until convergence to an equilibrium. Algorithm 1 shows the pseudocode for this process.

4.2.6 Active transport

I modelled active transport $\mathbf{ACT}_{i,j\leftarrow\bar{i},\bar{j}}(t)$ (Eq. 4.8) based on data for the axonal transport of tau protein [47, 181]. I concluded that tau showed anterograde movement 15.4% of the time, no movement 73% of the time, and retrograde movement 11.6% of the time. Due to lack of evidence for transport rates in dendrites and somas, I adjusted these percentages for all neuronal compartments, favouring anterograde movement overall.

Algorithm 1 Input: Network, $\mathrm{NND}_{\mathrm{thr}}$, $\mathbf{NND}_{i,j\leftarrow\bar{i},\bar{j}}$. Output: $\mathbf{NNDF}_{i,j\leftarrow\bar{i},\bar{j}}$

for *each compartment as source* **do**
  Initialise $\mathbf{NNDF}_{source,source} = 1$
  Create empty queue $Queue_{Sources}$ *(sources queue)*
  Create empty queue $Queue_{Fractions}$ *(fractions queue)*
  Append source to $Queue_{Sources}$
  Append 1 to $Queue_{Fractions}$
  while $Queue_{Sources}$ *is not empty* **do**
    $Current_{Source} \leftarrow Queue_{Source}(1)$
    $Current_{Fraction} \leftarrow Queue_{Fraction}(1)$
    Remove first element from $Queue_{Sources}$
    Remove first element from $Queue_{Fractions}$
    $\mathbf{NNDF}_{Current_{Source},source} \leftarrow \mathbf{NNDF}_{Current_{Source},source} - Current_{Fraction}$
    for *i from 1 to 3NNeu* **do**
      $To_{Add}(i) = 0$
    $To_{Add}(Current_{Source}) \leftarrow \mathbf{NND}_{Current_{Source},Current_{Source}}$
    for *each neighbour compartment of* $Current_{Source}$ *as destination* **do**
      $To_{Add}(destination) \leftarrow \mathbf{NND}_{Current_{Source},destination}$
    $Temp \leftarrow \sum_{i=1}^{3\mathrm{NNeu}} To_{Add}(i)$
    for *i from 1 to 3NNeu* **do**
      $To_{Add}(i) = Current_{Fraction} \frac{To_{Add}(i)}{Temp}$
    $\mathbf{NNDF}_{Current_{Source},source} \leftarrow \mathbf{NNDF}_{Current_{Source},source} + To_{Add}(Current_{Source})$
    for *each neighbouring compartment as destination* **do**
      $\mathbf{NNDF}_{destination,source} \leftarrow \mathbf{NNDF}_{destination,source} + To_{Add}(destination)$
      if $To_{Add}(destination) \geq \mathrm{NND}_{\mathrm{thr}}$ **then**
        Append destination to $Queue_{Sources}$
        Append $To_{Add}(destination)$ *to* $Queue_{Fractions}$

$$\mathbf{ACT}_{i,j\leftarrow\bar{i},\bar{j}}(t) = \begin{cases} 0.8258, \text{ if } i=\bar{i}, \text{ and } \bar{j}=1, j=1 \\ 0.1742, \text{ if } i=\bar{i}, \text{ and } \bar{j}=1, j=2 \\ 0.1160, \text{ if } i=\bar{i}, \text{ and } \bar{j}=2, j=1 \\ 0.73, \text{ if } i=\bar{i}, \text{ and } \bar{j}=2, j=2 \\ 0.1540, \text{ if } i=\bar{i}, \text{ and } \bar{j}=2, j=3 \\ 0.1371, \text{ if } i=\bar{i}, \text{ and } \bar{j}=3, j=2 \\ 0.8629, \text{ if } i=\bar{i}, \text{ and } \bar{j}=3, j=3 \\ 0, \text{otherwise} \end{cases} \tag{4.8}$$

4.2.7 Synaptic transfer

Synaptic transfer modelled the hypothesis that every action potential transferred a large quantity of protein to postsynaptic neurons (see Section 2.3.5). I defined $\mathbf{SYN}_{i,j\leftarrow\bar{i},\bar{j}}(t)$ (Eq. 4.9) as the probability of protein spreading via synaptic transfer to neuronal compartment i,j whenever an action potential occurred at neuron $\bar{i}$.

$$\mathbf{SYN}_{i,j\leftarrow\bar{i},\bar{j}}(t) = \begin{cases} 1, \text{ if } i=\bar{i}, j=\bar{j}, \bar{i} \text{ no action potential} \\ 1, \text{ if } i=\bar{i}, j=\bar{j}, \bar{i} \text{ action potential}, \bar{j}\neq 3 \\ \frac{\mathbf{SS}_{i,j\leftarrow\bar{i},\bar{j}}\mathbf{SEL}_{i,j\leftarrow\bar{i},\bar{j}}}{\sum_k\sum_u \mathbf{SS}_{k,u\leftarrow\bar{i},\bar{j}}\mathbf{SEL}_{k,u\leftarrow\bar{i},\bar{j}}}, \text{if } i\neq\bar{i}, \bar{i} \text{ action potential}, \bar{j}=3 \\ 0, \text{ otherwise} \end{cases} \tag{4.9}$$

4.2.8 Neuronal toxicity, toxic effects, and neuronal death

I assumed that protein accumulation gradually increased the overall toxicity level $\text{Txc}_i(t)$ (Eq. 4.10) within each neuron, where toxicity represented the cumulative negative effects on the neuron. Toxicity was initialised with a value of zero in simulations. It then increased based on an exponential function of the mean protein concentration within each respective neuron, as well as on the toxicity rate R_{Txc}. Once it reached a value of one, the corresponding neuron would die at timestep tdeath_i (Eq. 4.11). For dead neurons, only the mechanisms of misfolding, and outward neuronal scale diffusion would continue functioning. Figure 4.11 displays the exponential function that was used to update toxicity levels.

There are many hypotheses regarding the toxic effects of pathogenic proteins on neurons (see Section 2.3.6). I modelled that the toxicity level within a neuron had a direct, linear effect on the voltage threshold $\text{Vth}_i(t)$ [241] that had to be reached in order for an action potential to occur (Eq. 4.12), which I varied whether it was a toxic loss of function, or a toxic gain of function: as toxicity increased, the threshold also increased, thereby reducing the respective neuron's firing frequency (a toxic loss of function), or, as toxicity increased, the threshold decreased, thereby increasing the respective neuron's firing frequency (a toxic gain of function).

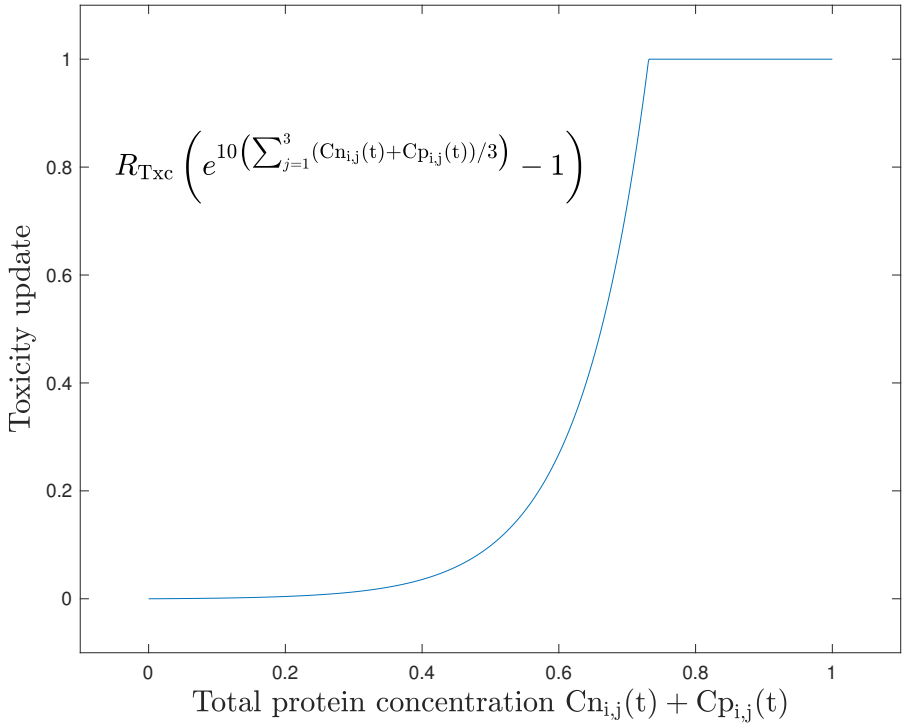

Figure 4.11: The exponential function that updated toxicity with $R_{\mathrm{Txc}} = 1/1500$.

$$\mathrm{Txc}_i(t) = \begin{cases} 0, \text{ if t=0} \\ \mathrm{Txc}_i(t-1) + R_{\mathrm{Txc}}\left[\exp\left(10\sum_{j=1}^{3}\frac{\mathrm{Cn}_{i,j}(t)+\mathrm{Cp}_{i,j}(t)}{3}\right)-1\right], \ldots \\ \ldots \text{ if } t>0, \mathrm{Txc}_i(t-1)<1 \\ 1, \text{ if } t>0, \mathrm{Txc}_i(t-1)\geq 1 \end{cases} \tag{4.10}$$

$$\mathrm{tdeath}_i = \arg\min_t \mathrm{Txc}_i(t) = 1 \tag{4.11}$$

$$\mathrm{Vth}_i(t) = \begin{cases} -40 \pm 10\mathrm{Txc}_i(t), \text{ if } t<\mathrm{tdeath}_i, \ \forall i \in \{\mathrm{RS,IB,FS}\} \\ -47 \pm 10\mathrm{Txc}_i(t), \text{ if } t<\mathrm{tdeath}_i, \ \forall i \in \{\mathrm{LTS}\} \\ +100, \text{ if } t \geq \mathrm{tdeath}_i, \ \forall i \end{cases} \tag{4.12}$$

4.2.9 Protein quantity update

Updating protein quantities for the next timestep required the summation of the changes from the different modelled mechanisms. I defined $\mathrm{QnAcc}_{i,j}(t)$, and

$\mathrm{QpAcc}_{i,j}(t)$ as the net change in protein quantity from accumulation (Eq. 4.13). I defined $\mathrm{QnNSS}_{i,j}(t)$, and $\mathrm{QpNSS}_{i,j}(t)$ as the net change in protein quantity from spread mechanisms (Eq. 4.14). Combining the contributions to protein quantity change from accumulation and spread mechanisms, I updated protein quantities at each timestep using the following equation (Eq. 4.15).

$$
\begin{aligned}
\mathrm{QnAcc}_{i,j}(t) = \quad & \left[\mathrm{CnProd}_{i,j}(t) + \mathrm{CnClear}_{i,j}(t) + \mathrm{CnMis}_{i,j}(t)\right] \mathrm{Vol}_{i,j} \\
\mathrm{QpAcc}_{i,j}(t) = \quad & \left[\mathrm{CpProd}_{i,j}(t) + \mathrm{CpClear}_{i,j}(t) + \mathrm{CpMis}_{i,j}(t)\right] \mathrm{Vol}_{i,j} \qquad (4.13) \\
\mathrm{QnNSS}_{i,j}(t) = \quad & \sum_{\bar{i}=1}^{\mathrm{NNeu}} \sum_{\bar{j}=1}^{3} f_{\mathrm{NND}} \mathbf{NNDF}_{i,j\leftarrow\bar{i},\bar{j}}(t) \mathrm{Qn}_{\bar{i},\bar{j}}(t) + \\
& f_{\mathrm{ACT}} \mathbf{ACT}_{i,j\leftarrow\bar{i},\bar{j}}(t) \mathrm{Qn}_{\bar{i},\bar{j}}(t) + \\
& f_{\mathrm{SYN}} \mathbf{SYN}_{i,j\leftarrow\bar{i},\bar{j}}(t) \mathrm{Qn}_{\bar{i},\bar{j}}(t) - \\
& (f_{\mathrm{NND}} + f_{\mathrm{ACT}} + f_{\mathrm{SYN}}) \mathrm{Qn}_{i,j}(t) \\
\mathrm{QpNSS}_{i,j}(t) = \quad & \sum_{\bar{i}=1}^{\mathrm{NNeu}} \sum_{\bar{j}=1}^{3} f_{\mathrm{NND}} \mathbf{NNDF}_{i,j\leftarrow\bar{i},\bar{j}}(t) \mathrm{Qp}_{\bar{i},\bar{j}}(t) + \\
& f_{\mathrm{ACT}} \mathbf{ACT}_{i,j\leftarrow\bar{i},\bar{j}}(t) \mathrm{Qp}_{\bar{i},\bar{j}}(t) + \\
& f_{\mathrm{SYN}} \mathbf{SYN}_{i,j\leftarrow\bar{i},\bar{j}}(t) \mathrm{Qp}_{\bar{i},\bar{j}}(t) - \\
& (f_{\mathrm{NND}} + f_{\mathrm{ACT}} + f_{\mathrm{SYN}}) \mathrm{Qp}_{i,j}(t) \qquad (4.14) \\
\mathrm{Qn}_{i,j}(t+1) = \quad & \mathrm{Qn}_{i,j}(t) + \mathrm{QnAcc}_{i,j}(t) + \mathrm{QnNSS}_{i,j}(t) \\
\mathrm{Qp}_{i,j}(t+1) = \quad & \mathrm{Qp}_{i,j}(t) + \mathrm{QpAcc}_{i,j}(t) + \mathrm{QpNSS}_{i,j}(t) \qquad (4.15)
\end{aligned}
$$

4.3 Simulation setup

In order to explore the effect of changing network and mechanism parameters on protein and network behaviour, I ran simulations, systematically varying parameter values. In all simulations, the timestep interval was $dt = 0.025$msec, toxicity rate was $R_{\mathrm{Txc}} = 1/1500$, probability of neuronal network diffusion was $f_{\mathrm{NND}} = 0.05$, production and clearance rates were $R_{\mathrm{nProd}} = R_{\mathrm{nClear}} = 0.0002$, and $R_{\mathrm{pProd}} = R_{\mathrm{pClear}} = 0.00002$, and the healthy concentration levels were $\mathrm{CnHealth} = \mathrm{CpHealth} = 0.01$. I varied eight parameters: (1) two random instances of neural net-

work connectivities based on the connection densities in Figure 4.3 and Figure 4.5, (2) soluble, or insoluble pathogenic protein (in the latter case there was no clearance and negligible production of pathogenic protein, only initial seeding and misfolding), (3) 17 types of protein seeds - with the first three types ('Seed All 1', 'Seed All 2', and 'Seed All 3'), all neurons started with $\mathrm{Cn}_{i,j}(0) = \mathrm{Cp}_{i,j}(0) = 0.01$ in simulations with soluble pathogenic protein, and $\mathrm{Cn}_{i,j}(0) = 0.01, \mathrm{Cp}_{i,j}(0) = 0.0001$ in simulations with insoluble pathogenic protein, with the difference between the three being a change in the seed of the random number generator of NEURON; for the remaining types of seeds, I added extra pathogenic protein at the start of the simulation to a single neuron of the first cortical column, varying the cortical layer and neuronal type of the seeded neuron (e.g., 'Seed L2RS', 'Seed L2IB', etc.), (4) low misfolding rate $R_{\mathrm{Mis}} = 0.08$, or high misfolding rate $R_{\mathrm{Mis}} = 0.09$, (5) no diffusion, low diffusion speed $\sigma_{\mathrm{NND}} = 50$, or high diffusion speed $\sigma_{\mathrm{NND}} = 500$, (6) no active transport $f_{\mathrm{ACT}} = 0$, weak active transport $f_{\mathrm{ACT}} = 0.0001$, or strong active transport $f_{\mathrm{ACT}} = 0.001$, (7) three settings for synaptic transfer and the toxic effect of the pathogenic protein - no synaptic transfer $f_{\mathrm{SYN}} = 0$ with an increase of voltage thresholds $\mathrm{Vth}_i(t)$, low synaptic transfer $f_{\mathrm{SYN}} = 0.154$ with an increase of voltage thresholds, or high synaptic transfer $f_{\mathrm{SYN}} = 0.154$ with a decrease of voltage thresholds, (8) selectivity to avoid intercolumnar connections $\mathbf{SEL}_{i,j\leftarrow\bar{i},\bar{j}} = 0.01$, no spread selectivity $\mathbf{SEL}_{i,j\leftarrow\bar{i},\bar{j}} = 1$, or selectivity to spread via intercolumnar connections $\mathbf{SEL}_{i,j\leftarrow\bar{i},\bar{j}} = 100$ (for $i,\bar{i}$ that belonged to different cortical columns). All of these variations required 11016 different simulation runs.

4.4 Results

In order to assess the vulnerability of specific neurons I calculated for each neuron its Geodesic Distance to the Seed (GDS), GDS_i and its 'Synaptic Strength Gradient' (SSG), SSG_i, (Eq. 4.16), which was the difference between the sum of its presynaptic connection strengths and the sum of its postsynaptic connection strengths. Neurons with a high SSG had many and/or strong presynaptic connections, but few and/or weak postsynaptic connections (here termed 'bottleneck' neurons). Neurons

have widely varying input:output relations [245]. I hypothesised that neurons with a high SSG or a low GDS value would accumulate protein faster, and thus reach neuronal death earlier. In Figure 4.12, every neuron is plotted as a point using their respective SSG and GDS values against the simulation time that they reached neuronal death (tdeath_i multiplied with dt); I performed linear regression to capture the relation between these two neuronal characteristics and time to neuronal death. I will refer to SSG R^2 as the 'bottleneck' neuron survival characteristic and to GDS R^2 as the distance to seed survival characteristic.

$$\text{SSG}_i = \sum_{\forall \bar{i} \setminus i} \sum_{\bar{j}=1}^{3} \sum_{j=1}^{3} \mathbf{SS}_{i,j \leftarrow \bar{i},\bar{j}} - \sum_{\forall \hat{i} \setminus i} \sum_{\hat{j}=1}^{3} \sum_{j=1}^{3} \mathbf{SS}_{\hat{i},\hat{j} \leftarrow i,j} \tag{4.16}$$

I quantified the asymmetry of network toxicity over time by calculating the corrected sample standard deviation of the toxicity of every neuron at each timestep $\sigma_{\text{Txc}}(t)$ (Eq. 4.18). In order to summarise this information over time to get the overall asymmetry of protein accumulation for each simulation, I defined ASY as the maximum value of $\sigma_{\text{Txc}}(t)$ over time (Eq. 4.19). This maximum value typically occurred during the first few neuronal deaths. I also compared the time it took for all neurons to reach neuronal death (time to network breakdown - TTNB) in each simulation. In Table 4.1, I indicate the magnitude of the effect that each parameter had on SSG R^2, GDS R^2, ASY, and TTNB.

$$\mu_{\text{Txc}}(t) = \frac{\sum_i \text{Txc}_i(t)}{\text{NNeu}} \tag{4.17}$$

$$\sigma_{\text{Txc}}(t) = \sqrt{\frac{\sum_i (\text{Txc}_i(t) - \mu_{\text{Txc}}(t))^2}{\text{NNeu} - 1}} \tag{4.18}$$

$$\text{ASY} = \max_t \sigma_{\text{Txc}}(t) \tag{4.19}$$

In order to assess each parameter's impact on protein spread patterns, I quantified the similarity and time to convergence between the orders of neuronal deaths for all pairs of simulations. I defined the set $G_s(n), n \in \{1, ..., \text{NNeu}\}$, indicating

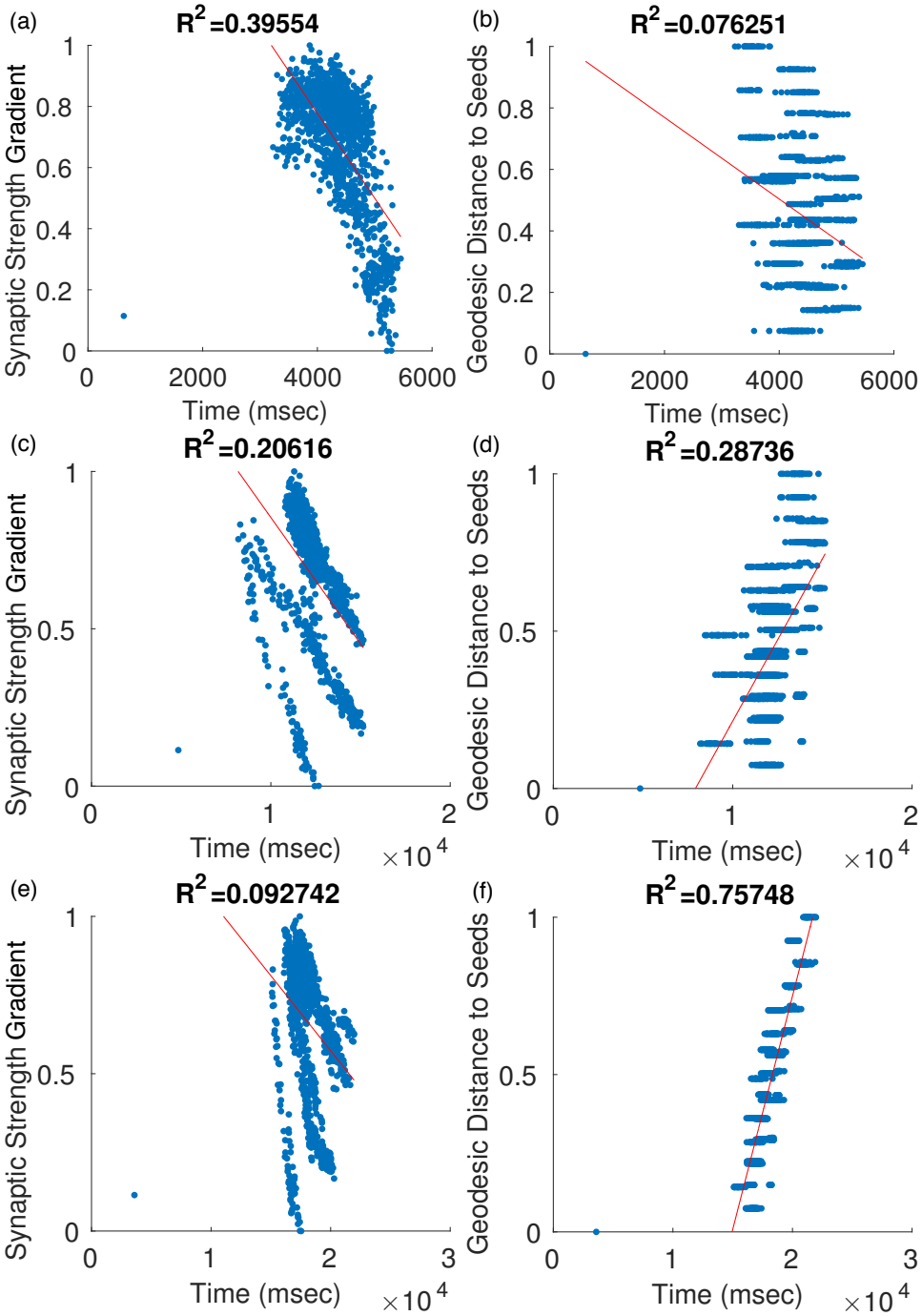

Figure 4.12: Synaptic strength gradient and geodesic distance to seed as metrics of neuronal vulnerability for certain simulations. Each point indicates a neuron i plotted against the simulation time of its neuronal death $\text{tdeath}_i \times dt$, and its respective SSG_i (left) or GDS_i (right) value for simulations primarily driven by passive diffusion of pathogenic protein (seed L2FS, low misfolding rate, strong active transport, no synaptic transfer, and no spread selectivity). (a) SSG and (b) GDS with soluble pathogenic protein and low diffusion speed. (c) SSG and (d) GDS with soluble pathogenic protein and high diffusion speed. (e) SSG and (f) GDS with insoluble pathogenic protein and high diffusion speed. Note that the single outlier points correspond to the seed neurons.

Table 4.1: Impact of simulation parameters on 'bottleneck' neuron survival characteristic (SSG R^2), distance to seed survival characteristic (GDS R^2), asymmetry of network toxicity (ASY) and time to network breakdown (TTNB). Number of +/- signs indicate strength of impact on the metric compared to a baseline observation, with 0 indicating no impact (e.g., increasing the misfolding rate has the effect of a small increase on the value of ASY). Note that +/- signs were used instead of values as simulations with different initial conditions are not directly comparable, thus a mean and standard deviation would not be too meaningful - this table was primarily meant to capture consistent behaviour and the number of +/- signs can be seen as orders of magnitude of the effect. [1] positive sign indicates the value of the metric for insoluble protein was higher than the value for soluble protein. [2] not applicable since initial protein seed concentrations were different (for similar starting concentrations, network breakdown would occur orders of magnitude later with soluble pathogenic protein). [3] The first three seeds had higher values. [4] Layer 4 and 5 seeds had lower values, whereas layer 6 had the highest values. [5] *,* indicates the relationships: [tendency of pathogenic protein to avoid intercolumnar connections vs no spread selectivity], [tendency of pathogenic protein to spread via intercolumnar connections vs no spread selectivity].

Parameter	SSG R^2	GDS R^2	ASY	TTNB
1) Network connectivity	0	0	0	0
2) (In)soluble protein[1]	- -	++	++	N/A[2]
3) Seed location	[3]	[4]	0	0
4) Misfolding rate	0	0	+	-
5) Diffusion speed	+++	+++	++	0
6) Active transport strength	++	+	++	- -
7) Synaptic transfer strength	++	+	++	+
8) Spread selectivity[5]	+++, +	- -, - -	+, +++	0, 0

the set of the first n neurons to reach neuronal death in a simulation s. I calculated the Dice coefficient (a measure of similarity between two sets) $\text{Dice}_{s,\bar{s}}(n)$ (Eq. 4.20) between sets $G_s(n)$ and $G_{\bar{s}}(n)$ for $n \in \{1,...,\text{NNeu}\}$. The higher the Dice coefficient value was for two sets, the larger the number of common dead neurons was. I defined time to convergence as the time $\text{tConv}_{s,\bar{s}}$ (Eq. 4.21), that the Dice coefficient reached and continued to exceed a threshold value $\text{ConvThr} = 0.8$. After convergence, since the Dice coefficient remains high, the simulations show similar spread patterns. Simulations with a low $\text{tConv}_{s,\bar{s}}$ (i.e., early convergence) had similar spread patterns during the entire simulation.

Figure 4.13 summarises the time to convergence for all pairs of simulations. I created the sets $H_{par}, par \in \{1,...,35\}$, each of which includes all simulations with

one common parameter value indicated by the underscript *par*. The value of *par* is indicated on the *par*-th row of the y-axis of Figure 4.13. For example, all simulations with a 'Low misfolding rate' belong to set H_{22}. I defined $\mathbf{CONV}_{par1,par2}$ as the mean time to convergence between all simulations in set H_{par1} against all simulations in set H_{par2} (Eq. 4.22). By comparing diagonal elements, one can study the effect of a single parameter value on time to convergence, whereas by comparing non-diagonal elements within a row or a column, one can study how variation of a second parameter affects time to convergence given that the first parameter remains constant.

$$\text{Dice}_{s,\bar{s}}(n) = \frac{\#\{G_s(n) \cap G_{\bar{s}}(n)\}}{n} \tag{4.20}$$

$$\text{tConv}_{s,\bar{s}} = \arg\min_n \left|\text{Dice}_{s,\bar{s}}(n) - \text{ConvThr}\right|, \quad s.t.\ \text{Dice}_{s,\bar{s}}(m) \geq \text{ConvThr}, \forall m \in \{\text{tConv}_{s,\bar{s}}, ..., \text{NNeu}\} \tag{4.21}$$

$$\mathbf{CONV}_{par1,par2} = \frac{\sum_{s \in H_{par1}} \sum_{\bar{s} \in H_{par2}} \text{tConv}_{s,\bar{s}}}{|H_{par1}||H_{par2}|} \tag{4.22}$$

Figure 4.14 displays the mean firing frequencies and mean toxicity over time for certain neuron types in a simulation where a toxic effect was expressed as an increase of firing voltage thresholds.

4.5 Discussion

In the absence of any protein spread, neuronal deaths occurred in random order across the network (result not shown). Across simulations, neuronal network diffusion was the primary driver of the patterns of protein spread (Figure 4.13), strongly influencing neuronal survival characteristics based on distance to seed (GDS) and synaptic input:output relations (SSG), as well as the asymmetry of network breakdown (Figure 4.12, Table 4.1). In simulations where neuronal network diffusion was strong and pathogenic protein was soluble, the spread pattern showed a relationship primarily with the input:output (SSG) metric, whereas with insoluble pathogenic protein, the spread pattern showed a relationship primarily with the dis-

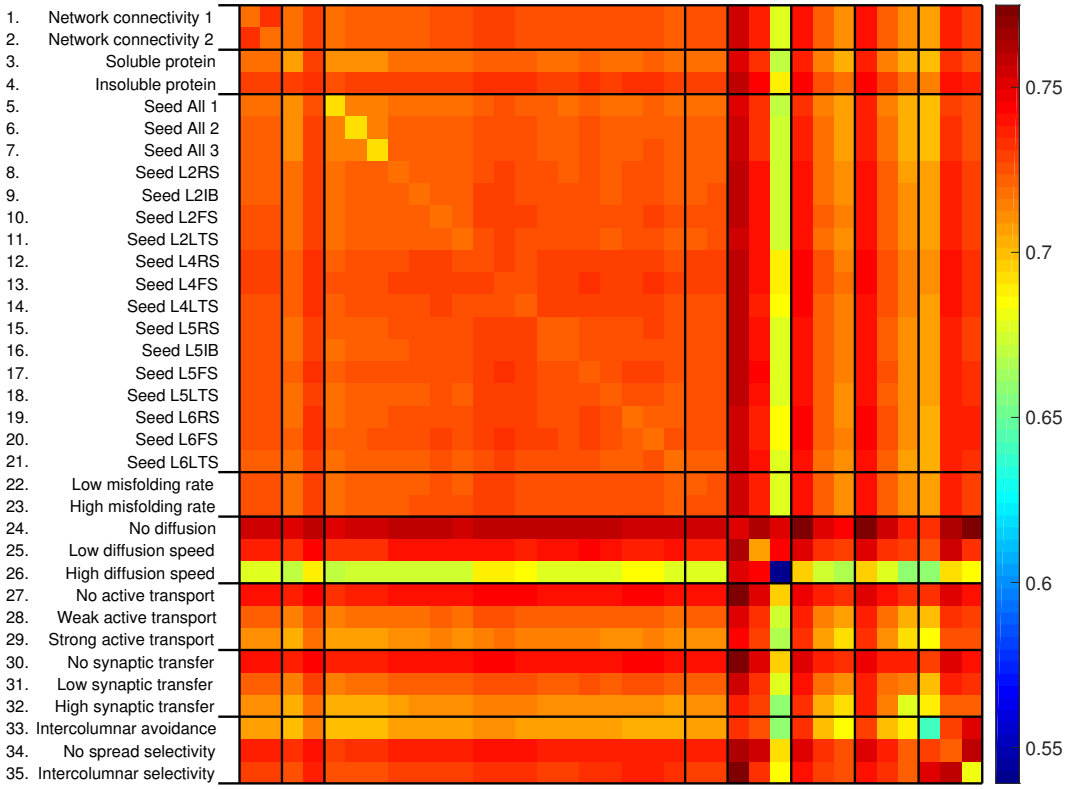

Figure 4.13: Heatmap of mean time to convergence between all pairs of simulation sets H_{par}. For example, a value of 0.65 indicates that convergence occurred after 65% of neurons reached neuronal death. The x-axis labels are replicated from the y-axis labels.

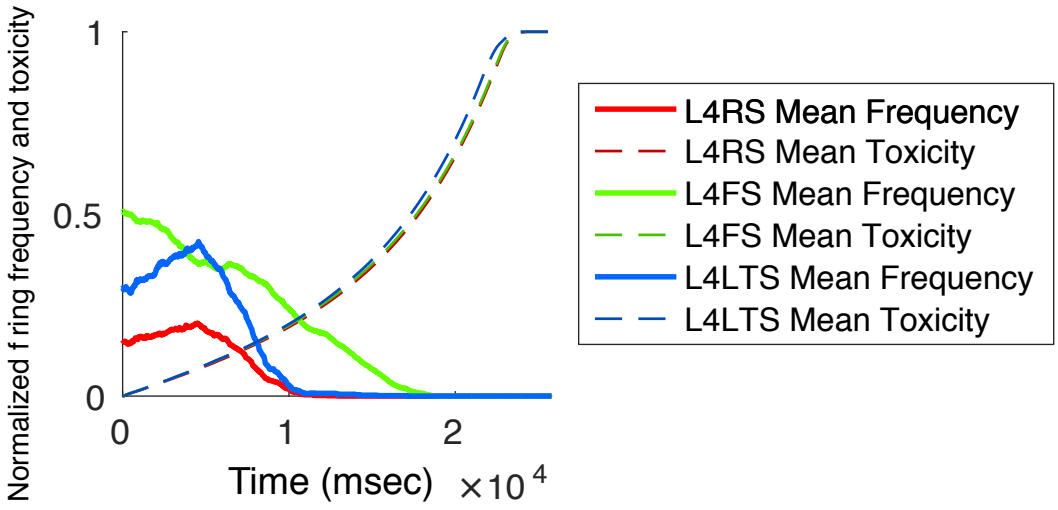

Figure 4.14: Mean toxicity and mean firing frequencies over time for layer 4 neurons of the first cortical column, grouped by neuronal type.

tance to seed (GDS) metric. This agrees with recent findings assigning the diffusive spread of pathogenic proteins a central role in the evolution of neurodegenerative diseases [30, 36, 37, 40, 41, 148], and with evidence from animal models of protein propagation [44]. “Enhanced insolubility" could reflect the presence of non-aggregated pathogenic oligomers that mediate local cellular toxicity: a factor that may drive rapidly evolving neurodegenerative disease pathologies such as amyotrophic lateral sclerosis and prion [246].

Increased misfolding rate and active transport of pathogenic protein hastened network breakdown, consistent with an amplification of intracellular toxic effects, as predicted empirically [44, 130, 148]. While of course in actual patients there is no ‘higher seed’ comparatively, in-vivo animal studies and in-vitro experiments can be done varying the seed. In my results, I found that a higher misfolding rate hastened neurodegeneration far more than a higher initial seed concentration in the case of insoluble pathogenic protein, in agreement with in-vivo data [145].

The asymmetry of network breakdown increased with insoluble protein, or with increased misfolding, diffusion speed, active transport strength, synaptic transfer strength, as well as when protein had the tendency to spread selectively via intercolumnar connections. These mechanisms tend to focus neuronal toxicity in specific network elements, a mechanism previously proposed to underpin the strikingly asymmetric atrophy profiles of TDP-43-opathies [36]. Inspection of Figure 4.13 suggests that the conjunction of particular protein and network factors promoted the more rapid convergence of patterns of network breakdown, in keeping with a ‘molecular nexopathy’ mechanism [36]. Pathogenic protein solubility, higher diffusion speed, stronger active transport, stronger synaptic transfer, and any spread selectivity all consistently accelerated the convergence of protein spread patterns.

My findings further endorse an important role of local neuronal geometry in modulating network breakdown. Whereas changing the overall network connectivity had no effect, the laminar location of neurons within the simulated cortical columns affected the impact of pathogenic protein seeding and diffusion. This computational evidence supports the exquisite histopathological se-

lectivity and regional vulnerability that characterise a range of neurodegenerative diseases [16, 30, 36, 37, 40, 41, 44, 148]. In addition, although my simulations were not designed primarily to capture alterations in neuronal electrophysiology, the relatively simple model parameters yielded complex neuronal activity profiles that showed dependence on neuronal type, and time. For example, in Figure 4.14, L4LTS neurons showed an initial increase in firing frequency under a 'loss of function' effect, reflecting the removal of inhibitory effects from connected neurons, and in line with previous predictions based on biological disease models [16].

Especially pertinently, my framework can identify factors that might constitute targets for therapeutic manipulation. For example, increased diffusion speed in the context of a soluble (in contrast to an insoluble) pathogenic protein tended to prolong overall network survival, even when I also increased the misfolding rate. This unintuitive result can be explained, as faster diffusion would spread protein more evenly in the network, promoting overall clearance of soluble pathogenic protein. This is a potential therapeutic mechanism that has attracted much recent interest [130, 133, 173]. Similar considerations apply to synaptic transfer, which was also protective in my simulations (Table 4.1), and has also been proposed as a target for future interventions [72]. In Alzheimer's disease, amyloid-beta is associated with toxic hyperexcitability [179, 247] (which, in turn, leads to even more pathogenic protein to be released from affected neurons). The mechanism of synaptic transfer was protective for individual neurons with a high firing frequency, but in combination with the hyperexcitability toxic gain effect, it was protective on the entire network-scale (increased TTNB, Table 4.1) for both soluble and insoluble pathogenic protein. Alzheimer's disease is the result of a complex interplay between amyloid-beta and tau proteins. The neuronal loss caused by tau coupled with the neuronal hyperexcitability caused by amyloid-beta could have the effect of spreading tau outside zones of amyloid deposition, leading to differential tissue distributions of the two proteins, in line with recent cellular and neuroimaging data [247, 248].

4.6 Limitations

In this chapter, I have shown that pathogenic protein and network properties drove patterns of network breakdown in a simulated, cortical microcircuit model of neurodegenerative diseases. This computational model captured certain key characteristics of pathogenic protein spread that are in accord with observed features of neurodegenerative diseases. Although the results and conclusions had no validation and did not apply to a specific pathogenic protein or disease, the more general concepts that emerged, such as soluble pathogenic protein targeting bottleneck neurons versus insoluble pathogenic protein targeting neurons near the seed, are likely to hold true in most, if not all, cases.

The potential of computational modelling techniques to simulate neural network disintegration remains largely unexplored. Such techniques seem ideally suited to define the 'structural logic that governs the biological effects' of neurodegenerative diseases [145]. My findings suggest that a small artificial neural network under a handful of relevant parameters can generate diverse, biologically plausible behaviour that is broadly relevant to human neurodegenerative diseases and consistent with empirical data.

A major limitation of computational modelling approaches is the need to simplify (sometimes radically) in order to capture a few mechanisms of pathogenic proteins which are likely to be of general relevance. This work could be refined in a number of ways. Some commonly assumed contributors of pathogenesis in neurodegenerative diseases that I did not model include multiple proteins (e.g., tau, amyloid-beta, etc.), chaperone proteins, glial cell interactions with neurons, protein aggregates of different sizes and the recruitment of additional proteins by larger aggregates, extracellular protein spread, endosomes, etc. Each of these processes could be modelled in order to develop this framework into a more realistic simulation of the complexity of actual neurodegenerative diseases.

The primary limitation of this work is the lack of substantial validation. Further work is required to test the models against a range of empirical data derived in-vitro and from animal models. The way to do this would be to create an artificial

neural network which simulates the same network as that used by an in-vivo animal study or by an in-vitro study, and then replicating similar starting conditions, i.e., the initial seed of pathogenic protein being simulated at the same area that pathogenic protein was inoculated into the animal or into the in-vitro culture. As pathogenic protein spreads over time in the animal or in-vitro model and atrophy occurs, this can serve as validation for the simulated spread within the artificial neural network. However, due to the complexity of such an undertaking, another route is to link the modelled mechanisms here to validation that uses brain imaging of disease progression. To that end, in Chapter 5, I create a framework of computational modelling at the brain scale using magnetic resonance imaging for validation, and in Chapter 6, I link the work presented in this chapter with the work of Chapter 5.

Chapter 5

Computational modelling at the brain scale: application to AD

While pathogenic protein mechanisms occur at the neuronal and the molecular scale, disease phenotypes in patients are typically observed with medical imaging at the brain scale. Being able to use imaging as empirical data of disease progression allows my work to be validated to a degree, and therefore test which models and model parameters best fit empirical data of disease progression, and by extension how much merit the respective modelling hypotheses have. Therefore, to link pathogenic protein mechanisms to disease phenotypes, a computational modelling framework at the brain scale is required.

There has been previous work that modelled pathogenic protein mechanisms at the brain scale. An fMRI study determined disease-specific regions as epicentres, whose functional connectivity in health correlated with atrophy progression [37, 68], suggesting that functional connectivity plays a role in disease progression. Graph theoretical analyses revealed that hub regions and regions with shorter functional paths to the syndrome-specific epicentre showed greater vulnerability. Raj et al. [41] modelled brain network mediated trans-synaptic diffusive spread. Their predictions of regional atrophy achieved a strong correlation with atrophy measurements of follow-up scans. Compared to their work, I model many additional pathogenic protein mechanisms, and additionally, the data they used were limited to four-year follow-up scans, whereas I aimed to predict disease progression

patterns in their entirety. The recent work of Weickenmeier et al. [70] is the most similar to this work, modelling transcription and translation, and misfolding identically, while having a different model for clearance, structural connectivity related spread, and extracellular diffusion. The authors attempted to replicate the disease progression of amyloid-beta and tau in AD, alpha-synuclein in Parkinson's disease, and TDP-43 in amyotrophic lateral sclerosis, but their validation consists of only visual assessment of results, thus not quantitative. Iturria et al. [69] modelled the spatiotemporal spread of amyloid-beta concentration using an epidemic spread model and validated their methodology using amyloid-beta concentration PET imaging of Alzheimer's disease subjects. They modelled protein production, clearance, and structural connectivity related spread. They discovered the anterior and posterior cingulate as the best fitting seed regions, and found structural connectivity to be a determinant of amyloid-beta spread in Alzheimer's disease. Compared to these works, I modelled additional mechanisms of spread, including functional, structural, and effective connectivity related spread, extracellular diffusion, and firing frequency related spread. I also simulated brain regional volume and atrophy, and my validation methodology was population based, rather than individual subject or qualitative.

To develop the framework for this work, I first constructed models for mechanisms of pathogenic protein accumulation, spread, and atrophy at the brain scale. I represented the healthy human brain as a network of 27 grey matter brain regions, with connections based on Euclidean distance, functional connectivity, structural connectivity, and effective connectivity, all derived from MRI scans. After seeding pathogenic protein into the network, I ran simulations and kept track of the timestep when each brain region began showing abnormally low volume (or high atrophy) for the first time. I then compared the sequence of brain regional volume losses becoming abnormally high during the simulation to the sequence derived from an event based model fitted to ApoE 4 positive AD patient data [64] (considered as ground truth). This comparison allowed me to find the optimal models and model parameters that best fitted AD ApoE 4 positive disease progression.

Functional, structural, and effective connectivity are the common connectivities that can be derived easily from patient scan data. While similar work has used them to model connections, in this chapter I attempt to discover which connectivities are linked to disease progression. Additionally, I briefly evaluated the merit behind a few of my modelling hypotheses and demonstrate how my framework could be informative for drug development. While further experiments could have been done in this chapter, these were left for the next chapter with the combined brain scale and neural scale model.

5.1 Brain scale modelling

Structural, functional, and diffusion-weighted MRIs from 10 healthy subjects were used to generate a graph representation of a healthy brain network, consisting of 27 grey matter regions and related by Euclidean distance, functional connectivity, structural connectivity, and effective connectivity (see Section 2.1.3). The scans were from the young onset Alzheimer's disease dataset, which included 22 healthy controls [249] with mean age of 60.6 (standard deviation 5.6), of which I randomly chose 10 controls. I believed that 10 subjects were enough as my work did not require subject-specific intricate details, but rather a population-average brain, where atrophy is quantified in large brain regions. While it is possible that results could change with more scans, I believe that it would be a small change. Similarly to the previous chapter, I modelled an abstract non-pathogenic and pathogenic protein concentration within each brain region, and also modelled the mechanisms of production, clearance, misfolding, extracellular diffusion, network-mediated diffusion, firing frequency related spread and atrophy. After initialising the network and seeding pathogenic protein into it, I ran simulations, using the modelled mechanisms to update the network state at each timestep t until the entire network atrophied (i.e., the brain volumes became zero).

5.1.1 Image processing

T1-weighted MR images were parcellated into 208 brain regions [92]. I kept $\mathrm{NReg} = 27$ symmetric grey matter regions (Fig. 5.3), denoted with $r \in$

$\{1,...,\text{NReg}\}$. The 27 regions chosen were the same as the regions which were found to be significant by the EBM. Regions were symmetrised because the EBM also performs this operation, although this has ramifications for certain diseases which have left-right asymmetry, as they cannot be modelled accurately enough. Each region had associated coordinates $\mathbf{Coor}_r$ and volume $V_r(t)$. Subject volumes were normalised by their total intracranial volume, then for each region $V_r(0)$ was set to the average regional volume of the population. I defined $\mathbf{D}_{r\leftarrow\bar{r}}$ as the Euclidean distance connectivity matrix among brain regions.

Resting-state functional MRIs were motion and EPI corrected and high-pass filtered (0.01Hz). Time courses were extracted, then centred and variance-normalised. The parcellations were affinely registered from the T1w to the fMRI image space. I computed the per region, per subject synaptic signals based on the methodology of Karahanoğlu, Caballero-Gaudes, Lazeyras, and Van De Ville [250] (using what they call 'activity inducing signals' in their work), which were averaged over subjects to get the population regional synaptic signals $\mathbf{Sig}_r$. I calculated the functional connectivity matrix $\mathbf{F}_{r\leftarrow\bar{r}}$ using the correlation coefficient between all pairs of synaptic signals $\mathbf{Sig}_r$. Although typically functional connectivity is based on BOLD signal correlations, it attempts to correlate synaptic signals, so I used this definition instead. The per region, per subject synaptic signals were also used to compute the synaptic activity's power spectrum, which were averaged over subjects. Using the per region power spectrums, I computed the mean frequency per region $\text{freq}_r(t)$.

Diffusion data were corrected for motion, eddy-currents, and EPI distortion using field maps before tensors were fitted. Tractography was then performed [251], which was then filtered using the approach proposed by Smith, Tournier, Calamante, and Connelly [252]. I defined $\mathbf{S}_{r\leftarrow\bar{r}}$ as the structural connectivity matrix extracted from the tractography and defined using the brain parcellation of the T1w images. I varied whether $\mathbf{S}_{r\leftarrow\bar{r}}$ was constructed before or after the filtering approach [252].

Resting-state fMRI scans were used to compute each subject's effective connectivity [253]. The population average effective connectivity $\mathbf{E}_{r\leftarrow\bar{r}}$ was calculated

by performing Bayesian model reduction [254]. Effective connectivity estimation can incorporate structural connectivity $\mathbf{S}_{r\leftarrow\bar{r}}$ as prior information [255]. I varied whether $\mathbf{E}_{r\leftarrow\bar{r}}$ was calculated based only on the rsfMRI scans, or using the rsfMRI scans in conjunction with the structural connectivity constructed without the filtering step [252], or finally using the rsfMRI scans in conjunction with the structural connectivity constructed with the filtering step [252].

The variations in the definition of structural and effective connectivity were used to check whether results were sensitive to them.

5.1.2 General modelling

I modelled the mechanisms of protein production, clearance, misfolding, extracellular diffusion, network-mediated diffusion, firing frequency related spread, and atrophy. Brain regions had associated non-pathogenic protein concentration $\mathrm{Cn}_r(t)$, pathogenic protein concentration $\mathrm{Cp}_r(t)$, non-pathogenic protein quantity $\mathrm{Qn}_r(t) = \mathrm{Cn}_r(t) * V_r(t)$, pathogenic protein quantity $\mathrm{Qp}_r(t) = \mathrm{Cp}_r(t) * V_r(t)$, atrophy $A_r(t)$, and radius $\rho_r(t)$ (I simplified brain regions to have a spherical shape). Atrophy was initialised to $A_r(0) = 0$ and increased as a function of the regional protein concentration (Eq. 5.1), with AThr defining the protein concentration threshold below which no additional atrophy occurs and R_A controlling the atrophy rate. Once $A_r(t) = 1$, then the region had fully atrophied. As atrophy increased, it linearly decreased volumes $V_r(t)$ (Eq. 5.2, also requiring an updating of radii), as well as the regional synaptic frequency $\mathrm{freq}_r(t)$ (Eq. 5.3), as I assumed that as brain regions atrophy, less synaptic activity would occur.

$$A_r(t+1) = A_r(t) + \max\left[0, R_A\left(e^{10(\mathrm{Cn}_r(t)+\mathrm{Cp}_r(t)-\mathrm{AThr})} - 1\right)\right] \quad (5.1)$$

$$V_r(t) = (1 - A_r(t))\, V_r(0) \quad (5.2)$$

$$\mathrm{freq}_r(t) = (1 - A_r(t))\, \mathrm{freq}_r(0) \quad (5.3)$$

5.1.3 Production, clearance, and misfolding

I modelled production, clearance, and misfolding in a similar manner to the models presented in Section 4.2.1, Section 4.2.2, and Section 4.2.3, respectively. Given production rates of non-pathogenic protein R_{nProd} and pathogenic protein R_{pProd}, I defined $\text{CnProd}_r(t)$ and $\text{CpProd}_r(t)$ as non-pathogenic protein production and pathogenic protein production, respectively (Eq. 5.5). I modelled clearance as $\text{CnClear}_r(t)$ and $\text{CpClear}_r(t)$ (Eq. 5.7), with healthy protein concentration levels CnHealth and CpHealth, and clearance rates R_{nClear} and R_{pClear}. Given a misfolding rate R_{Mis}, I defined $\text{CnMis}_r(t)$ and $\text{CpMis}_r(t)$ as the misfolding terms (Eq. 5.9).

$$\text{CnProd}_r(t) = R_{\text{nProd}} \tag{5.4}$$

$$\text{CpProd}_r(t) = R_{\text{pProd}} \tag{5.5}$$

$$\text{CnClear}_r(t) = -R_{\text{nClear}} \log\left(1 + (e-1)\frac{\text{Cn}_r(t)}{\text{CnHealth}}\right) \tag{5.6}$$

$$\text{CpClear}_r(t) = -R_{\text{pClear}} \log\left(1 + (e-1)\frac{\text{Cp}_r(t)}{\text{CpHealth}}\right) \tag{5.7}$$

$$\text{CnMis}_r(t) = -R_{\text{Mis}}\text{Cn}_r(t)\text{Cp}_r(t) \tag{5.8}$$

$$\text{CpMis}_r(t) = R_{\text{Mis}}\text{Cn}_r(t)\text{Cp}_r(t) \tag{5.9}$$

5.1.4 Protein spread

I modelled seven mechanisms of spread. I modelled extracellular diffusion $\mathbf{ED}_{r\leftarrow\bar{r}}(t)$ (Eq. 5.11), network-mediated diffusion using functional, structural, and effective connectivity $\mathbf{ND}|\mathbf{F}_{r\leftarrow\bar{r}}(t)$, $\mathbf{ND}|\mathbf{S}_{r\leftarrow\bar{r}}(t)$, and $\mathbf{ND}|\mathbf{E}_{r\leftarrow\bar{r}}(t)$ (Eq. 5.13), respectively, and firing frequency related spread using functional, structural, and effective connectivity $\mathbf{FS}|\mathbf{F}_{r\leftarrow\bar{r}}(t)$, $\mathbf{FS}|\mathbf{S}_{r\leftarrow\bar{r}}(t)$, and $\mathbf{FS}|\mathbf{E}_{r\leftarrow\bar{r}}(t)$ (Eq. 5.14), respectively, with the notation indicating the probability of protein spreading from region $\bar{r}$ to r.

Although protein can clearly only spread via fibre tracts, and functional connectivity is not directly related to fibre tract connections, there has been evidence that atrophy patterns correlate with functional networks [37], thus modelling it and

its contribution to spread is of interest. Spread based on functional connectivity or effective connectivity could be thought of as spread that physically occurs through fibre tracts, but the "strength" of that spread is modulated not only by the number of connections, but also by the electrical activity correlation between two regions (functional connectivity) or the strength of the connections (effective connectivity). Additionally, while structural connectivity can have many false positives, this should not have a significant impact on results if we assume that the false positives are roughly uniformly distributed in the structural connectivity matrix.

I defined $\mathbf{NAF}_{r\leftarrow\bar{r}}(t)$, $\mathbf{NAS}_{r\leftarrow\bar{r}}(t)$, and $\mathbf{NAE}_{r\leftarrow\bar{r}}(t)$ as the normalised absolute functional, structural, and effective connectivity matrices, respectively (Eq. 5.10).

$$\begin{aligned}
\mathbf{NAF}_{r\leftarrow\bar{r}}(t) &= \begin{cases} \frac{|\mathbf{F}_{r\leftarrow\bar{r}}|}{\sum_{k=1}^{\mathrm{NReg}}\sum_{\bar{k}=1}^{\mathrm{NReg}}|\mathbf{F}_{k\leftarrow\bar{k}}|}, \text{ if } A_r(t)<1 \text{ and } A_{\bar{r}}(t)<1 \\ 0, \text{ otherwise} \end{cases} \\
\mathbf{NAS}_{r\leftarrow\bar{r}}(t) &= \begin{cases} \frac{|\mathbf{S}_{r\leftarrow\bar{r}}|}{\sum_{k=1}^{\mathrm{NReg}}\sum_{\bar{k}=1}^{\mathrm{NReg}}|\mathbf{S}_{k\leftarrow\bar{k}}|}, \text{ if } A_r(t)<1 \text{ and } A_{\bar{r}}(t)<1 \\ 0, \text{ otherwise} \end{cases} \\
\mathbf{NAE}_{r\leftarrow\bar{r}}(t) &= \begin{cases} \frac{|\mathbf{E}_{r\leftarrow\bar{r}}|}{\sum_{k=1}^{\mathrm{NReg}}\sum_{\bar{k}=1}^{\mathrm{NReg}}|\mathbf{E}_{k\leftarrow\bar{k}}|}, \text{ if } A_r(t)<1 \text{ and } A_{\bar{r}}(t)<1 \\ 0, \text{ otherwise} \end{cases}
\end{aligned} \tag{5.10}$$

5.1.5 Extracellular diffusion

Extracellular diffusion modelled Brownian motion in the extracellular space. I simplified the modelling to assume that protein would spread out of the centre of a spherical brain region based on an isotropic 3D normal distribution. Under this assumption, the probability of protein spreading to a brain region was determined by the integral of the 3D normal distribution. To simplify this further, I approximated the calculation of the integral of the 3D normal distribution by calculating instead the integral a 1D normal distribution with zero mean and standard deviation σ_{ED} between the destination-region's nearest point and the destination-region's furthest point from the source-region. An illustration of extracellular diffusion is shown in

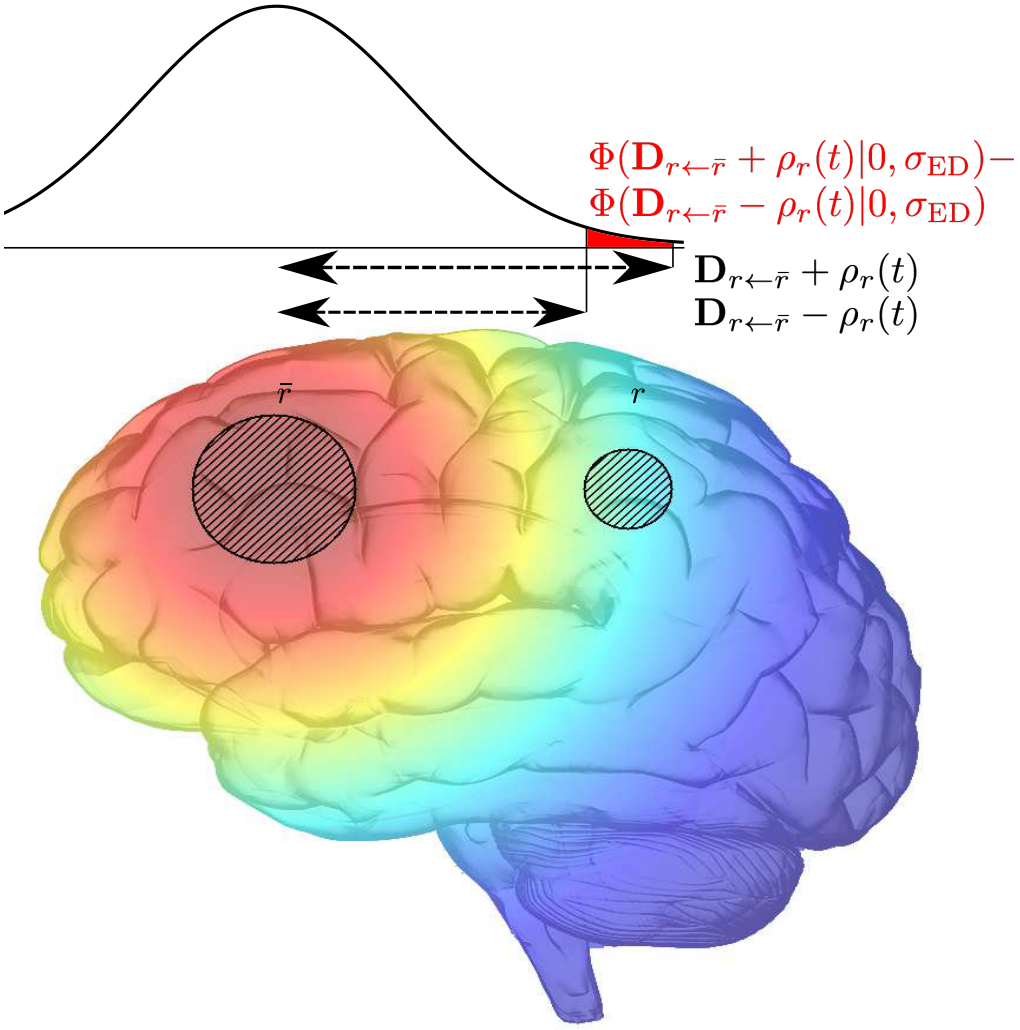

Figure 5.1: An illustration of extracellular diffusion. In this example protein spreads from brain region $\bar{r}$ to brain region r. Figure was created after modification of the image downloaded from http://clipart-library.com/clip-art/brain-transparent-image-24.htm.

Figure 5.1 (Eq. 5.11).

$$\mathbf{ED}_{r\leftarrow\bar{r}}(t) = \frac{\Phi\left(\mathbf{D}_{r\leftarrow\bar{r}} + \rho_r(t)|0, \sigma_{\mathrm{ED}}\right) - \Phi\left(\mathbf{D}_{r\leftarrow\bar{r}} - \rho_r(t)|0, \sigma_{\mathrm{ED}}\right)}{\sum_{\hat{r}=1}^{\mathrm{NReg}} \Phi\left(\mathbf{D}_{\hat{r}\leftarrow\bar{r}} + \rho_{\hat{r}}(t)|0, \sigma_{\mathrm{ED}}\right) - \Phi\left(\mathbf{D}_{\hat{r}\leftarrow\bar{r}} - \rho_{\hat{r}}(t)|0, \sigma_{\mathrm{ED}}\right)} \tag{5.11}$$

5.1.6 Network-mediated diffusion

Network-mediated diffusion modelled Brownian motion intracellularly and intercellularly. The probability of protein spreading out of region $\bar{r}$ is given by NDout|$\mathrm{F}_{\bar{r}}$,

NDout|S$_{\bar{r}}$, and NDout|E$_{\bar{r}}$ (Eq. 5.12), and it was based on the integral of a one dimensional normal distribution, with the standard deviation $\sigma_{\text{ND|F}}$, $\sigma_{\text{ND|S}}$, and $\sigma_{\text{ND|E}}$ controlling the speed of diffusion, as well as a term for the relative connection strength per unit of volume for region $\bar{r}$ (note that the multiplication with the minimum volume is simply to normalise the values to a desired scale). The spread into a region r depended on the connection strengths given by the normalised absolute functional $\mathbf{NAF}_{r\leftarrow\bar{r}}(t)$, structural $\mathbf{NAS}_{r\leftarrow\bar{r}}(t)$, or effective $\mathbf{NAE}_{r\leftarrow\bar{r}}(t)$ connectivity matrices (Eq. 5.13). An illustration of network-mediated diffusion is shown in Figure 5.2.

$$
\begin{aligned}
\text{NDout|F}_{\bar{r}}(t) &= 2\Phi\left(-\rho_{\bar{r}}(t)|0,\sigma_{ND|F}\right)\sum_{r}\frac{\mathbf{NAF}_{r\leftarrow\bar{r}}(t)}{V_{\bar{r}}(0)}\min_{\hat{r}}V_{\hat{r}}(0)\\
\text{NDout|S}_{\bar{r}}(t) &= 2\Phi\left(-\rho_{\bar{r}}(t)|0,\sigma_{ND|S}\right)\sum_{r}\frac{\mathbf{NAS}_{r\leftarrow\bar{r}}(t)}{V_{\bar{r}}(0)}\min_{\hat{r}}V_{\hat{r}}(0)\\
\text{NDout|E}_{\bar{r}}(t) &= 2\Phi\left(-\rho_{\bar{r}}(t)|0,\sigma_{ND|E}\right)\sum_{r}\frac{\mathbf{NAE}_{r\leftarrow\bar{r}}(t)}{V_{\bar{r}}(0)}\min_{\hat{r}}V_{\hat{r}}(0)
\end{aligned}
\tag{5.12}
$$

$$
\begin{aligned}
\mathbf{ND|F}_{r\leftarrow\bar{r}}(t) &= \begin{cases}\text{NDout|F}_{\bar{r}}(t)\frac{\mathbf{NAF}_{r\leftarrow\bar{r}}(t)}{\sum_{\hat{r}}\mathbf{NAF}_{\hat{r}\leftarrow\bar{r}}(t)}, \text{ if } r\neq\bar{r}\\ \text{NDout|F}_{\bar{r}}(t)\frac{\mathbf{NAF}_{r\leftarrow\bar{r}}(t)}{\sum_{\hat{r}}\mathbf{NAF}_{\hat{r}\leftarrow\bar{r}}(t)}+\left(1-\text{NDout|F}_{\bar{r}}(t)\right), \text{ if } r=\bar{r}\end{cases}\\
\mathbf{ND|S}_{r\leftarrow\bar{r}}(t) &= \begin{cases}\text{NDout|S}_{\bar{r}}(t)\frac{\mathbf{NAS}_{r\leftarrow\bar{r}}(t)}{\sum_{\hat{r}}\mathbf{NAS}_{\hat{r}\leftarrow\bar{r}}(t)}, \text{ if } r\neq\bar{r}\\ \text{NDout|S}_{\bar{r}}(t)\frac{\mathbf{NAS}_{r\leftarrow\bar{r}}(t)}{\sum_{\hat{r}}\mathbf{NAS}_{\hat{r}\leftarrow\bar{r}}(t)}+\left(1-\text{NDout|S}_{\bar{r}}(t)\right), \text{ if } r=\bar{r}\end{cases}\\
\mathbf{ND|E}_{r\leftarrow\bar{r}}(t) &= \begin{cases}\text{NDout|E}_{\bar{r}}(t)\frac{\mathbf{NAE}_{r\leftarrow\bar{r}}(t)}{\sum_{\hat{r}}\mathbf{NAE}_{\hat{r}\leftarrow\bar{r}}(t)}, \text{ if } r\neq\bar{r}\\ \text{NDout|E}_{\bar{r}}(t)\frac{\mathbf{NAE}_{r\leftarrow\bar{r}}(t)}{\sum_{\hat{r}}\mathbf{NAE}_{\hat{r}\leftarrow\bar{r}}(t)}+\left(1-\text{NDout|E}_{\bar{r}}(t)\right), \text{ if } r=\bar{r}\end{cases}
\end{aligned}
\tag{5.13}
$$

5.1.7 Firing frequency related spread

I assumed that the more frequent synaptic activity was, the more protein would spread out of a region. The probability of protein spreading out of region $\bar{r}$ was based on the general strength of firing frequency related spread $R_{\text{FS|F}}$, $R_{\text{FS|S}}$, or $R_{\text{FS|E}}$, as well as on the firing frequency of the source region $\text{freq}_{\bar{r}}(t)$ (normalised for convenience). The probability of protein spreading into region r depended on the connection strengths of the normalised absolute functional $\mathbf{NAF}_{r\leftarrow\bar{r}}(t)$, structural $\mathbf{NAS}_{r\leftarrow\bar{r}}(t)$, or effective $\mathbf{NAE}_{r\leftarrow\bar{r}}(t)$ connectivity matrices (Eq. 5.14).

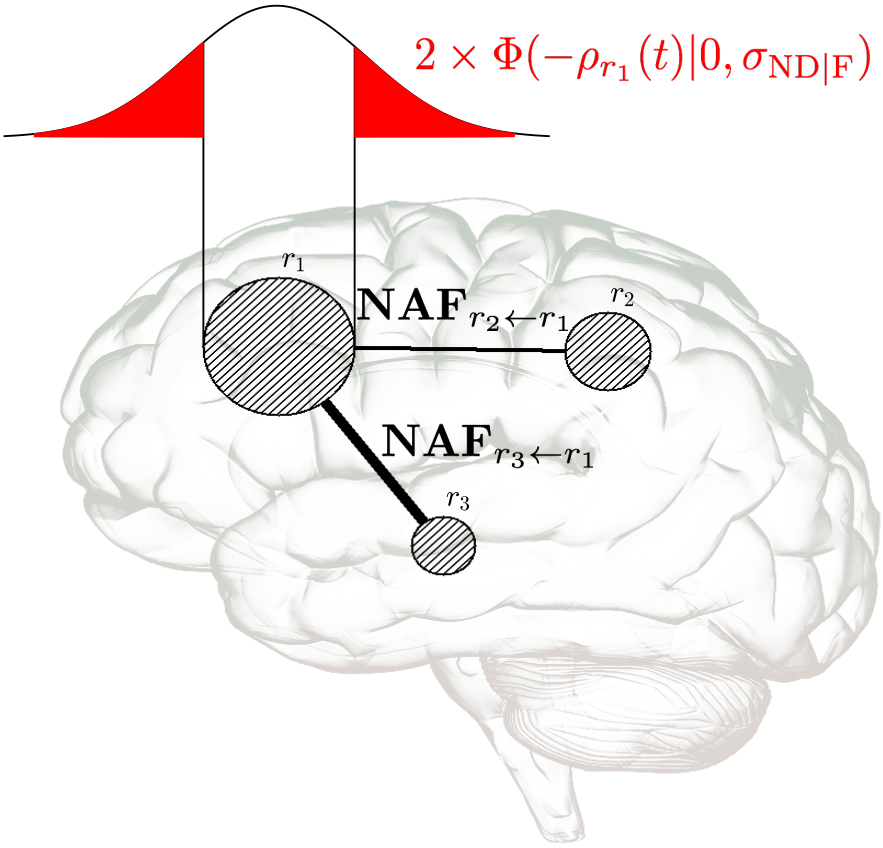

Figure 5.2: An illustration of functional connectivity related network-mediated diffusion. The integral of the normal distribution $2\Phi\left(-\rho_{r_1}(t)|0, \sigma_{ND|F}\right)$ indicates the probability of protein attempting to diffuse out of region r_1. However, this is also limited by the total connectivity of the region, which I calculated using the relative connection strength per unit of volume, which in this example is $\frac{\mathbf{NAF}_{r_2 \leftarrow r_1}(t) + \mathbf{NAF}_{r_3 \leftarrow r_1}(t)}{V_{r_1}(0)} \min_{\hat{r}} V_{\hat{r}}(0)$. Intuitively this implies that regions with stronger or more connections, but equal volumes will spread more protein. Similarly, regions with similar total connectivity, but higher volume will spread less protein. Since I use the initial volume to normalise, I am making an assumption that connectivity is not affected from atrophy. The product of the previous two terms is the probability of protein diffusing out of region r_1, with the relative connection strengths to r_2 and r_3 determining the probability of diffusion to each respective region. Figure was created after modification of the image downloaded from http://clipart-library.com/clip-art/brain-transparent-image-24.htm.

$$
\begin{aligned}
\mathbf{FS}|\mathbf{F}_{r\leftarrow\bar{r}}(t) &= \begin{cases} R_{\mathrm{FS|F}}\frac{f_{\bar{r}}(t)}{\max_{\hat{r}} f_{\hat{r}}(0)}\frac{\mathbf{NAF}_{r\leftarrow\bar{r}}(t)}{\sum_{\tilde{r}}\mathbf{NAF}_{\tilde{r}\leftarrow\bar{r}}(t)}, \text{ if } r\neq\bar{r} \\ R_{\mathrm{FS|F}}\frac{f_{\bar{r}}(t)}{\max_{\hat{r}} f_{\hat{r}}(0)}\frac{\mathbf{NAF}_{r\leftarrow\bar{r}}(t)}{\sum_{\tilde{r}}\mathbf{NAF}_{\tilde{r}\leftarrow\bar{r}}(t)} + 1 - R_{\mathrm{FS|F}}\frac{f_{\bar{r}}(t)}{\max_{\hat{r}} f_{\hat{r}}(0)}, \text{ if } r=\bar{r} \end{cases} \\
\mathbf{FS}|\mathbf{S}_{r\leftarrow\bar{r}}(t) &= \begin{cases} R_{\mathrm{FS|S}}\frac{f_{\bar{r}}(t)}{\max_{\hat{r}} f_{\hat{r}}(0)}\frac{\mathbf{NAS}_{r\leftarrow\bar{r}}(t)}{\sum_{\tilde{r}}\mathbf{NAS}_{\tilde{r}\leftarrow\bar{r}}(t)}, \text{ if } r\neq\bar{r} \\ R_{\mathrm{FS|S}}\frac{f_{\bar{r}}(t)}{\max_{\hat{r}} f_{\hat{r}}(0)}\frac{\mathbf{NAS}_{r\leftarrow\bar{r}}(t)}{\sum_{\tilde{r}}\mathbf{NAS}_{\tilde{r}\leftarrow\bar{r}}(t)} + 1 - R_{\mathrm{FS|S}}\frac{f_{\bar{r}}(t)}{\max_{\hat{r}} f_{\hat{r}}(0)}, \text{ if } r=\bar{r} \end{cases} \\
\mathbf{FS}|\mathbf{E}_{r\leftarrow\bar{r}}(t) &= \begin{cases} R_{\mathrm{FS|E}}\frac{f_{\bar{r}}(t)}{\max_{\hat{r}} f_{\hat{r}}(0)}\frac{\mathbf{NAE}_{r\leftarrow\bar{r}}(t)}{\sum_{\tilde{r}}\mathbf{NAE}_{\tilde{r}\leftarrow\bar{r}}(t)}, \text{ if } r\neq\bar{r} \\ R_{\mathrm{FS|E}}\frac{f_{\bar{r}}(t)}{\max_{\hat{r}} f_{\hat{r}}(0)}\frac{\mathbf{NAE}_{r\leftarrow\bar{r}}(t)}{\sum_{\tilde{r}}\mathbf{NAE}_{\tilde{r}\leftarrow\bar{r}}(t)} + 1 - R_{\mathrm{FS|E}}\frac{f_{\bar{r}}(t)}{\max_{\hat{r}} f_{\hat{r}}(0)}, \text{ if } r=\bar{r} \end{cases}
\end{aligned} \tag{5.14}
$$

5.1.8 Protein quantity update

Updating protein quantities for the next timestep required the summation of the changes from the different modelled mechanisms (Eq. 5.17). I defined $\mathrm{QnAcc}_r(t)$, and $\mathrm{QpAcc}_r(t)$ as the net change in protein quantity from accumulation (Eq. 5.15). The different spread models were combined into a single matrix $\mathbf{BSS}(t) \in \mathbb{R}^{\mathrm{NReg}\times\mathrm{NReg}}$ (Eq. 5.16). While the order in which the matrices were multiplied can change the values of $\mathbf{BSS}(t)$, this should be reflected in the parameters of each spread model, thus the multiplication order had no genuine impact on the models or the results. This means that with a certain multiplication order the optimal parameters for the individual mechanisms will result in the matrix $\mathbf{BSS}(t)$ being similar to what it would be with a different multiplication order and thus different optimal parameters for the individual mechanisms.

$$\begin{aligned}
\mathrm{QnAcc}_r(t) = &\quad [\mathrm{CnProd}_r(t) + \mathrm{CnClear}_r(t) + \mathrm{CnMis}_r(t)]\, V_r(t) \\
\mathrm{QpAcc}_r(t) = &\quad [\mathrm{CpProd}_r(t) + \mathrm{CpClear}_r(t) + \mathrm{CpMis}_r(t)]\, V_r(t) \qquad (5.15) \\
\mathbf{BSS}(t) = &\quad \mathbf{FS}|\mathbf{F}(t) \times \mathbf{FS}|\mathbf{S}(t) \times \mathbf{FS}|\mathbf{E}(t) \times ... \\
&\quad \times \mathbf{ND}|\mathbf{F}(t) \times \mathbf{ND}|\mathbf{S}(t) \times \mathbf{ND}|\mathbf{E}(t) \times \mathbf{ED}(t) \qquad (5.16) \\
\mathrm{Qn}_r(t+1) = &\quad \sum_{\bar{r}=1}^{\mathrm{NReg}} \mathbf{BSS}_{r\leftarrow\bar{r}}(t)\, [\mathrm{Qn}_{\bar{r}}(t) + \mathrm{QnAcc}_{\bar{r}}(t)] \\
\mathrm{Qp}_r(t+1) = &\quad \sum_{\bar{r}=1}^{\mathrm{NReg}} \mathbf{BSS}_{r\leftarrow\bar{r}}(t)\, [\mathrm{Qp}_{\bar{r}}(t) + \mathrm{QpAcc}_{\bar{r}}(t)] \qquad (5.17)
\end{aligned}$$

5.1.9 Simulation initialisation

In all simulations, the initial non-pathogenic protein concentration was set to $\mathrm{Cn}_r(0) = 0.01$, the production rate of non-pathogenic protein was set to $R_{\mathrm{nProd}} = 2e-4$, the clearance rate of non-pathogenic protein was set to $R_{\mathrm{nClear}} = 2e-4$, and the atrophy concentration threshold was set to $\mathrm{AThr} = 0.04$ (i.e., no atrophy occurred unless the protein concentration was at least 0.04, or $\mathrm{Cn}_r(t) + \mathrm{Cp}_r(t) > 0.04$). I varied whether pathogenic protein was soluble ($R_{\mathrm{pClear}} = 2e-5$) or insoluble ($R_{\mathrm{pClear}} = 0$), whether there was pathogenic protein production ($\mathrm{Cp}_r(0) = 0.01, R_{\mathrm{pProd}} = 2e-5$) or not ($\mathrm{Cp}_r(0) = 0, R_{\mathrm{pProd}} = 0$), and whether there was pathogenic protein seeding of concentration CpSeed at the hippocampus, at the parahippocampal gyrus, or at the entorhinal area (e.g., for seeding the hippocampus: $\mathrm{Cp}_{r=hippocampus}(0) = \mathrm{CpSeed}$).

5.1.10 Event based model fitting

In order to evaluate how accurately a specific set of models and modelling parameters represented a particular neurodegenerative disease, I compared the simulation's atrophy prediction against the prediction of an event based model [77]. For this work, the EBM was informed from cross-sectional data of ApoE 4 positive AD patients, MCI patients, and healthy controls. The data used was the same as in Young et al. [77] from the Alzheimer's Disease Neuroimaging Initiative (ADNI) database.

The EBM assumed that brain regional volumes were probabilistically healthy or abnormal, fitting a normal and a uniform distribution to each brain region's volume data, which calculated the probability of health and abnormality, respectively. Volume abnormality threshold Vthres_r for a brain region was defined as the volume value such that the probability of health was equal to the probability of abnormality for that region. The EBM computed an uncertainty matrix $\mathbf{UM}_{r,i}$, such as the one shown in Figure 1 of Young et al. [77], which indicated the probability of region r being i-th in the order of brain regional volumes becoming abnormal (e.g., if $\mathbf{UM}_{r=hippocampus,i=1} = 0.37, \mathbf{UM}_{r=hippocampus,i=2} = 0.5, \mathbf{UM}_{r=hippocampus,i=3} = 0.13$, then the hippocampus has 0.37 probability of showing abnormal volume before any other brain region does, 0.5 probability of showing abnormal volume after one other brain region shows abnormal volume first, and 0.13 probability of showing abnormal volume after two other brain regions show abnormal volume first). Thus, for each simulation, I had to keep track of the exact timestep that each region's volume became abnormal (i.e., $\arg\min_t V_r(t) \leq \text{Vthres}_r$). I defined OS_r as the event position that brain region r became abnormal during a simulation. I used the following metric to determine the goodness of fit for each set of models and model parameters and to optimise the parameter set θ (Eq. 5.19):

$$\theta^{\star} = \arg\min_{\theta} \sum_{r} \log(\mathbf{UM}_{r,\text{OS}_r}) \tag{5.18}$$

$$\theta = \{R_{\text{Mis}}, R_A, \text{CpSeed}, \sigma_{\text{ED}}, \sigma_{\text{ND|F}}, \sigma_{\text{ND|S}}, \sigma_{\text{ND|E}}, R_{\text{FS|F}}, R_{\text{FS|S}}, R_{\text{FS|E}}\} \tag{5.19}$$

5.2 Results

A model of pathogenic protein without production or clearance (i.e., an insoluble pathogenic protein), and with seeding at the hippocampus best fitted empirical data (Fig. 5.3) with parameters $\{R^{\star}_{Mis} = 0.297, R^{\star}_A = 0.00152, \text{CpSeed}^{\star} = 0.0969, \sigma^{\star}_{\text{ED}} = 0.000243, \sigma^{\star}_{\text{ND|F}} = 0,\ \sigma^{\star}_{\text{ND|S}} = 0.0829, \sigma^{\star}_{\text{ND|E}} = 0.00276, R^{\star}_{\text{FS|F}} = 0, R^{\star}_{\text{FS|S}} = 0, R^{\star}_{\text{FS|E}} = 0\}$. The brain region atrophy order given with the optimal parameters had a normalised Kendall Tau distance of 0.188 with the atrophy order

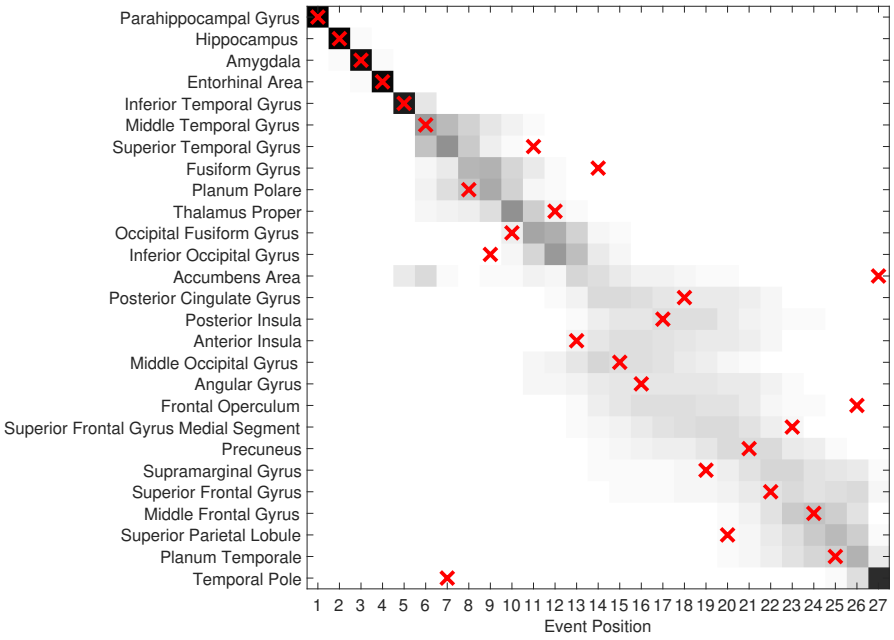

Figure 5.3: Illustration of the fit between the simulation with optimal parameters and the atrophy order given by an EBM for ApoE 4 positive AD. The matrix **UM** indicates in greyscale the event position uncertainty for each region. The red crosses are based on the sequence OS_r that was computed after running a simulation using the optimal parameters $\theta^\star$.

given by the EBM. When attempting to fit with a soluble pathogenic protein and/or a pathogenic protein with a non-zero production rate, the fit was not as good.

5.3 Discussion and limitations

The simulation with the optimal parameters predicted the early stages of atrophy progression well, whereas later stages had higher variance from the diagonal sequence given by the EBM (Fig. 5.3). All other parameters being equal, simulations where pathogenic protein had no production or clearance fitted the data better, evidence that is in favour of the 'prion-like' spread hypothesis [30, 36]. Spread was primarily driven by the structural connectivity, whereas functional connectivity ($\sigma^\star_{\mathrm{ND|F}} = 0$), extracellular diffusion ($\sigma^\star_{\mathrm{ED}} = 0.000243$), and effective connectivity ($\sigma^\star_{\mathrm{ND|E}} = 0.00276$) only had small contributions. Firing frequency related spread ($R^\star_{\mathrm{FS|F}} = 0, R^\star_{\mathrm{FS|S}} = 0, R^\star_{\mathrm{FS|E}} = 0$) also did not contribute to the spread. This evidence suggests protein spread is driven by structural fibre tract connectivity, and not by synaptic activity in ApoE 4 positive AD. Previous modelling approaches have also

had success in modelling spread using structural fibre tract connectivity [41, 69], or with functional connectivity [37], but none have modelled both.

On the assumption that my models with the optimal parameters $\theta^{\star}$ represent ApoE 4 positive AD disease progression sufficiently well, then hypothetically my framework can easily evaluate (within its limits) candidate therapies by simulating therapies that have an effect on one or more of the models. For example, altering the speed of extracellular diffusion had little effect on atrophy progression speed, whereas decreasing the speed of network-mediated diffusion significantly slowed down atrophy progression speed, thus my framework would suggest that researchers focus on therapies that reduce network-mediated diffusion, rather than extracellular diffusion.

In this work, many simplifying assumptions were made in order to keep the models computationally efficient and in the interest of time, I prioritised modelling many mechanisms rather than fewer mechanisms with higher accuracy. In future work, additional mechanisms (e.g., further proteostasis related mechanisms, amyloid-beta and tau interaction, etc.) could be modelled and their contribution to disease progression assessed for a variety of neurodegenerative diseases, under the hypothesis that different parameter values are linked to different diseases. Modelling the entirety of the brain and without symmetrising the brain regions would allow for more accurate modelling of diseases, especially those with asymmetric atrophy profiles. Voxel-based modelling, rather than region-based spheres would also increase the model's ability to capture atrophy progression, albeit at higher computational complexity. Extracellular diffusion was assumed to be isotropic for simplicity, which is not biologically accurate. A more advanced model would restrict it to be within the skull, with more restricted spread in grey matter and less restricted in white matter, and much less restricted in cerebrospinal fluid. This could be implemented as a matrix which could be calculated before any simulations that would determine the spread from each voxel to another.

Adding appropriate regularisation terms to the cost function and estimating the structural and functional connectivities from a larger population of healthy controls

would also be desirable. In this work, connectivity metrics were assumed to remain constant under atrophy, which is not the case in reality [40], and is an assumption that could be relaxed in future work. This could simply be done by reducing the structural connectivity "strengths" from one region to another as that region atrophies, or another way would be to model the connections independently as, e.g., tubes. This would likely have the effect that white matter that has a lot of protein spreading through it would deteriorate faster compared to less trafficked white matter. A sensitivity analysis altering parameter values around the best fit or looking at other local optima would also enhance the validity of the results. Another limitation is the use of the EBM for validation, as instead of training my model directly on the data itself, I am also taking into account the assumptions made by the EBM model. Additionally, more recent work with EBMs [256] has been able to find the atrophy orders of subtypes of diseases. It would be interesting to model these subtypes with either completely different parameters for each subtype and notice what are the similarities and differences among them, or to model them as one set of parameters for the disease, where its subtypes occur simply based on seeding different brain regions. Another way to fit the parameters so as to not depend on the EBM would be to use longitudinal data as done for example by Raj et al. [41].

In Chapter 6, I link the work presented in this chapter with the work of Chapter 4, changing the brain scale modelling to a certain extent, while the neuronal scale modelling remains largely unchanged.

Chapter 6

Linking the neuronal scale with the brain scale

In Chapter 4, I presented computational modelling of neurodegenerative diseases at the neuronal scale, where the neurobiological mechanisms that govern pathogenic proteins occur, but there is no viable validation methodology. On the other hand, in Chapter 5, I presented computational modelling of neurodegenerative diseases at the brain scale, where most patient empirical data is acquired, but the brain scale is remote from the neurobiological processes. In this chapter, I link the two scales, so that models of neurobiological mechanisms that occur at the neuronal scale can be validated based on their ability to predict atrophy progression for different neurodegenerative diseases with data that is available at the brain scale.

There has not been previous similar work that has attempted to link these two scales. In order to link them, I combined the work of the previous two chapters by modelling a brain network where each brain region is modelled as a number of cortical columns. At the neuronal scale, each neuron's dendrites, soma, and axon contained a concentration of non-pathogenic and pathogenic protein, and the mechanisms modelled were similar to those of Chapter 4: production, clearance, misfolding, neuronal network diffusion, active transport, neuronal frequency related spread, a toxic effect on the firing frequencies of the neurons, neuronal toxicity, and neuronal death. At the brain scale, I modelled symmetric grey matter brain regions as spherical volumes, modelling atrophy, extracellular diffusion, and four types of

spread based on functional, structural, or effective connectivity: (1) fast spread, (2) diffusive spread, (3) brain regional frequency related fast spread, and (4) brain regional frequency related diffusive spread.

For each simulation, I tracked brain atrophy, which was compared to the population average atrophy progression given by event based models [64, 77]: one for ApoE 4 positive Alzheimer's disease, and one for each of the three genetic variants of frontotemporal dementia related to chromosome 9 open reading frame 72, progranulin, and the microtubule associated protein tau mutations (hereafter simply referred to as AD, C9orf72, GRN, and MAPT, respectively). The EBMs constructed were similar to the one I used in Chapter 5, except that the grey matter regions used in this chapter were larger, and accounted for most of the grey matter of the brain. The decision for the change in the modelled regions was two-fold: a) calculating effective connectivity for many regions is memory-intensive, and based on the parcellation scheme used, there were 27 large grey matter regions given by default, and b) unlike the previous chapter, I wanted to compare results among the four diseases, thus the same regions had to be used, rather than the specific regions which were most relevant to each specific disease.

I determined the optimal model and model parameters for each neurodegenerative disease, thus determining their underlying controlling mechanisms. Finding the seed locations is of interest since they could potentially be different than the first region to show atrophy in the EBM. I also discovered the primary mechanisms responsible for protein spread in each disease. Additionally, I performed a sensitivity analysis to discover how much alteration of each parameter is required before the atrophy order given with the altered parameters diverges (where divergence was assumed to occur when the Kendall Tau distance was higher than 0.017, or six changes in the atrophy order) from the atrophy order given by the simulation with the optimal parameters. Lastly, I showcase how such information can suggest targets for therapeutic intervention.

6.1 Methodology

Structural, functional, and diffusion-weighted MRI scans from 10 healthy subjects were used to generate a graph representation of the healthy brain network, where symmetric grey matter brain regions were the nodes of the graph. Each brain region was represented at the neuronal scale as a number of cortical columns. I modelled multiple pathogenic protein mechanisms. After initialising the network, and seeding pathogenic protein into it, I ran simulations, using the modelled mechanisms to update the network state at each timestep t, until the entire network atrophied.

6.1.1 Image dataset and processing

The images used and the image processing procedures used were exactly the same as those presented in Section 5.1.1, although the brain region parcellation was used to extract larger regions of interest for the work of this chapter. There were $\mathrm{NReg} = 27$ symmetric grey matter regions, denoted by $r \in \{1, ..., \mathrm{NReg}\}$, with associated barycentric coordinates $\mathbf{Coor}_r$, and volumes $V_r(t)$. I defined $\mathbf{D}_{r \leftarrow \bar{r}}$ as a matrix whose elements are the Euclidean distances among brain regions. I defined $\mathbf{F}_{r \leftarrow \bar{r}}$ as the functional connectivity matrix, $\mathbf{S}_{r \leftarrow \bar{r}}$ as the structural connectivity matrix, and $\mathbf{E}_{r \leftarrow \bar{r}}$ as the effective connectivity matrix. I defined the normalised absolute functional, structural, and effective connectivity matrices $\mathbf{NAF}_{r \leftarrow \bar{r}} = \frac{|\mathbf{F}_{r \leftarrow \bar{r}}|}{\sum_{k=1}^{\mathrm{NReg}} \sum_{\bar{k}=1}^{\mathrm{NReg}} |\mathbf{F}_{k \leftarrow \bar{k}}|}$, $\mathbf{NAS}_{r \leftarrow \bar{r}} = \frac{|\mathbf{S}_{r \leftarrow \bar{r}}|}{\sum_{k=1}^{\mathrm{NReg}} \sum_{\bar{k}=1}^{\mathrm{NReg}} |\mathbf{S}_{k \leftarrow \bar{k}}|}$, and $\mathbf{NAE}_{r \leftarrow \bar{r}} = \frac{|\mathbf{E}_{r \leftarrow \bar{r}}|}{\sum_{k=1}^{\mathrm{NReg}} \sum_{\bar{k}=1}^{\mathrm{NReg}} |\mathbf{E}_{k \leftarrow \bar{k}}|}$, respectively.

6.1.2 General modelling

Brain regions were represented as a number of cortical columns (between 1 and 15) $\mathrm{NCol}_r = \lceil 15 V_r(0) / \max_r V_r(0) \rceil$, with the number depending on their initial volumes, although the biologically realistic number of cortical columns is much higher (see Section 2.1.2). However, since the modelling of the cortical columns is not highly accurate, but a simplification, adding more columns would have no real impact on results, and 1 to 15 columns was a good balance between computational requirement and contrast between large and small brain regions. Cortical column and neuronal characteristics remained the same as in Chapter 4, with each region having a total of $\mathrm{NNeu}_r = 470 \times \mathrm{NCol}_r$ neurons. Each neuron $i | r \in$

$\{1,...,\text{NNeu}_r\}$ belonged to a cortical column $\text{Col}_{i|r} \in \{1,...,\text{NCol}_r\}$, cortical column layer $\text{Lay}_{i|r} \in \{2,4,5,6\}$, and had a type $\text{Type}_{i|r} \in \{\text{RS,IB,FS,LTS}\}$. I defined each compartment's diameter $\text{Diam}_{i,j=1|r} = 2, \text{Diam}_{i,j=2|r} = 30, \text{Diam}_{i,j=3|r} = 1$, length $\text{Len}_{i,j=1|r} = 500, \text{Len}_{i,j=2|r} = 30, \text{Len}_{i,j=3|r} = 200$, base area $\text{Area}_{i,j|r} = \pi(\text{Diam}_{i,j|r}/2)^2$, and volume $\text{Vol}_{i,j|r} = \text{Len}_{i,j|r} \times \text{Area}_{i,j|r}$. Each compartment contained a concentration of non-pathogenic protein $\text{Cn}_{i,j|r}(t)$ and pathogenic protein $\text{Cp}_{i,j|r}(t)$. These concentrations are easily convertible to and from quantities $\text{Qn}_{i,j|r}(t) = \text{Cn}_{i,j|r}(t) \times \text{Vol}_{i,j|r}$, $\text{Qp}_{i,j|r}(t) = \text{Cp}_{i,j|r}(t) \times \text{Vol}_{i,j|r}$. Concentrations were normalised at certain steps to ensure they were non-negative, and to ensure their sum was never higher than one ($\text{Cn}_{i,j|r}(t) + \text{Cp}_{i,j|r}(t) \leq 1$).

Each neuron had a voltage threshold $\text{Vth}_{i|r}(t)$ which determined whether a neuron had an action potential or not. In Chapter 4, I simulated neuronal activity and action potentials of neurons using the NEURON simulator. However, I did not use NEURON for this chapter due to its high computational overhead (approximately 10 times slower computation). The only interaction between neuronal activity and pathogenic protein mechanisms that NEURON simulated was protein spread related to action potentials. Therefore, I had to approximate action potentials by using NEURON to calculate the average firing frequencies of neurons of each type and layer for different values of $\text{Vth}_{i|r}(t)$, and then used a simple nearest neighbour regression to define the firing frequency of each neuron $\text{fr}_{i|r}(t)$ (firing frequencies were normalised so that the maximum firing frequency possible was equal to one) as a function of $\text{Vth}_{i|r}(t)$, the type of neuron i, and the layer of neuron i.

I assumed that whenever protein spread from one brain region to another through the brain network (as opposed to extracellular spread), it could only do so from axonal compartments from the set of 'output neurons' Out_r, and could only spread to dendritic compartments of the set of 'input neurons' In_r. Layer 2 and 3 excitatory neurons are generally considered as the neurons that receive input from, and project output to other cortical structures, as described in Section 2.1.2. Therefore, I set $\text{In}_r = \{i|r, s.t.\ \text{Type}_{i|r} = \text{RS,IB}, \text{Lay}_{i|r} = 2\}$ and $\text{Out}_r = \{i|r, s.t.\ \text{Type}_{i|r} = \{\text{RS,IB}\}, \text{Lay}_{i|r} = 2\}$. I defined $\mathbf{SS}_{i,j|r \leftarrow \bar{i},\bar{j}|r}$ as the strength of a synapse starting from

neuronal compartment $\bar{i}, \bar{j}|r$, and connecting to postsynaptic neuronal compartment $i, j|r$. When there was no synaptic connection, then $\mathbf{SS}_{i,j|r \leftarrow \bar{i},\bar{j}|r} = 0$ (see Neymotin et al. [241] for values).

6.1.3 Neuronal scale accumulation: production, clearance, and misfolding

I modelled protein production, clearance, and misfolding exactly as I did in Chapter 4. I assumed production $\text{CnProd}_{i,j|r}(t)$ and $\text{CpProd}_{i,j|r}(t)$ occurred at constant production rates R_{nProd} and R_{pProd}, respectively, until neuronal death (Eq. 6.1). Given clearance rates R_{nClear} and R_{pClear}, and healthy protein concentration levels CnHealth and CpHealth, I defined $\text{CnClear}_{i,j|r}(t)$ and $\text{CpClear}_{i,j|r}(t)$ as clearance terms (Eq. 6.2). Given a misfolding rate R_{Mis}, I defined $\text{CnMis}_{i,j|r}(t)$ and $\text{CpMis}_{i,j|r}(t)$ as the misfolding terms (Eq. 6.3). I defined $\text{QnAcc}_{i,j|r}(t)$ and $\text{QpAcc}_{i,j|r}(t)$ as the net change in protein quantity from accumulation (Eq. 6.4).

$$\begin{aligned}
\text{CnProd}_{i,j|r}(t) &= \begin{cases} R_{\text{nProd}}, \text{ if } j = 2 \\ 0, \text{ otherwise} \end{cases} \\
\text{CpProd}_{i,j|r}(t) &= \begin{cases} R_{\text{pProd}}, \text{ if } j = 2 \\ 0, \text{ otherwise} \end{cases}
\end{aligned} \tag{6.1}$$

$$\begin{aligned}
\text{CnClear}_{i,j|r}(t) &= -R_{\text{nClear}} \log\left(1 + (e-1)\frac{\text{Cn}_{i,j|r}(t)}{\text{CnHealth}}\right) \\
\text{CpClear}_{i,j|r}(t) &= -R_{\text{pClear}} \log\left(1 + (e-1)\frac{\text{Cp}_{i,j|r}(t)}{\text{CpHealth}}\right)
\end{aligned} \tag{6.2}$$

$$\begin{aligned}
\text{CnMis}_{i,j|r}(t) &= -R_{\text{Mis}}\text{Cn}_{i,j|r}(t)\text{Cp}_{i,j|r}(t) \\
\text{CpMis}_{i,j|r}(t) &= +R_{\text{Mis}}\text{Cn}_{i,j|r}(t)\text{Cp}_{i,j|r}(t)
\end{aligned} \tag{6.3}$$

$$\begin{aligned}
\text{QnAcc}_{i,j|r}(t) &= \left[\text{CnProd}_{i,j|r}(t) + \text{CnClear}_{i,j|r}(t) + \text{CnMis}_{i,j|r}(t)\right] \text{Vol}_{i,j|r} \\
\text{QpAcc}_{i,j|r}(t) &= \left[\text{CpProd}_{i,j|r}(t) + \text{CpClear}_{i,j|r}(t) + \text{CpMis}_{i,j|r}(t)\right] \text{Vol}_{i,j|r}
\end{aligned} \tag{6.4}$$

6.1.4 Neuronal scale spread: neuronal network diffusion, active transport, and neuronal frequency related spread

I modelled three types of neuronal scale spread with minor changes compared to their modelling presented in Chapter 4. Specifically, Algorithm 1 shown in Section 4.2.5 was not used in order to reduce computational and memory requirements requirements, and neuronal frequency related spread was based on the estimated firing frequencies of neurons, rather than individual action potentials.

Neuronal network diffusion $\mathbf{NND}_{i,j|r\leftarrow\bar{i},\bar{j}|r}(t)$ (Eq. 6.7) modelled passive slow Brownian motion of protein, with speed σ_{NND}, and weights $\mathbf{WNND}_{i,j|r\leftarrow\bar{i},\bar{j}|r}$ (Eq. 6.5). I defined $\mathbf{Ent}_{i,j|r\leftarrow\bar{i},\bar{j}|r}$ as the probability of protein managing to pass through the entrance from $\bar{i},\bar{j}$ to i,j (Eq. 6.6).

$$\mathbf{WNND}_{i,j|r\leftarrow\bar{i},\bar{j}|r} = \begin{cases} 20, \text{ if } i=\bar{i}, \text{ and } \bar{i},\bar{j} \text{ neighbour of } i,j \\ \mathbf{SS}_{i,j|r\leftarrow\bar{i},\bar{j}|r}, \text{ if } i\neq\bar{i}, \text{ and } \bar{i},\bar{j} \text{ neighbour of } i,j \\ 0, \text{ if } \bar{i},\bar{j} \text{ not a neighbour of } i,j \end{cases} \quad (6.5)$$

$$\mathbf{Ent}_{i,j|r\leftarrow\bar{i},\bar{j}|r} = \frac{\min(\mathrm{Area}_{i,j|r},\mathrm{Area}_{\bar{i},\bar{j}|r})}{\mathrm{Area}_{\bar{i},\bar{j}|r}} \quad (6.6)$$

$$\mathbf{NND}_{i,j|r\leftarrow\bar{i},\bar{j}|r}(t) = \mathbf{WNND}_{i,j|r\leftarrow\bar{i},\bar{j}|r}\mathbf{Ent}_{i,j|r\leftarrow\bar{i},\bar{j}|r} \times\Phi\left(-\mathrm{Len}_{\bar{i},\bar{j}|r}/2|0,1000\sigma_{\mathrm{NND}}\right) \quad (6.7)$$

I modelled active transport $\mathbf{ACT}_{i,j|r\leftarrow\bar{i},\bar{j}|r}(t)$ (Eq. 6.8) similarly to Chapter 4.

$$\mathbf{ACT}_{i,j|r\leftarrow\bar{i},\bar{j}|r}(t) = \begin{cases} 0.8258, \text{ if } i=\bar{i}, \text{ and } \bar{j}=1, j=1 \\ 0.1742, \text{ if } i=\bar{i}, \text{ and } \bar{j}=1, j=2 \\ 0.1160, \text{ if } i=\bar{i}, \text{ and } \bar{j}=2, j=1 \\ 0.73, \text{ if } i=\bar{i}, \text{ and } \bar{j}=2, j=2 \\ 0.1540, \text{ if } i=\bar{i}, \text{ and } \bar{j}=2, j=3 \\ 0.1371, \text{ if } i=\bar{i}, \text{ and } \bar{j}=3, j=2 \\ 0.8629, \text{ if } i=\bar{i}, \text{ and } \bar{j}=3, j=3 \\ 0, \text{otherwise} \end{cases} \tag{6.8}$$

Neuronal frequency related spread $\mathbf{NFS}_{i,j|r\leftarrow\bar{i},\bar{j}|r}(t)$ modelled protein spread between neurons based on the firing frequency of the source neuron, and their synaptic strengths (Eq. 6.9).

$$\mathbf{NFS}_{i,j|r\leftarrow\bar{i},\bar{j}|r}(t) = \mathbf{SS}_{i,j|r\leftarrow\bar{i},\bar{j}|r}\mathrm{fr}_{\bar{i}|r}(t) \tag{6.9}$$

I also defined f_{NND}, f_{ACT}, and f_{NFS} as the intrinsic probability of protein spreading with each respective neuronal scale spread mechanism. These parameters could only take non-negative values, and their sum had to be lower or equal to one, as they are probabilities and if their sum was higher than one, then it would be possible for a compartment to spread more protein in a timestep than it originally had. Note that each of the columns of the matrices $\mathbf{NND}_{i,j|r\leftarrow\bar{i},\bar{j}|r}(t)$, $\mathbf{ACT}_{i,j|r\leftarrow\bar{i},\bar{j}|r}(t)$, and $\mathbf{NFS}_{i,j|r\leftarrow\bar{i},\bar{j}|r}(t)$ indicate what fraction of protein spreads out of $\bar{i},\bar{j}|r$ towards each other compartment (including itself), and thus the columns were normalised at every timestep so that they summed to one. I defined $\mathrm{QnNSS}_{i,j|r}(t)$ and $\mathrm{QpNSS}_{i,j|r}(t)$ as the net change in protein quantity from neuronal scale spread mechanisms (Eq. 6.10).

$$
\begin{aligned}
\mathrm{QnNSS}_{i,j|r}(t) = \sum_{\bar{i}=1}^{\mathrm{NNeu}_r} \sum_{\bar{j}=1}^{3} \quad & f_{\mathrm{NND}}\mathbf{NND}_{i,j|r\leftarrow\bar{i},\bar{j}|r}(t)\mathrm{Qn}_{\bar{i},\bar{j}|r}(t) + \\
& f_{\mathrm{ACT}}\mathbf{ACT}_{i,j|r\leftarrow\bar{i},\bar{j}|r}(t)\mathrm{Qn}_{\bar{i},\bar{j}|r}(t) + \\
& f_{\mathrm{NFS}}\mathbf{NFS}_{i,j|r\leftarrow\bar{i},\bar{j}|r}(t)\mathrm{Qn}_{\bar{i},\bar{j}|r}(t) - \\
& (f_{\mathrm{NND}} + f_{\mathrm{ACT}} + f_{\mathrm{NFS}})\mathrm{Qn}_{i,j|r} \\
\mathrm{QpNSS}_{i,j|r}(t) = \sum_{\bar{i}=1}^{\mathrm{NNeu}_r} \sum_{\bar{j}=1}^{3} \quad & f_{\mathrm{NND}}\mathbf{NND}_{i,j|r\leftarrow\bar{i},\bar{j}|r}(t)\mathrm{Qp}_{\bar{i},\bar{j}|r}(t) + \\
& f_{\mathrm{ACT}}\mathbf{ACT}_{i,j|r\leftarrow\bar{i},\bar{j}|r}(t)\mathrm{Qp}_{\bar{i},\bar{j}|r}(t) + \\
& f_{\mathrm{NFS}}\mathbf{NFS}_{i,j|r\leftarrow\bar{i},\bar{j}|r}(t)\mathrm{Qp}_{\bar{i},\bar{j}|r}(t) - \\
& (f_{\mathrm{NND}} + f_{\mathrm{ACT}} + f_{\mathrm{NFS}})\mathrm{Qp}_{i,j|r}
\end{aligned} \tag{6.10}
$$

6.1.5 Neuronal scale toxicity: toxicity levels, toxic effect, and neuronal death

I defined $\mathrm{Txc}_{i|r}(t)$ (Eq. 6.11) as the toxicity level within a neuron, given a toxicity rate R_{Txc}, and a minimum concentration Cmin. Toxicity levels started at zero $\mathrm{Txc}_{i|r}(0) = 0$, and increased as a function of protein concentration. I modelled that neuronal toxicity levels directly increased or decreased the firing frequencies of neurons. After the toxicity level of a neuron reached a value of one, the neuron would be considered dead for the remainder of the simulation. I defined the set of dead neurons $\mathrm{Dead}_r(t) = \{i|r, s.t.\ \mathrm{Txc}_{i|r}(t) = 1\}$, and the set of alive neurons $\mathrm{Alive}_r(t) = \{i|r, s.t.\ \mathrm{Txc}_{i|r}(t) < 1\}$. I also defined the set of alive outputs $\mathrm{OutAl}_r(t) = \{i|r, s.t.\ i|r \in \mathrm{Out}_r \text{ and } i|r \in \mathrm{Alive}_r(t)\}$, and the set of alive inputs $\mathrm{InAl}_r(t) = \{i|r, s.t.\ i|r \in \mathrm{In}_r \text{ and } i|r \in \mathrm{Alive}_r(t)\}$. Neuronal death affected the modelled mechanisms: (a) protein production and clearance could not occur at dead neuronal compartments, (b) protein misfolding could still occur at dead neuronal compartments, (c) protein could not spread into dead neuronal compartments via neuronal network diffusion, neuronal frequency related spread, extracellular diffusion, or any of the brain network related spread mechanisms, but could still do so

via active transport, and (d) protein could not spread out of dead neuronal compartments via neuronal frequency related spread, or any of the brain network related spread mechanisms, but could still do so via neuronal network diffusion, active transport, and extracellular diffusion.

$$\mathrm{Txc}_{i|r}(t) = \mathrm{Txc}_{i|r}(t-1) + \max\left\{0, R_{\mathrm{Txc}}\left[\exp\left(10\sum_{j}\frac{\mathrm{Cn}_{i,j|r}(t)+\mathrm{Cp}_{i,j|r}(t)}{3} - \mathrm{Cmin}\right) - 1\right]\right\} \quad (6.11)$$

6.1.6 Brain scale atrophy

I defined atrophy $A_r(t)$, which is equal to the proportion of dead neurons of the respective brain region's cortical columns (Eq. 6.12). Atrophy had a reverse relationship with regional volume $V_r(t)$ (Eq. 6.13), and regional radius $\rho_r(t)$ (Eq. 6.14).

$$A_r(t) = \frac{|\mathrm{Dead}_r(t)|}{\mathrm{NNeu}_r} \quad (6.12)$$

$$V_r(t) = (1 - A_r(t))\, V_r(0) \quad (6.13)$$

$$\rho_r(t) = (1 - A_r(t))\, \rho_r(0) \quad (6.14)$$

6.1.7 Brain scale spread: extracellular diffusion, fast network spread, diffusive network spread, fast frequency related spread, and diffusive frequency related spread

I modelled thirteen types of brain scale spread mechanisms (explained below), using information from the Euclidean distances, as well as the functional connectivity, structural connectivity, and effective connectivity to study whether such information plays a role in neurodegenerative disease progression. This information was used to model combinations of fast spread through network connections, slow diffusive spread through network connections and via the extracellular space, and spread related to brain regional neuronal activity.

Functional and structural connectivity have been modelled before in similar work and found to be predictive of neurodegeneration progression, but never in conjunction. Along with effective connectivity, they are the three connectivity metrics that can be fairly easily calculated for individual subjects. I chose to model fast, slow diffusive, and electrical activity based spread as they are three vastly different, but also basic and simple mechanisms of spread. Additionally, extracellular diffusion is commonly thought of as a potential mechanism of spread.

Extracellular diffusion $\mathbf{ED}_{i,j|r\leftarrow\bar{i},\bar{j}|\bar{r}}(t)$ (Eq. 6.16) was modelled similarly to Chapter 5, and it modelled Brownian motion in the extracellular space. I simplified the modelling by assuming that protein spread out of a brain region was based on an isotropic 3D normal distribution, with mean equal to the source region's coordinates $\mathbf{Coor}_r$, and standard deviation equal to the extracellular diffusion speed σ_{ED}. Under this assumption, the probability of protein spreading to a brain region was determined by the integral of that normal distribution. To simplify this further, I calculated the integral of a 1D normal distribution instead (with zero mean) between the destination region's closest and furthest point from the source region. An illustration of extracellular diffusion is shown in Figure 5.1.

$$\begin{aligned}\mathbf{Int}_{r\leftarrow\bar{r}}(t) &= \Phi\left(\mathbf{D}_{r\leftarrow\bar{r}}+\rho_r(t)|0,\sigma_{\text{ED}}\right)- \\ &\quad \Phi\left(\mathbf{D}_{r\leftarrow\bar{r}}-\rho_r(t)|0,\sigma_{\text{ED}}\right) \qquad (6.15)\end{aligned}$$

$$\mathbf{ED}_{i,j|r\leftarrow\bar{i},\bar{j}|\bar{r}}(t) = \begin{cases} \frac{\text{Vol}_{i,j|r}}{\sum_{k\in\text{Alive}_r(t)}\sum_{l=1}^{3}\text{Vol}_{k,l|r}} f_{\text{ED}} \frac{\mathbf{Int}_{r\leftarrow\bar{r}}(t)}{\sum_{m=1}^{\text{NReg}}\mathbf{Int}_{m\leftarrow\bar{m}}(t)},\ldots \\ \ldots \text{ if } i|r\in\text{InAl}_r(t) \\ 0, \text{ otherwise}\end{cases} \qquad (6.16)$$

I also modelled four types of brain network spread: fast (FW), diffusive (DW), fast frequency related (FF), and diffusive frequency related (DF). Each of the four types of spread was used in conjunction with each of the three network connectivity matrices $\mathbf{F}_{r\leftarrow\bar{r}}$, $\mathbf{S}_{r\leftarrow\bar{r}}$, or $\mathbf{E}_{r\leftarrow\bar{r}}$, for a total of twelve brain network spread mechanisms. All of these mechanisms spread protein out of axons of alive output neurons

$\mathrm{OutAl}_r(t)$, and into dendrites of alive input neurons $\mathrm{InAl}_r(t)$, where $\mathbf{CA}_{i,j|r\leftarrow\bar{i},\bar{j}|\bar{r}}(t)$ indicates whether there was a connection from $\bar{i},\bar{j}|\bar{r}$ to $i,j|r$ at timestep t (Eq. 6.17).

$$\mathbf{CA}_{i,j|r\leftarrow\bar{i},\bar{j}|\bar{r}}(t) = \begin{cases} 1, \text{ if } i|r \in \mathrm{InAl}_r(t) \text{ and } \bar{i}|\bar{r} \in \mathrm{OutAl}_{\bar{r}}(t) \text{ and } ... \\ ... \ r \neq \bar{r} \text{ and } j = 1 \text{ and } \bar{j} = 3 \\ 0, \text{ otherwise} \end{cases} \tag{6.17}$$

Fast spread was a simple linear model of the absolute values of the respective connectivity matrices, representing direct and quick spread between brain regions, unaffected by synaptic activity or distance. Diffusive spread was the same as fast spread, but also took into account distance between brain regions, assuming that protein could spread faster to closer regions. This intracellular diffusion was modelled as Brownian motion by using the cumulative distribution function of the 1D normal distribution $\Phi(x|\mu,\sigma)$ with $\mu = 0,\ \sigma = \sigma_{\mathrm{ID}}$ and $x = -\mathbf{D}_{r\leftarrow\bar{r}}/2$, which is the half of the distance between two regions, assuming that any protein that spread past the half of the distance between them, would continue and actually reach the destination brain region. Fast frequency related and diffusive frequency related spread were similar to fast spread, and diffusive spread, respectively, but the quantity of protein that spread out of each output neuron axon was also determined by its firing frequency, under the assumption that the amount of protein molecules spreading out of a neuron depended on its electrical activity.

I defined f_{ED}, $f_{\mathrm{FW|F}}$, $f_{\mathrm{FW|S}}$, $f_{\mathrm{FW|E}}$, $f_{\mathrm{DW|F}}$, $f_{\mathrm{DW|S}}$, $f_{\mathrm{DW|E}}$, $f_{\mathrm{FF|F}}$, $f_{\mathrm{FF|S}}$, $f_{\mathrm{FF|E}}$, $f_{\mathrm{DF|F}}$, $f_{\mathrm{DF|S}}$, and $f_{\mathrm{DF|E}}$ as the intrinsic probability of protein spreading with each respective mechanism. These took non-negative values, and their sum was restricted to be less than or equal to one. The probability of protein spreading from $\bar{i},\bar{j}|\bar{r}$ to $i,j|r$ with each of these mechanisms is given by $\mathbf{ED}_{i,j|r\leftarrow\bar{i},\bar{j}|\bar{r}}(t)$ (Eq. 6.16) for extracellular diffusion; by $\mathbf{FW|F}_{i,j|r\leftarrow\bar{i},\bar{j}|\bar{r}}(t)$, $\mathbf{FW|S}_{i,j|r\leftarrow\bar{i},\bar{j}|\bar{r}}(t)$, and $\mathbf{FW|E}_{i,j|r\leftarrow\bar{i},\bar{j}|\bar{r}}(t)$ (Eq. 6.18) for fast spread related to functional, structural, and effective connectivity, respectively; by $\mathbf{DW|F}_{i,j|r\leftarrow\bar{i},\bar{j}|\bar{r}}(t)$, $\mathbf{DW|S}_{i,j|r\leftarrow\bar{i},\bar{j}|\bar{r}}(t)$, and $\mathbf{DW|E}_{i,j|r\leftarrow\bar{i},\bar{j}|\bar{r}}(t)$ (Eq. 6.19) for diffusive spread; by $\mathbf{FF|F}_{i,j|r\leftarrow\bar{i},\bar{j}|\bar{r}}(t)$,

$\mathbf{FF}|\mathbf{S}_{i,j|r\leftarrow\bar{i},\bar{j}|\bar{r}}(t)$, and $\mathbf{FF}|\mathbf{E}_{i,j|r\leftarrow\bar{i},\bar{j}|\bar{r}}(t)$ (Eq. 6.20) for fast frequency related spread; and by $\mathbf{DF}|\mathbf{F}_{i,j|r\leftarrow\bar{i},\bar{j}|\bar{r}}(t)$, $\mathbf{DF}|\mathbf{S}_{i,j|r\leftarrow\bar{i},\bar{j}|\bar{r}}(t)$, and $\mathbf{DF}|\mathbf{E}_{i,j|r\leftarrow\bar{i},\bar{j}|\bar{r}}(t)$ (Eq. 6.21) for diffusive frequency related spread. Equations are shown below for functional connectivity related spread only; those based on structural or effective connectivity were similarly defined. Fig 6.1 is an illustration of these twelve brain scale spread mechanisms. Note that Fig 6.1 describes the spread between cortical columns of different brain regions. Cortical columns within the same brain region are highly interconnected as well, as described in Chapter 4.

$$\mathbf{FW}|\mathbf{F}_{i,j|r\leftarrow\bar{i},\bar{j}|\bar{r}}(t) = f_{\mathrm{FW|F}}\frac{\mathbf{NAF}_{r\leftarrow\bar{r}}}{|\mathrm{In}_r|} \tag{6.18}$$

$$\mathbf{DW}|\mathbf{F}_{i,j|r\leftarrow\bar{i},\bar{j}|\bar{r}}(t) = f_{\mathrm{DW|F}}\frac{\mathbf{NAF}_{r\leftarrow\bar{r}}}{|\mathrm{In}_r|}2\left[\Phi(-\mathbf{D}_{r\leftarrow\bar{r}}/2|0,\sigma_{\mathrm{ID}})\right] \tag{6.19}$$

$$\mathbf{FF}|\mathbf{F}_{i,j|r\leftarrow\bar{i},\bar{j}|\bar{r}}(t) = f_{\mathrm{FF|F}}\mathrm{fr}_{\bar{i}|\bar{r}}(t)\frac{\mathbf{NAF}_{r\leftarrow\bar{r}}}{|\mathrm{In}_r|} \tag{6.20}$$

$$\mathbf{DF}|\mathbf{F}_{i,j|r\leftarrow\bar{i},\bar{j}|\bar{r}}(t) = f_{\mathrm{DF|F}}\mathrm{fr}_{\bar{i}|\bar{r}}(t)\frac{\mathbf{NAF}_{r\leftarrow\bar{r}}}{|\mathrm{In}_r|}2\left[\Phi(-\mathbf{D}_{r\leftarrow\bar{r}}/2|0,\sigma_{\mathrm{ID}})\right] \tag{6.21}$$

6.1.8 Neuronal and brain scale interaction

I defined $\mathbf{BSS}_{i,j|r\leftarrow\bar{i},\bar{j}|\bar{r}}(t)$ (Eq. 6.22) as the overall probability of protein spreading via brain scale spread mechanisms from $\bar{i},\bar{j}|\bar{r}$ to $i,j|r$.

$$\begin{aligned}\mathbf{BSS}_{i,j|r\leftarrow\bar{i},\bar{j}|\bar{r}}(t) = \mathbf{ED}_{i,j|r\leftarrow\bar{i},\bar{j}|\bar{r}}(t) + \mathbf{CA}_{i,j|r\leftarrow\bar{i},\bar{j}|\bar{r}}(t)\times\\ [\mathbf{FW}|\mathbf{F}_{i,j|r\leftarrow\bar{i},\bar{j}|\bar{r}}(t) + \mathbf{FW}|\mathbf{S}_{i,j|r\leftarrow\bar{i},\bar{j}|\bar{r}}(t) + \mathbf{FW}|\mathbf{E}_{i,j|r\leftarrow\bar{i},\bar{j}|\bar{r}}(t) +\\ \mathbf{DW}|\mathbf{F}_{i,j|r\leftarrow\bar{i},\bar{j}|\bar{r}}(t) + \mathbf{DW}|\mathbf{S}_{i,j|r\leftarrow\bar{i},\bar{j}|\bar{r}}(t) + \mathbf{DW}|\mathbf{E}_{i,j|r\leftarrow\bar{i},\bar{j}|\bar{r}}(t) +\\ \mathbf{FF}|\mathbf{F}_{i,j|r\leftarrow\bar{i},\bar{j}|\bar{r}}(t) + \mathbf{FF}|\mathbf{S}_{i,j|r\leftarrow\bar{i},\bar{j}|\bar{r}}(t) + \mathbf{FF}|\mathbf{E}_{i,j|r\leftarrow\bar{i},\bar{j}|\bar{r}}(t) +\\ \mathbf{DF}|\mathbf{F}_{i,j|r\leftarrow\bar{i},\bar{j}|\bar{r}}(t) + \mathbf{DF}|\mathbf{S}_{i,j|r\leftarrow\bar{i},\bar{j}|\bar{r}}(t) + \mathbf{DF}|\mathbf{E}_{i,j|r\leftarrow\bar{i},\bar{j}|\bar{r}}(t)]\end{aligned} \tag{6.22}$$

I defined $\mathrm{QnBSSadd}_{i,j|r}(t)$ and $\mathrm{QpBSSadd}_{i,j|r}(t)$ (Eq. 6.23) as the protein quantity that spread via brain scale spread mechanisms into $i,j|r$. I similarly defined $\mathrm{QnBSSrem}_{i,j|r}(t)$ and $\mathrm{QpBSSrem}_{i,j|r}(t)$ (Eq. 6.24) for the protein quantity

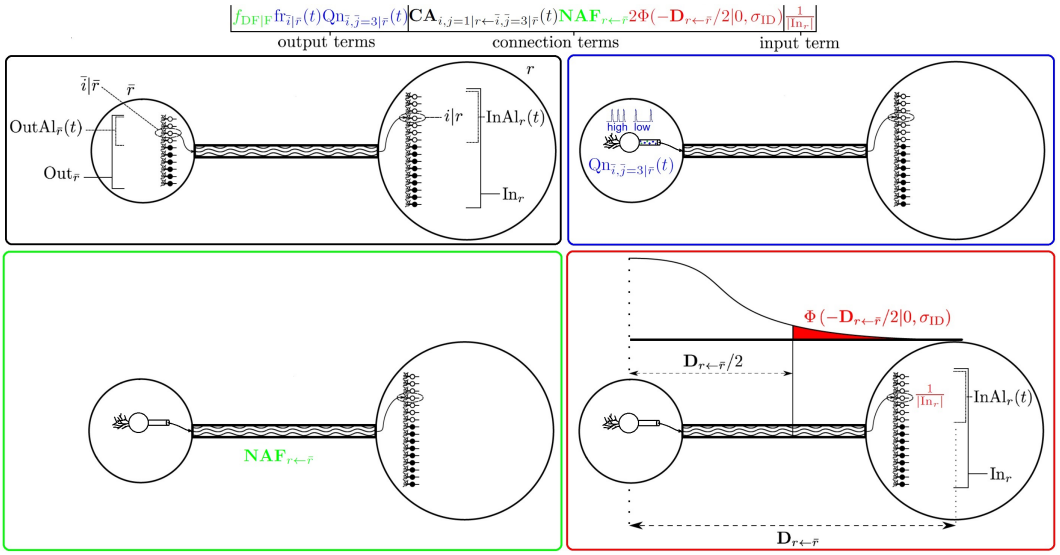

Figure 6.1: An illustration of the brain scale network based spread mechanisms. This figure demonstrates how protein would spread from the axon of neuron $\bar{i}|\bar{r}$ to the dendrites of neuron $i|r$. The equation at the top is the quantity of non-pathogenic protein that would spread via diffusive frequency-related functional connectivity based spread (Eq. 6.21 along with the quantity of normal protein $\mathrm{Qn}_{\bar{i},\bar{j}=3|\bar{r}}(t)$). Top left - black: The connectivity term $\mathbf{CA}_{i,j|r\leftarrow\bar{i},\bar{j}|\bar{r}}(t)$ determines whether the output neuron $\bar{i}|\bar{r}$ is a cortical column output neuron and is alive and the input neuron $i|r$ is a cortical column input neuron and is also alive, and thus whether a connection exists between them or not. Top right - blue: Given a specific output neuron, the amount of protein that will spread depends on the protein quantity currently available at the axon of the output neuron $\mathrm{Qn}_{\bar{i},\bar{j}=3|\bar{r}}(t)$, which, for frequency-related spread mechanisms only, is further modulated by the firing frequency of that neuron $\mathrm{fr}_{\bar{i}|\bar{r}}(t)$ (which are normalised between 0 and 1), with more protein spreading with a higher firing frequency. Bottom left - green: The term $f_{\mathrm{DF|F}}$ is the intrinsic probability of protein spreading via a specific mechanism (in this case diffusive frequency-related functional connectivity based spread), with $\mathbf{NAF}_{r\leftarrow\bar{r}}$ being the weight given from the functional connectivity data. Bottom right - red: In the case of diffusive-based spread mechanisms, protein spreads to r only if it diffuses past the midpoint $\mathbf{D}_{r\leftarrow\bar{r}}/2$, where the term $2\Phi(-\mathbf{D}_{r\leftarrow\bar{r}}/2|0,\sigma_{\mathrm{ID}})$ gives the probability of that event occurring. Finally, the protein that arrives at r is spread into all alive neurons equally, by dividing by In_r, which means that as neurons die, less protein spreads to that region, thus accounting to a degree for axonal loss. Note that all terms take values between 0 and 1 (except for $\mathrm{Qn}_{\bar{i},\bar{j}=3|\bar{r}}(t)$), thus only reducing the quantity that spreads.

that spread out of $i, j|r$. Lastly, I defined $\mathrm{QnBSS}_{i,j|r}(t)$ and $\mathrm{QpBSS}_{i,j|r}(t)$ (Eq. 6.25) as the net change in protein quantity from brain scale spread mechanisms.

$$
\begin{aligned}
\mathrm{QnBSSadd}_{i,j|r}(t) &= \sum_{\bar{i}=1}^{\mathrm{NNeu}_r} \sum_{\bar{j}=1}^{3} \sum_{\bar{r}=1}^{\mathrm{NReg}} \mathbf{BSS}_{i,j|r\leftarrow\bar{i},\bar{j}|\bar{r}}(t)\mathrm{Qn}_{\bar{i},\bar{j}|\bar{r}}(t) \\
\mathrm{QpBSSadd}_{i,j|r}(t) &= \sum_{\bar{i}=1}^{\mathrm{NNeu}_r} \sum_{\bar{j}=1}^{3} \sum_{\bar{r}=1}^{\mathrm{NReg}} \mathbf{BSS}_{i,j|r\leftarrow\bar{i},\bar{j}|\bar{r}}(t)\mathrm{Qp}_{\bar{i},\bar{j}|\bar{r}}(t) \qquad (6.23) \\
\mathrm{QnBSSrem}_{i,j|r}(t) &= \sum_{\bar{i}=1}^{\mathrm{NNeu}_r} \sum_{\bar{j}=1}^{3} \sum_{\bar{r}=1}^{\mathrm{NReg}} \mathbf{BSS}_{\bar{i},\bar{j}|\bar{r}\leftarrow i,j|r}(t)\mathrm{Qn}_{i,j|r}(t) \\
\mathrm{QpBSSrem}_{i,j|r}(t) &= \sum_{\bar{i}=1}^{\mathrm{NNeu}_r} \sum_{\bar{j}=1}^{3} \sum_{\bar{r}=1}^{\mathrm{NReg}} \mathbf{BSS}_{\bar{i},\bar{j}|\bar{r}\leftarrow i,j|r}(t)\mathrm{Qp}_{i,j|r}(t) \qquad (6.24) \\
\mathrm{QnBSS}_{i,j|r}(t) &= \mathrm{QnBSSadd}_{i,j|r}(t) - \mathrm{QnBSSrem}_{i,j|r}(t) \\
\mathrm{QpBSS}_{i,j|r}(t) &= \mathrm{QpBSSadd}_{i,j|r}(t) - \mathrm{QpBSSrem}_{i,j|r}(t) \qquad (6.25)
\end{aligned}
$$

Combining the contributions to protein quantity change from accumulation (Eq. 6.4), neuronal based spread (Eq. 6.10), and brain scale spread (Eq. 6.25), I updated protein quantities at each timestep using the following equation (Eq. 6.26).

$$
\begin{aligned}
\mathrm{Qn}_{i,j|r}(t+1) &= \mathrm{Qn}_{i,j|r}(t) + \mathrm{QnACC}_{i,j|r}(t) + \mathrm{QnNSS}_{i,j|r}(t) + \mathrm{QnBSS}_{i,j|r}(t) \\
\mathrm{Qp}_{i,j|r}(t+1) &= \mathrm{Qp}_{i,j|r}(t) + \mathrm{QpACC}_{i,j|r}(t) + \mathrm{QpNSS}_{i,j|r}(t) + \mathrm{QpBSS}_{i,j|r}(t) \qquad (6.26)
\end{aligned}
$$

6.1.9 Event based modelling

I used EBMs similarly to Chapter 5 with data for each of the four neurodegenerative diseases of this chapter in order to evaluate the atrophy predictive power of the models. I defined $\mathbf{UM}|\mathbf{dis}_{r,o}$, as the probability of region r being o-th in the order of brain regional volumes becoming abnormal based on cross-sectional MR data. More specifically, the EBMs were constructed using the data used by Young et al. [256], which included 1369 AD subjects from Alzheimer's Disease Neuroimaging Initiative (ADNI) and 63 C9orf72, 76 GRN, and 33 MAPT subjects from GE-

Netic Frontotemporal dementia Initiative (GENFI). Thus, for each simulation with parameter set θ, I kept track of the exact timestep that each region's volume became abnormal (i.e., $\text{Tatr}_r(\theta) = \arg\min_t V_r(t) \leq \text{Vthres}_r$). I defined $\text{SO}_r(\theta)$ as the event order position that brain region r became abnormal during a simulation. Thus, the cost function was defined as (Eq. 6.27):

$$\text{C}|\text{dis}(\theta) \quad = \quad -\sum_{r=1}^{\text{NReg}} \log\left(\mathbf{UM}|\mathbf{dis}_{r,\text{SO}_r(\theta)}\right) \tag{6.27}$$

6.2 Results

In all simulations, the initial non-pathogenic protein concentration was set to $\text{Cn}_{i,j|r}(0) = 0.01$, the production rate of non-pathogenic protein was set to $R_{\text{nProd}} = 2e-4$, and the clearance rate of non-pathogenic protein was set to $R_{\text{nClear}} = 2e-4$. Pathogenic protein was assumed to be insoluble ($R_{\text{pClear}} = 0$), and without production ($\text{Cp}_{i,j|r}(0) = 0,\ R_{\text{pProd}} = 0$). The minimum concentration for toxicity was set to $\text{Cmin} = 0.011$.

6.2.1 Neurodegenerative disease parameter optimisation

The parameter set θ included (Eq. 6.28):

$$\begin{aligned}\theta = \{&\text{SeedLoc}, \text{FReffect}, \text{CpSeed}, f_{\text{ED}}, \sigma_{\text{ED}}, f_{\text{FW|F}}, f_{\text{FW|S}}, f_{\text{FW|E}}, f_{\text{DW|F}}, f_{\text{DW|S}}, \cdots \\ &f_{\text{DW|E}}, f_{\text{FF|F}}, f_{\text{FF|S}}, f_{\text{FF|E}}, f_{\text{DF|F}}, f_{\text{DF|S}}, f_{\text{DF|E}}, \sigma_{\text{ID}}, R_{\text{Mis}}, \sigma_{\text{NND}}, f_{\text{NND}}, f_{\text{ACT}}, \cdots \\ &f_{\text{NFS}}, R_{\text{Txc}}\},\end{aligned} \tag{6.28}$$

where SeedLoc determined which brain region had a pathogenic protein seed CpSeed, such that $\text{Cp}_{i,j|r=\text{SeedLoc}}(0) = \text{CpSeed},\ \forall i, j$, and FReffect refers to whether the toxic effect on the firing frequencies was positive or negative.

I computed the optimal set of models and model parameters for ApoE 4 positive AD, θ^{AD}, for C9orf72 FTD, $\theta^{C9orf72}$, for GRN FTD, θ^{GRN}, and for MAPT FTD, θ^{MAPT}, by minimising the cost function with each respective uncertainty ma-

trix using (Eq. 6.29):

$$\theta^{dis} = \arg\min_{\theta} \mathrm{C}|\mathrm{dis}(\theta) \tag{6.29}$$

The best two algorithms (TOMLAB/MULTIMIN and TOMLAB/LGO) based on Figure 2.14 (see Section 2.4.1) are part of a commercial software. I instead chose to download and try the PSWARM and MCS algorithms, which performed well in the tests. In addition, since my code was written in MATLAB, I used MATLAB's own generalised pattern search, particle swarm, and simulated annealing functions (*patternsearch, particleswarm, simulannealbnd*), as they were easy to include in my implementation. MATLAB's particle swarm software consistently optimised and converged faster than the other four algorithms, although it is impossible to know if it converged to the global optimum, or if another algorithm would overtake it and perform better in the long-run. Additionally, certain parameters had to be sampled in a different manner, as suggested in Section 2.4.2. More specifically, CpSeed, f_{ED}, R_{Mis}, f_{NND}, f_{ACT}, f_{NFS}, and R_{Txc} were sampled in a logarithmic space, as the order of magnitude that is appropriate for these parameter values is not known in advance, e.g., viable values for R_{Mis} could be in the 0.0001 to 0.001 range, in the 0.1 to 1 range, etc. The convergence rate can be seen in Figure 6.2 (note that this figure does not contain all of the optimisation runs I performed; I also ran another similar set, for $\approx$180 days, but unfortunately only saved the final best fits).

The log likelihood of the fits were -497 for AD, -81 for C9orf72, -1979 for GRN, and -83 for MAPT. Note that the maximum log likelihood possible, given by the EBM was -38.6007 for AD, -41.9721 for C9orf72, -32.8946 for GRN, and -50.2392 for MAPT. The Kendall Tau distance was 0.34 for AD, 0.13 for C9orf72, 0.26 for GRN, and 0.23 for MAPT.

The optimal parameters are shown in the left part of Figure 6.3. I visualised atrophy in the brain from sagittal and transverse planes in Figure 6.4 at certain timesteps of the simulations that ran with the optimal parameters for each disease. Figure 6.5 displays the confusion matrices calculated by the event based model

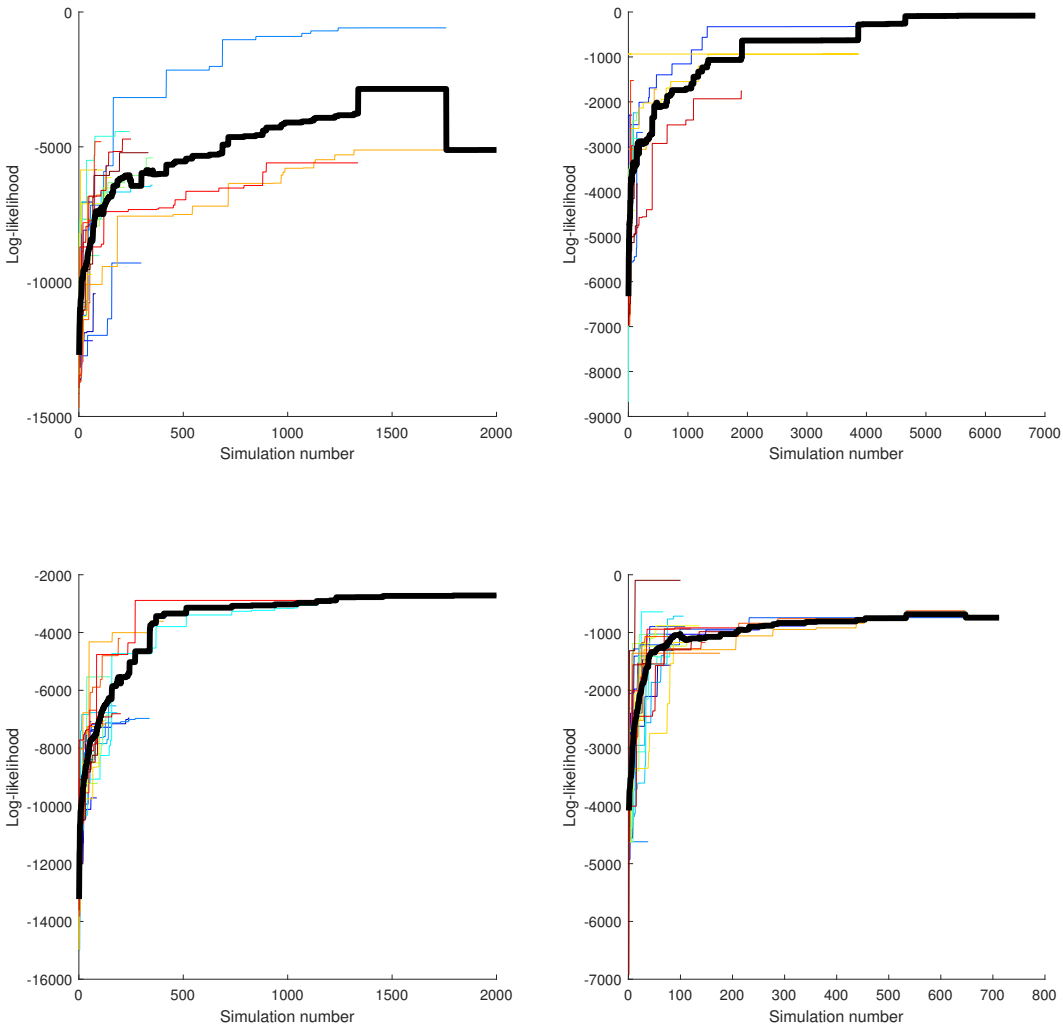

Figure 6.2: Convergence rate of optimisation. Figure displays the maximum log-likelihood found from the optimisation after a certain number of simulations (function evaluations) have occurred. We ran the optimisation with 24 different random initialisations for each disease (each line representing one of them). The thicker black line represents the mean value of the 24 optimisation runs. The optimisation was ran for approximately 35 days. Note that the number of simulations in each case varies, as simulations can run from anywhere between a few timesteps and 1,000,000 timesteps, depending on the chosen parameters. Top left: AD, top right: C9orf72, bottom left: GRN, bottom right: MAPT.

for each of the four neurodegenerative diseases, with the atrophy order from the simulations with the optimal parameters overlaid.

6.2.2 Contribution of protein spread mechanisms

Delineating the degree of protein spread from each spread mechanism in each neurodegenerative disease is of interest. I first performed an analysis to determine whether a simple model where Euclidean distances (suggesting extracellular diffusion), functional connectivity, structural connectivity, or effective connectivity from a predetermined seed region could predict atrophy progression. In AD, decreasing structural connectivity strength from the amygdala best fitted EBM atrophy progression (log likelihood -3913, Kendall Tau distance 0.39). In C9orf72, decreasing functional connectivity strength from the supratemporal best fitted EBM atrophy progression (log likelihood -1398, Kendall Tau distance 0.24). In GRN, there were no good fits, but the best one was with decreasing functional connectivity strength from the medial parietal (log likelihood -6634, Kendall Tau distance 0.39). In MAPT, the best fit was with increasing Euclidean distance from the temporal pole (log likelihood -92, Kendall Tau distance 0.23). Figure 6.6 displays the confusion matrices calculated by the event based model for each of the four neurodegenerative diseases, with the atrophy order from the respective aforementioned connectivity measurements.

Figure 6.7 shows the percentage of protein that spread with each mechanism in the simulations with the optimal parameters for each respective disease.

Figure 6.8 atrophy over time (timesteps) during simulations with the optimal parameters.

6.2.3 Sensitivity analysis via divergence from atrophy pattern

I performed a sensitivity analysis, displayed in Figure 6.3, by starting with the optimal set of parameters values θ^{dis} for each disease as the baseline values, and then increased or decreased one parameter's value at a time until a change occurred in the atrophy order of brain regions $\mathrm{SO}_r(\theta^{dis} \pm \theta^{\mathrm{offset}})$. This procedure determined what the minimally required change in a parameter was in order to produce changes in the

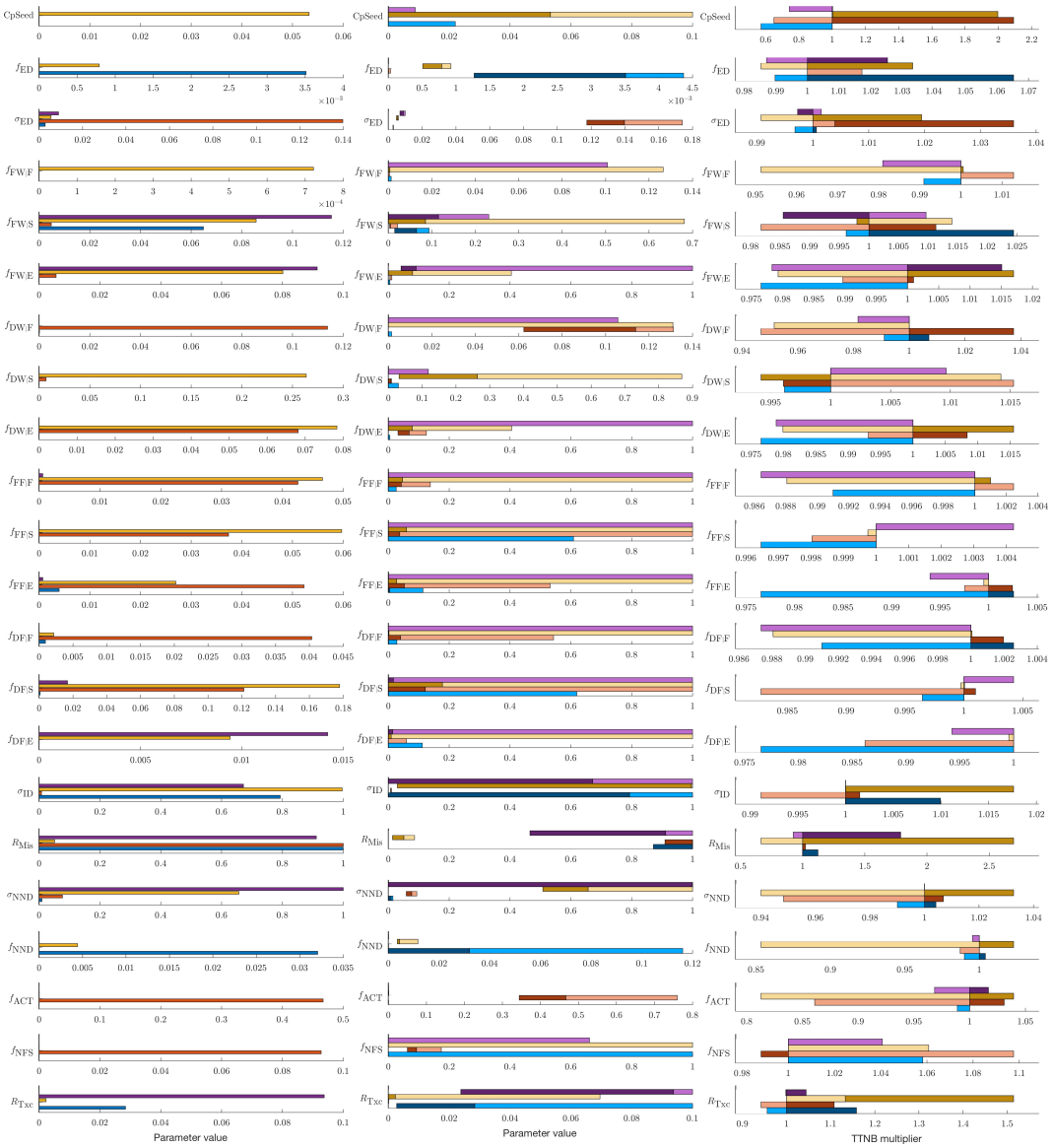

Figure 6.3: Optimal parameters, sensitivity analysis and TTNB analysis for each parameter and each disease. Left: optimal parameters for each disease. Middle: sensitivity analysis indicating the minimum parameter change required for divergence from the atrophy pattern of the simulation with optimal parameters, where divergence required a minimum of six changes in the atrophy order. Each parameter consists of a darker bar and a lighter bar. At the left edge of the dark bar is the value that parameter had to decrease to in order to cause divergence, and similarly for the right edge of the lighter bar for increasing the parameter value. The baseline values (θ^{dis}) are in-between the dark and light bar. Generally speaking, parameters with large bars signify that the atrophy pattern was not sensitive to this parameter. Right: associated change in TTNB from the sensitivity analysis, e.g., decreasing R_{Mis} from ≈ 0.08 to ≈ 0.03 in GRN resulted in almost tripling TTNB, delaying disease progression. Blue: AD, red: C9orf72, yellow: GRN, purple: MAPT.

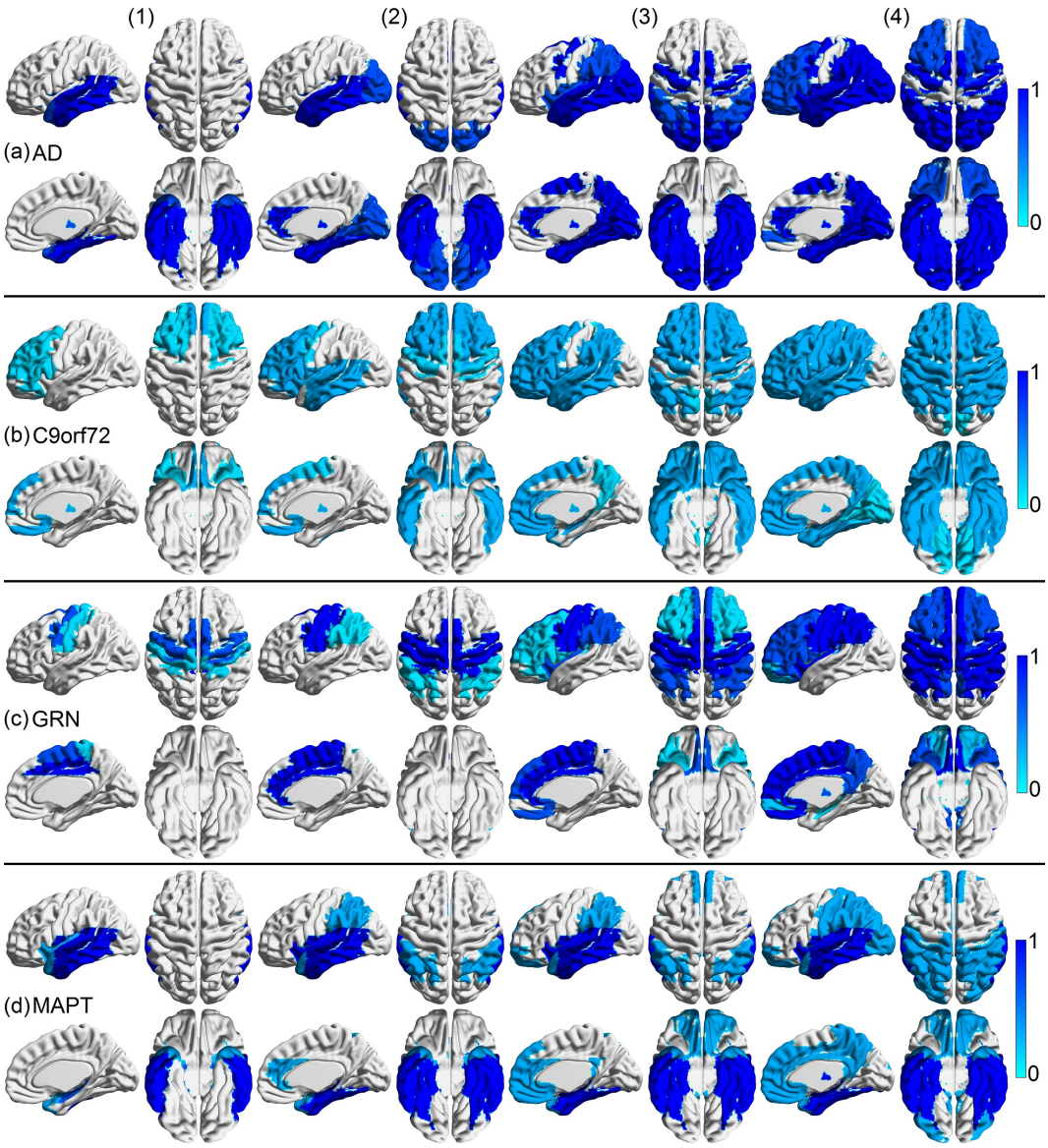

Figure 6.4: Visualisation of brain atrophy progression for each disease from sagittal, coronal, and transverse planes from the simulations with optimal parameters: (a) simulation for AD with parameters θ^{AD} after (1) 6, (2) 10, (3) 19, and (4) 22 regions showed abnormal atrophy, (b) simulation for C9orf72 with parameters $\theta^{C9orf72}$ after (1) 4, (2) 12, (3) 18, and (4) 22 regions showed abnormal atrophy, (c) simulation for GRN with parameters θ^{GRN} after (1) 3, (2) 6, (3) 13, and (4) 20 regions showed abnormal atrophy, and (d) simulation for MAPT with parameters θ^{MAPT} after (1) 10, (2) 15, (3) 18, and (4) 23 regions showed abnormal atrophy. The color indicates atrophy $A_r(t)$. These figures were created with the BrainNet Viewer (Xia, Wang, and He [257], 2013, http://www.nitrc.org/projects/bnv/).

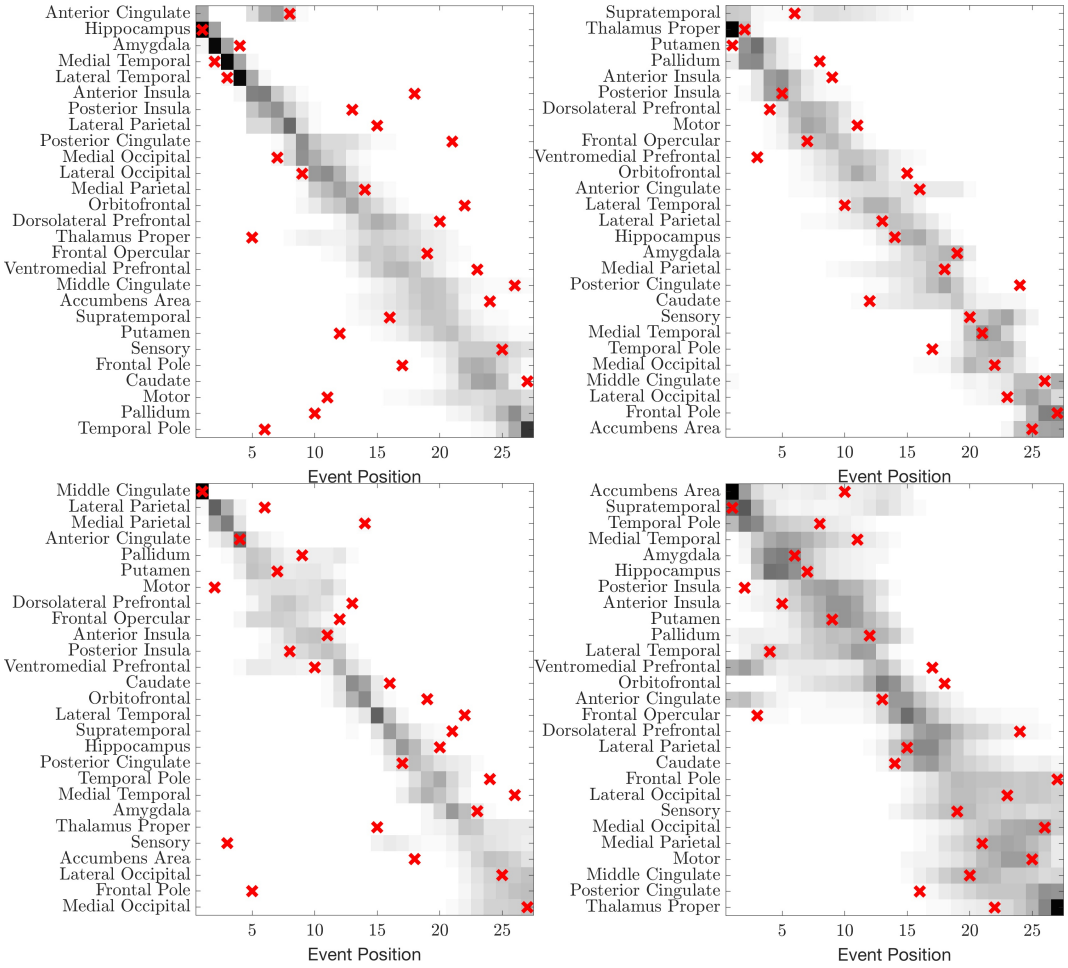

Figure 6.5: Comparison of atrophy prediction from simulations against population average atrophy progression given by the EBM. Greyscale indicates the atrophy order position probability for each brain region given by each disease's respective EBM's uncertainty matrix $\mathbf{UM}|\mathbf{dis}_{r,o}$. The red Xs are based on the atrophy order $\mathrm{SO}_r(\theta^{dis})$ that was computed after running simulations using the optimal parameters θ^{dis}. Top left: AD, top right: C9orf72, bottom left: GRN, bottom right: MAPT.

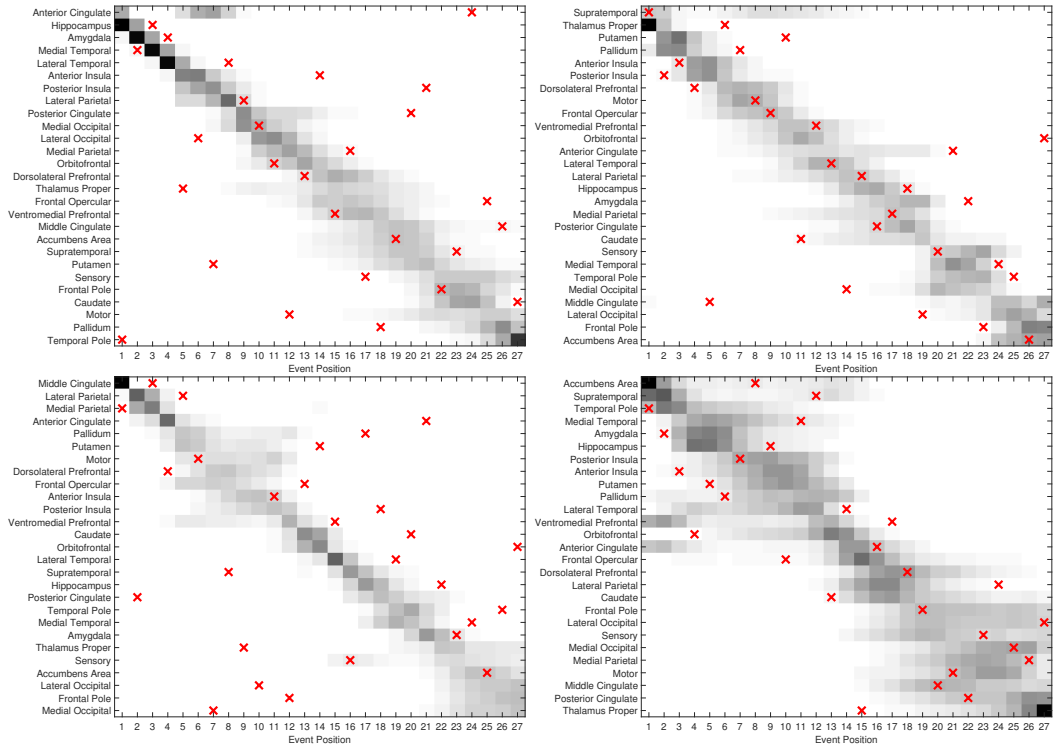

Figure 6.6: Comparison of atrophy prediction from simple models against population average atrophy progression given by the EBM. Greyscale indicates the order position probability for each brain region given by each disease's respective EBM's uncertainty matrix $\mathbf{UM}|\mathbf{dis}_{r,o}$. The red Xs are based on the atrophy order determined by the increasing or decreasing order of functional connectivity, structural connectivity, effective connectivity, or Euclidean distances. Top left: AD with order determined by decreasing structural connectivity strength from the amygdala, top right: C9orf72 with order determined by decreasing functional connectivity strength from the supratemporal, bottom left: GRN with order determined by decreasing functional connectivity strength from the medial parietal, bottom right: MAPT with order determined by increasing Euclidean distance from the temporal pole.

atrophy order, and we repeated this step until there were at least six changes in the atrophy order of brain regions. Additionally, it determined how long the network survived before atrophy spread in the entire brain, which was defined by timesteps to network breakdown (TTNB). Figure 6.9 is a different sensitivity analysis, which for multiple simulations of higher log-likelihood displays the related parameters (note that this figure does not contain all of the optimisation runs I performed; I also ran another similar set, for ≈180 days, but only saved the final best fits).

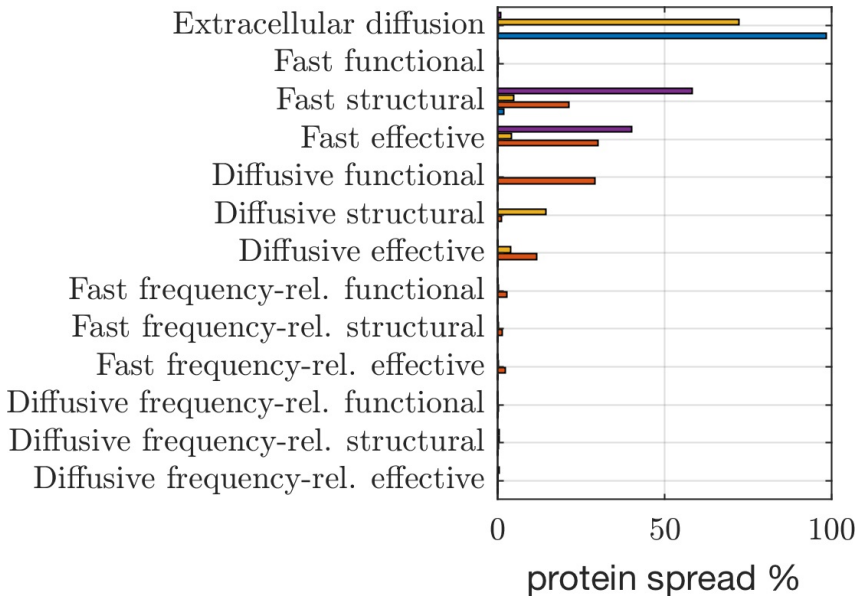

Figure 6.7: Percentage of protein spread via each modelled mechanism during simulations with the optimal parameters. Blue: AD, red: C9orf72, yellow: GRN, purple: MAPT.

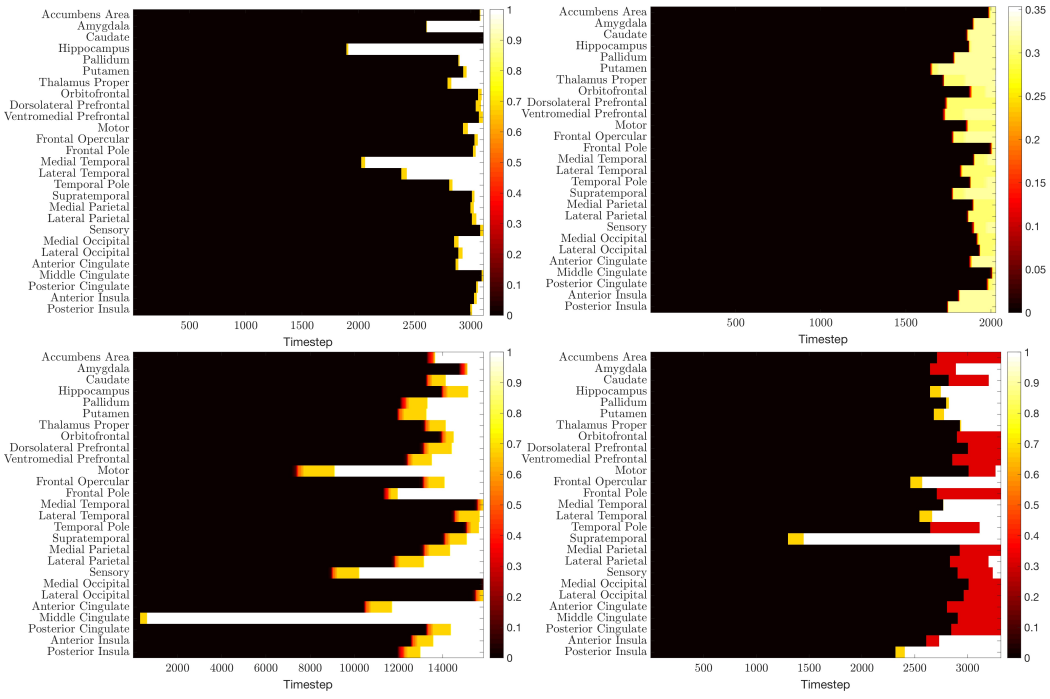

Figure 6.8: Atrophy over time during simulations with the optimal parameters. Top left: AD, top right: C9orf72, bottom left: GRN, bottom right: MAPT.

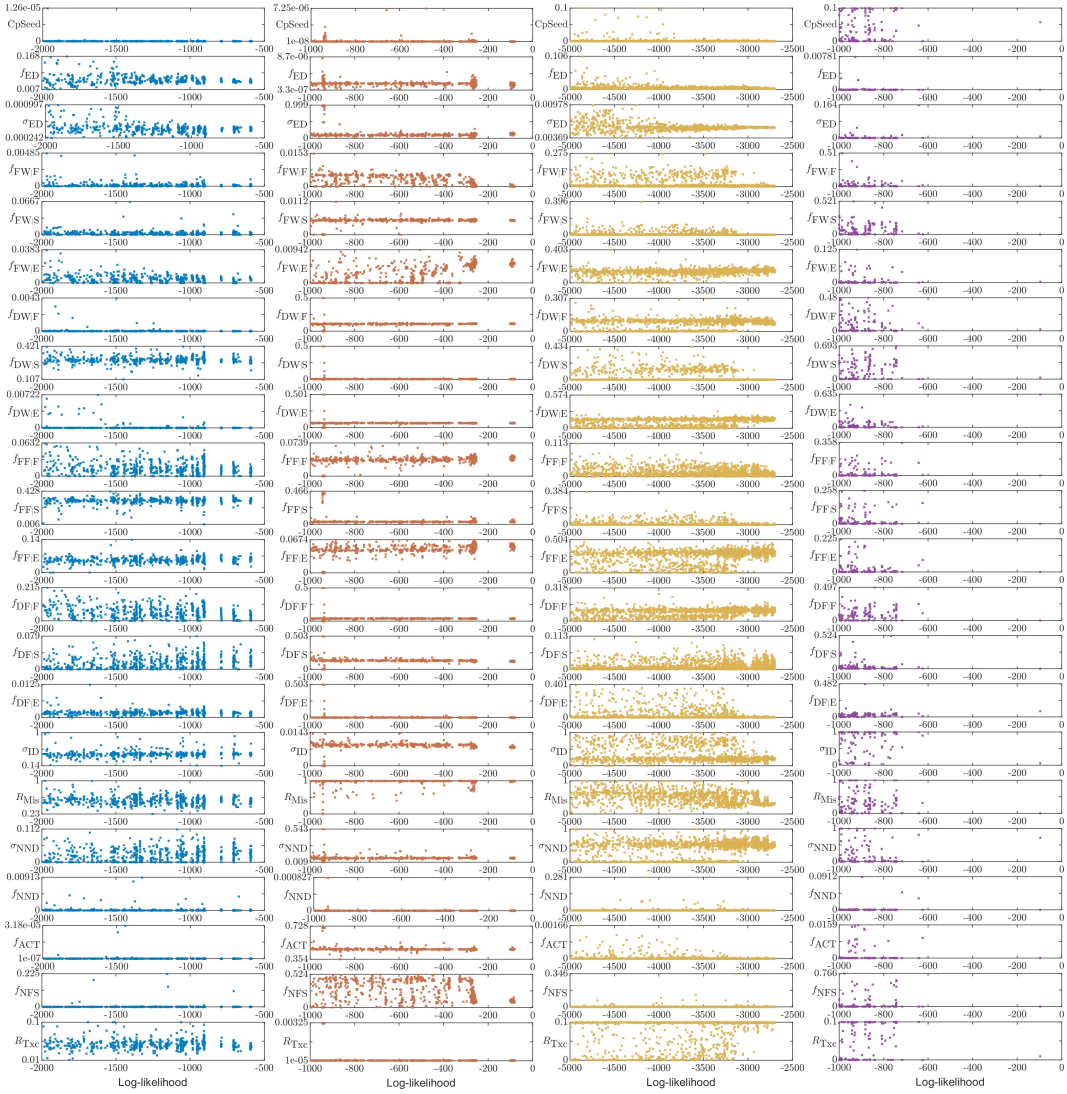

Figure 6.9: Various parameter regimes and their related log-likelihood. Each point corresponds to a parameter value on the y-axis, and to a simulation whose log-likelihood is given by the x-axis. Blue: AD, red: C9orf72, yellow: GRN, purple: MAPT.

6.3 Discussion

The optimisation procedure discovered optimal parameters that best fitted population average atrophy progression in AD, C9orf72, GRN, and MAPT, as seen in the left part of Figure 6.3. The most likely seed regions were: hippocampus in AD, thalamus proper in C9orf72, middle cingulate in GRN, and supratemporal in MAPT. Neurofibrillary tangles first present themselves in the entorhinal cortex in AD. Although the entorhinal cortex was not specifically parcellated, the closest simulated region was the medial temporal lobe, which showed atrophy early on, and empirically, the hippocampus is the next region to manifest neurofibrillary tangles (see Section 2.2.2). Atrophy in AD is more prominent on the hippocampus, mesial temporal, lateral temporoparietal, posterior cingulate and the precuneus bilaterally (see Section 2.2.2). There is no general consensus on the seed location of the FTD subtypes, but their general atrophy patterns have been observed to include: symmetric thalamus and cerebellum atrophy in patients with C9orf72 mutations, asymmetric frontal, temporal, and parietal lobe atrophy in patients with GRN mutations, and anterior and medial temporal lobe atrophy in patients with MAPT mutations (see Section 2.2.3). As can be seen in Figure 6.4, my results of atrophy progression qualitatively agree with qualitative literature based on radiologist and neuroscientific opinion (although this work cannot capture left-right brain asymmetry, as I symmetrised the brain for my analysis), except for a few outlier errors shown in Figure 6.5 for AD, C9orf72, and GRN. When comparing these results to the result of Figure 5.3, it appears on first sight that the fit has worsened, however the brain regions used in both cases were different, thus the fits can't be directly compared; I used larger brain regions in this chapter in order to capture most of the brain grey matter and to be able to compare between the four diseases.

Additionally, in the simulations with the optimal parameters, there was a long incubation time with each disease before atrophy started becoming noticeable (Figure 6.8, except for GRN, perhaps because it had the worst fit), in agreement with previous results [69, 70]. The first region to show atrophy in each disease did so after 60% to 77% of the total timesteps that were required before all regions showed

atrophy.

From Figure 6.6, one can note how well simple models fitted atrophy progression. AD best fitted (although the fit is poor) with structural connectivity, C9orf72 best fitted with functional connectivity, GRN best fitted (although the fit is poor) with functional connectivity, and MAPT best fitted with Euclidean distance. By comparison, Figure 6.7 shows that with my more complex model, protein spread: primarily via extracellular diffusion, and to a lesser extent via fast structural connectivity related connections in AD; primarily via fast and diffusive functional, effective, and structural connectivity related spread, and secondarily via fast frequency-related spread in C9orf72; primarily via extracellular diffusion, but also a significant portion spread via both structural connectivity and effective connectivity related connections in GRN; via fast structural and effective connectivity related connections in MAPT. Interestingly, the models of frequency related spread had little impact, and indeed, when I reran the simulations with the related parameter values set to zero, there was no significant change on atrophy progression. This implies that either I did not model the underlying neurobiological mechanisms sufficiently accurately, or that protein does not spread using these mechanisms. Overall, these results point to three mechanisms of protein spread, with their importance varying widely among diseases: (a) “Euclidean distance based spread" with extracellular diffusion, (b) bidirectional, fibre tract connection based spread, and (c) unidirectional synaptic connection based spread (which is what effective connectivity attempts to model).

It has been shown in-vitro that the ‘misfolding rate’ (or templating effectiveness) and the toxicity of pathogenic proteins varies a lot [145]. The products of the misfolding rates and toxicity rates of my optimal parameters were higher in AD and MAPT than C9orf72 and GRN. This coincided with an increase of neuronal frequencies toxic effect and lower neuronal frequency related spread in AD and MAPT, whereas the opposites were true for C9orf72 and GRN. Interestingly, AD and MAPT are associated with tau protein, whereas C9orf72 and GRN with TDP-43 protein (see Section 2.2.3 and Section 2.2.2).

6.3.1 Atrophy order and TTNB sensitivity to parameter value change

As is expected, increasing the protein seed concentration CpSeed, the misfolding rate R_{Mis}, or the toxicity rate R_{Txc} hastened disease progression (Figure 6.3). Noticeably, AD required a large change in these parameters to cause a substantial change in the atrophy order, and in some cases in the TTNB. The opposite case was true for C9orf72, where the atrophy order and TTNB were sensitive to smaller changes in these parameters. GRN was sensitive to changes in the misfolding rate, but not the initial seed or the toxicity rate. MAPT was the most sensitive to changes in these parameters. I hypothesise that the reason AD and GRN were less sensitive to these parameters is because AD and GRN had a stronger extracellular diffusion element, versus a more directed spread via structural or effective connectivity. Based on the results of this and of previous chapters, I have noticed that when spread is directed by certain criteria (such as fibre tracts), protein gathers in vulnerable 'bottleneck' elements (e.g., brain regions or neurons). These elements become a lot more vulnerable when directed spread is coupled with a higher misfolding rate, toxicity rate, or protein seed. On the other hand, in the case of undirected spread (such as extracellular diffusion), the ability of neurons to transmit or receive protein is equal for all neurons, thus there is no intrinsic vulnerability and vulnerability is determined by proximity to the seed region only. This result presents the counter-intuitive notion that in certain diseases a therapy that limits the spread mechanism can be more effective than a therapy that reduces the 'misfolding rate' or the 'toxicity rate' of pathogenic proteins. From Figure 6.9, we can see how different parameters fit the EBM, and how much variation is possible before changing the log-likelihood of the fit. From this figure, it seems that the best fits of the related optimisation runs (the figure does not show all of the optimisation runs we performed), are the only ones. More specifically, in AD, no other set of parameters that is non-local to the best fit was found; in C9orf72, increasing fast functional connectivity spread, decreasing fast effective connectivity spread, decreasing the misfolding rate, and increasing the neuronal frequency spread provide a different "good" fit that is

non-local to the best fit we found; in GRN there was another non-local fit but the best fit was poor anyway; and in MAPT there were no other non-local "good" fits.

Generally, increasing the strength of most spread mechanisms hastened disease progression, at varying degrees, with active transport hastening it the most, relatively speaking. In all diseases, their atrophy orders were most sensitive to changes in the parameter values of their respective primary brain scale spread mechanisms (extracellular diffusion in AD, fast structural connectivity related spread in C9orf72, extracellular diffusion in GRN, and fast structural and effective connectivity related spread in MAPT), as well as to changes with all of the neuronal scale spread mechanisms. In AD and GRN, despite extracellular diffusion being the primary spread mechanism, changes to its parameter values did not have a significant effect on TTNB, which further supports my earlier hypothesis stating that increased misfolding rate, toxicity rate, or protein seed has less of an effect when coupled with undirected spread. Typically, TTNB was most sensitive to changes with the parameters related to the neuronal scale spread mechanisms.

One notable exception where increasing the strength of the spread mechanism delayed disease progression (by approximately 10%) instead was neuronal frequency related spread, especially in the cases where the toxic effect was an increase of firing frequencies in neurons. This result agrees with the result of Chapter 4, and the reasoning behind it is that this combination of mechanisms will spread protein more evenly among neurons, as neurons with higher protein concentrations will spread more protein out of them, whereas neurons with lower protein concentrations will not spread as much protein. This promotes overall clearance and reduces overall toxicity.

6.4 Conclusions and future work

I presented one of the first contributions that combined neuronal and brain scale modelling of neurodegenerative diseases, and the first one to use a compartment-based computational modelling approach, which is commonly used for modelling neurons (e.g., using the simulator NEURON [241]), making it easy to combine

the current approach with other work in that field. Optimal parameters that fitted atrophy progression of four neurodegenerative diseases were found, highlighting differences between them with regards to: their seed regions, their primary spread mechanisms, potential therapeutic targets, and the consistency of their atrophy patterns to changes.

However, this work is still preliminary. A Bayesian model selection framework would better determine which modelled mechanisms play a role which ones do not. Performing a sensitivity analysis around a number of locally optimal fits would help determine which mechanisms are consistently required. Additionally, the suggestions made regarding potential therapeutic targets are more demonstrative of how such a framework could produce them, although electrical-activity based spread of protein does indeed have potential to be neuroprotective under certain circumstances, and other studies have also reached the same conclusion.

As with all modelling approaches, this work could be improved with better modelling. I used cortical columns and similar connectivity patterns for all brain regions, but this could be improved with scaled down versions of the specific neural network that constitutes each brain region, as well as more biologically accurate modelling of the connectivity among different brain regions, rather than simply assuming all the excitatory neurons of layer II and III are inputs and outputs. This also would address the issue that currently the neuronal scale has less of an effect on results as it is the same in all regions, with the only differentiating element being the number of columns, although modelling the neuronal scale mechanisms theoretically increases the biological accuracy of the overall model compared to the previous chapter's model. This work can also be extended to perform individual patient atrophy prediction, by either learning and predicting directly on longitudinal data, or by combining the current framework as a prior on the parameters and learning the patient-specific adjusted parameters, at which point comparisons could be made with similar work [41, 177] which has focused on individual patient prognosis only, and not population-average. Positron emission tomography of protein concentration could be used to instantiate the brain regional protein concentration,

and also as (extra) validation [69]. Better informed values for parameters, and better modelling can be derived by combining this work with other neurodegenerative disease modelling work. For example, I did not model multiple proteins, such as tau and amyloid-beta in Alzheimer's disease, chaperones, multiple clearance pathways, spread that occurs only after neuronal death, aggregates of different sizes which are subject to different mechanisms, etc.

Chapter 7

Conclusions

This thesis presented work on computationally modelling the accumulation, spread, and toxic effects of pathogenic proteins on neurons and the brain in neurodegenerative diseases. I used a different approach compared to similar work, modelled additional and more complex neurobiological mechanisms, and linked the neuronal scale, where these neurobiological mechanisms exist, with the brain scale, where patient data that is used for validation is acquired.

In Chapter 4, an analysis of various neurobiological mechanisms of accumulation and spread was performed at the neuronal scale in a network of cortical columns. The modelled mechanisms captured key characteristics of pathogenic proteins, and observations were made regarding the effects of modifying the models on the atrophy patterns, with special interest given to how much alteration of parameter values was required before atrophy progression diverged from a specific pattern. Certain concepts emerged as significant, such as that soluble pathogenic protein spread is determined by the network's global connectivity and targets 'bottleneck' neurons, whereas the spread of insoluble pathogenic protein is determined more so by the network's local connectivity near the seed and targets nearby neurons. While far from solid evidence for specific diseases, these concepts can raise questions when observing disease phenotypes: are diseases where atrophy spreads locally and are heterogeneous more likely to have insoluble pathogenic proteins, whereas homogeneous diseases have more soluble pathogenic proteins? Finally, an analysis was performed to determine which mechanisms provided appealing can-

didates for progression-delaying therapies, consistently finding that strengthening mechanisms that spread protein more evenly among neurons to be notable candidates.

In Chapter 5, I attempted to learn which mechanisms govern the pathogenic proteins responsible for ApoE 4 positive AD. I computationally modelled mechanisms of accumulation, spread (including effective connectivity related spread, which had not been investigated by any previous similar work), and toxic effects at the brain scale, modelling a number of grey matter brain regions as nodes in a network. At the brain scale, I was able to use an event based model of population average disease progression as "ground truth", whereas related work has used only individual patient data. Optimal model parameters were found, with evidence consistently pointing to pathogenic protein being insoluble, rather than soluble, in agreement with the 'prion-like' hypothesis. Spread was primarily driven by structural connectivity (i.e., fibre tract connections), and to a lesser extent by extracellular diffusion and effective connectivity. Firing frequency related spread mechanisms did not spread any protein. These results are broadly in agreement with previous related work [41, 69]. They were not in agreement with the work of Zhou et al. [37], as functional connectivity was not found to be predictive, potentially because I modelled effective connectivity. A reduction of the strength of structural connectivity related spread was found to delay disease progression, and thus is suggested as a candidate target for therapy.

In Chapter 6, I combined and extended my previous two chapters, linking neurobiological mechanisms that occur at the neuronal scale with patient data that is acquired at the brain scale, thus enabling validation of those mechanisms. I modelled the neuronal scale mechanisms in the same manner as I did in Chapter 4, and modified and added additional mechanisms of spread at the brain scale. I used an event based model for ApoE 4 positive AD, and C9orf72, GRN, and MAPT mutations related frontotemporal dementias. Thus, in this work, I was able to find optimal model parameters for each of these four diseases, and I then performed a comparative study. The mechanisms of spread varied considerably among the

four diseases, as well as which mechanisms presented themselves as more alluring targets for therapeutic intervention. Seed regions for each disease were also determined through the optimisation procedure. As with the results presented in Chapter 5, the spread was found to be primarily driven by extracellular diffusion, structural connectivity related connections, and effective connectivity related connections, and not by functional connectivity or by firing frequency related spread mechanisms. Decreasing the strength of each mechanism of spread was found to delay disease progression, with the exception of neuronal frequency related spread, where strengthening it would delay disease progression. This result agrees with the previous results presented in Chapter 4.

In this thesis, I set out to gain a better understanding of pathogenic protein mechanisms in order to: (a) study the 'molecular nexopathies' paradigm, (b) predict pathogenic protein behaviour and by extension brain atrophy, (c) suggest potential therapeutic targets, (d) suggest which hypotheses regarding these mechanisms should be prioritised in future in-vivo and in-vitro research. Indeed, the results with AD and the three genetic FTD subtypes found that their respective pathogenic proteins were governed by very different mechanisms (represented by my model parameter values). In addition, their spread patterns heavily depended on the network's structural and effective connectivity, as well as "Euclidean distances", and the role each of these played varied highly among the four diseases, for example, AD spread via extracellular diffusion and via fast structural connectivity related connections, whereas C9orf72 spread via fast structural connectivity related connections and via slower effective connectivity related connections. These results suggest that further research is prioritised towards testing whether AD spreads via extracellular diffusion and rapidly via fibre tracts, whereas in C9orf72 the focus should be on its respective mechanisms. Furthermore, by delineating the optimal model parameters, their behaviour could be predicted, and by extension atrophy. This enabled atrophy prognosis (although not at an individual patient basis yet), as well as elucidated the seed region in each disease, information that might be helpful in developing biomarkers for earlier diagnosis. Additionally, being able to predict

protein behaviour also meant that hypothetical therapeutic interventions could be simulated to study which ones could delay disease progression, and thus suggestions of potential therapeutic targets were made, in particular enhancing electrical-activity based spread of protein. Lastly, certain mechanisms, such as electrical-activity based spread at the brain scale, were found to not contribute significantly to the disease process, whereas others were more important, such as extracellular diffusion or spread based on structural connectivity. Thus, prioritising further studies on the mechanisms that were stronger contributors is preferable.

7.1 Future work

The work of this thesis could be extended in a number of ways. While computational modelling has a lot of potential within the topic of neurodegenerative diseases, the major limitation for such work is the lack of neurobiological knowledge to inform the construction of the computational models, such as production rates of the soluble, non-pathogenic protein variants. A collaborative effort between neurobiologists and computational modellers could provide quicker results for both, where neurobiological results inform and refine the computational model, and computational modelling results can inform neurobiological research regarding which hypotheses hold more promise and warrant further, real-world studies. For example, a potential in-vivo or in-vitro study might be interested in observing how modification of different spread mechanisms might influence disease progression. From my results, it was found that strengthening a mechanism of action potential related spread would delay disease progression. This result can be used to give priority to testing this particular spread mechanism first, either in-vivo or in-vitro, as in-vivo and in-vitro studies are expensive and time consuming, so any proof that assists in prioritisation is beneficial.

However, there is already a lot of information in the literature that could be used to enhance the current model, which wasn't used in this thesis, as simplifications had to be made due to time restrictions and to build a model more gradually. More accurate representations of each brain region's neural network, and the con-

nections among them could improve the face validity of the results. Additionally, there has been a lot of related work in the systems biology (see Chapter 3) field, modelling the single neuron scale in detail, which could be integrated with the current approach. As more neurobiological knowledge is gathered, certain parameters of the models will no longer be parameters, but become known values, allowing for faster optimisation and less likelihood of overfitting, which in turn enables one to model additional neurobiological mechanisms. Additionally, multiple proteins (such as tau and amyloid-beta in AD) could be modelled, and PET protein tracer imaging data can be used to initialise protein concentrations in brain regions.

Most similar work has concerned itself with atrophy or protein concentration prediction of individual patients. Future work that would integrate individual patient prognosis would enable comparison of the predictive power among various approaches in the literature, if using the same datasets. One way to integrate individual patient prediction with the current work would be to use the population average model as a sort of “prior", and patient specific model parameters would be able to slightly modify the modelled mechanisms within a ‘hierarchical model’ framework. Within the context of providing therapy suggestions, there might be individual patient differences, whereby some patients would benefit more from a drug altering one pathogenic protein mechanism, whereas other patients might benefit more from a drug altering a different mechanism. These nuances are lost with the population-based framework used in this work, but with an individual patient framework therapy suggestions could become more personalised. Additionally, PET protein tracer imaging could be used within this context either on its own, or in conjunction with MRI atrophy quantification. Naturally, the optimal parameters found in each case would be different, but most likely the ones found when using PET and MRI data in conjunction would be most accurate. Lastly, within the individual-subject context, if the modelled mechanisms reach a point where they represent disease progression accurately enough, it would be possible given patient-specific data to run the simulation in reverse and “predict” the seed region, the results of which could be of interest for earlier diagnosis research.

Finally, the complexity of the overall model of my work meant that optimisation was very slow. Additionally, there is no guarantee that the optima that I found were the global optima and due to the nature of the optimisation function and my model, even if I had found a global optimum, there is no guarantee that it is the only one as there could multiple sets of parameters that give the optimal result. This could mean that with (much) faster optimisation my modelled mechanisms could fit the data of the EBM even better than in the results. Thus, where appropriate, simplifications to the model, especially of the neural network would help to address this issue. A more fundamental way to reduce the computational complexity in a more significant way would be to modify the models so that the cost function becomes smooth, differentiable, and, most importantly, convex, as this would allow the use of better optimisation techniques, and convergence would be much faster, although to what degree this is feasible is questionable. This would also open up the possibility, especially within the context of individual patient prediction, of using more advanced machine learning techniques for model selection, and techniques that reduce the likelihood of overfitting to the training or the test data, e.g., through comparing training performance with validation and test performance, cross validation, bootstrapping, boosting, etc.

Unfortunately, I personally will not be continuing work on this topic, however I wish the best of luck to anyone who does and hope this thesis helped them in their endeavour.

Bibliography

[1] Qaseem A, Snow V, Cross JT, Forciea MA, Hopkins R, Shekelle P, et al. Current pharmacologic treatment of dementia: a clinical practice guideline from the American College of Physicians and the American Academy of Family Physicians. Annals of Internal Medicine. 2008;148(5):370–378.

[2] Gauthier SG. Alzheimer's disease: the benefits of early treatment. European Journal of Neurology. 2005;12:11–16.

[3] Ferri CP, Prince M, Brayne C, Brodaty H, Fratiglioni L, Ganguli M, et al. Global prevalence of dementia: a Delphi consensus study. The Lancet. 2005;366(9503):2112–2117.

[4] Patterson C, Lynch C, Bliss A, Lefevre M, Wiedner W. World Alzheimer's report 2018: The state of the art of dementia research: New frontiers. London Alzheimer's Disease International (ADI). 2018;.

[5] Knapp M, Prince M, Albanese E, Banerjee S, Dhanasiri S, Fernandez JL, et al. Dementia UK: The full report. London: Alzheimer's society. 2007;.

[6] Jucker M, Walker LC. Self-propagation of pathogenic protein aggregates in neurodegenerative diseases. Nature. 2013;501(7465):45–51.

[7] Balch WE, Morimoto RI, Dillin A, Kelly JW. Adapting proteostasis for disease intervention. Science. 2008;319(5865):916–919.

[8] Edelstein-Keshet L, Spiros A. Exploring the formation of Alzheimer's disease senile plaques in silico. Journal of Theoretical Biology. 2002;216(3):301–326.

[9] Villemagne VL, Burnham S, Bourgeat P, Brown B, Ellis KA, Salvado O, et al. Amyloid β deposition, neurodegeneration, and cognitive decline in sporadic Alzheimer's disease: a prospective cohort study. The Lancet Neurology. 2013;12(4):357–367.

[10] Farlow M, Anand R, Messina Jr J, Hartman R, Veach J. A 52-week study of the efficacy of rivastigmine in patients with mild to moderately severe Alzheimer's disease. European Neurology. 2000;44(4):236–241.

[11] Misra C, Fan Y, Davatzikos C. Baseline and longitudinal patterns of brain atrophy in MCI patients, and their use in prediction of short-term conversion to AD: results from ADNI. Neuroimage. 2009;44(4):1415–1422.

[12] Carbonell F, Iturria-Medina Y, Evans AC. Mathematical modeling of protein misfolding mechanisms in neurological diseases: a historical overview. Frontiers in Neurology. 2018;9:37.

[13] Uchihara T, Giasson BI. Propagation of alpha-synuclein pathology: hypotheses, discoveries, and yet unresolved questions from experimental and human brain studies. Acta Neuropathologica. 2016;131(1):49–73.

[14] Lewis J, Dickson DW. Propagation of tau pathology: hypotheses, discoveries, and yet unresolved questions from experimental and human brain studies. Acta Neuropathologica. 2016;131(1):27–48.

[15] Eisele YS, Duyckaerts C. Propagation of Aß pathology: hypotheses, discoveries, and yet unresolved questions from experimental and human brain studies. Acta Neuropathologica. 2016;131(1):5–25.

[16] Garden GA, La Spada AR. Intercellular (mis)communication in neurodegenerative disease. Neuron. 2012;73(5):886–901.

[17] Winklhofer KF, Tatzelt J, Haass C. The two faces of protein misfolding: gain- and loss-of-function in neurodegenerative diseases. The EMBO journal. 2008;27(2):336–349.

[18] Kang JE, Lim MM, Bateman RJ, Lee JJ, Smyth LP, Cirrito JR, et al. Amyloid-β dynamics are regulated by orexin and the sleep-wake cycle. Science. 2009;326(5955):1005–1007.

[19] Polymenidou M, Cleveland DW. The seeds of neurodegeneration: prion-like spreading in ALS. Cell. 2011;147(3):498–508.

[20] Aguzzi A, Rajendran L. The transcellular spread of cytosolic amyloids, prions, and prionoids. Neuron. 2009;64(6):783–790.

[21] Ahmed RM, Devenney EM, Irish M, Ittner A, Naismith S, Ittner LM, et al. Neuronal network disintegration: common pathways linking neurodegenerative diseases. Journal of Neurology, Neurosurgery & Psychiatry. 2016;87(11):1234–1241.

[22] Haass C. Initiation and propagation of neurodegeneration. Nature Medicine. 2010;16(11):1201–1204.

[23] Thal DR, Rüb U, Orantes M, Braak H. Phases of Aβ-deposition in the human brain and its relevance for the development of AD. Neurology. 2002;58(12):1791–1800.

[24] Braak H, Braak E. Neuropathological stageing of Alzheimer related changes. Acta Neuropathologica. 1991;82(4):239–259.

[25] Braak H, Del Tredici K, Rüb U, De Vos RAI, Steur ENHJ, Braak E. Staging of brain pathology related to sporadic Parkinson's disease. Neurobiology of Aging. 2003;24(2):197–211.

[26] Brettschneider J, Del Tredici K, Toledo JB, Robinson JL, Irwin DJ, Grossman M, et al. Stages of pTDP-43 pathology in amyotrophic lateral sclerosis. Annals of Neurology. 2013;74(1):20–38.

[27] Seeley WW, Crawford RK, Zhou J, Miller BL, Greicius MD. Neurodegenerative diseases target large-scale human brain networks. Neuron. 2009;62(1):42–52.

[28] Raj A, Powell F. Models of network spread and network degeneration in brain disorders. Biological Psychiatry: Cognitive Neuroscience and Neuroimaging. 2018;3(9):788–797.

[29] Hardy JA, Higgins GA. Alzheimer's disease: the amyloid cascade hypothesis. Science. 1992;256(5054):184–185.

[30] Frost B, Diamond MI. Prion-like mechanisms in neurodegenerative diseases. Nature Reviews Neuroscience. 2010;11(3):155.

[31] Mietelska-Porowska A, Wasik U, Goras M, Filipek A, Niewiadomska G. Tau protein modifications and interactions: their role in function and dysfunction. International Journal of Molecular Sciences. 2014;15(3):4671–4713.

[32] Jucker M, Walker LC. Propagation and spread of pathogenic protein assemblies in neurodegenerative diseases. Nature Neuroscience. 2018;21(10):1341–1349.

[33] Bakshi S, Chelliah V, Chen C, van der Graaf PH. Mathematical biology models of Parkinson's disease. CPT: Pharmacometrics & Systems Pharmacology. 2018;8(2):77–86.

[34] Prusiner SB. Biology and genetics of prions causing neurodegeneration. Annual Review of Genetics. 2013;47:601–623.

[35] Haass C, Selkoe DJ. Soluble protein oligomers in neurodegeneration: lessons from the Alzheimer's amyloid β-peptide. Nature Reviews Molecular Cell Biology. 2007;8(2):101.

[36] Warren JD, Rohrer JD, Schott JM, Fox NC, Hardy J, Rossor MN. Molecular nexopathies: a new paradigm of neurodegenerative disease. Trends in Neurosciences. 2013;36(10):561–569.

[37] Zhou J, Gennatas ED, Kramer JH, Miller BL, Seeley WW. Predicting regional neurodegeneration from the healthy brain functional connectome. Neuron. 2012;73(6):1216–1227.

[38] Filippi M, Basaia S, Canu E, Imperiale F, Magnani G, Falautano M, et al. Changes in functional and structural brain connectome along the Alzheimer's disease continuum. Molecular Psychiatry. 2018;10.1038/s41380-018-0067-8.

[39] Iturria-Medina Y. Anatomical brain networks on the prediction of abnormal brain states. Brain Connectivity. 2013;3(1):1–21.

[40] Pievani M, de Haan W, Wu T, Seeley WW, Frisoni GB. Functional network disruption in the degenerative dementias. The Lancet Neurology. 2011;10(9):829–843.

[41] Raj A, LoCastro E, Kuceyeski A, Tosun D, Relkin N, Weiner M. Network diffusion model of progression predicts longitudinal patterns of atrophy and metabolism in Alzheimer's disease. Cell Reports. 2015;10(3):359–369.

[42] Clavaguera F, Akatsu H, Fraser G, Crowther RA, Frank S, Hench J, et al. Brain homogenates from human tauopathies induce tau inclusions in mouse brain. Proceedings of the National Academy of Sciences. 2013;110(23):9535–9540.

[43] Guo JL, Narasimhan S, Changolkar L, He Z, Stieber A, Zhang B, et al. Unique pathological tau conformers from Alzheimer's brains transmit tau pathology in nontransgenic mice. Journal of Experimental Medicine. 2016;213(12):2635–2654.

[44] Clavaguera F, Bolmont T, Crowther RA, Abramowski D, Frank S, Probst A, et al. Transmission and spreading of tauopathy in transgenic mouse brain. Nature Cell Biology. 2009;11(7):909.

[45] Zhang B, Higuchi M, Yoshiyama Y, Ishihara T, Forman MS, Martinez D, et al. Retarded axonal transport of R406W mutant tau in transgenic mice with a neurodegenerative tauopathy. Journal of Neuroscience. 2004;24(19):4657–4667.

[46] Rizzu P, Joosse M, Ravid R, Hoogeveen A, Kamphorst W, van Swieten JC, et al. Mutation-dependent aggregation of tau protein and its selective depletion from the soluble fraction in brain of P301L FTDP-17 patients. Human Molecular Genetics. 2000;9(20):3075–3082.

[47] Ahmed Z, Cooper J, Murray TK, Garn K, McNaughton E, Clarke H, et al. A novel in vivo model of tau propagation with rapid and progressive neurofibrillary tangle pathology: the pattern of spread is determined by connectivity, not proximity. Acta Neuropathologica. 2014;127(5):667–683.

[48] Rohrer JD, Lashley T, Schott JM, Warren JE, Mead S, Isaacs AM, et al. Clinical and neuroanatomical signatures of tissue pathology in frontotemporal lobar degeneration. Brain. 2011;134(9):2565–2581.

[49] Whitwell JL, Weigand SD, Boeve BF, Senjem ML, Gunter JL, DeJesus-Hernandez M, et al. Neuroimaging signatures of frontotemporal dementia genetics: C9ORF72, tau, progranulin and sporadics. Brain. 2012;135(3):794–806.

[50] Filippi M, Agosta F. Structural and functional network connectivity breakdown in Alzheimer's disease studied with magnetic resonance imaging techniques. Journal of Alzheimer's Disease. 2011;24(3):455–474.

[51] Agosta F, Pievani M, Geroldi C, Copetti M, Frisoni GB, Filippi M. Resting state fMRI in Alzheimer's disease: beyond the default mode network. Neurobiology of Aging. 2012;33(8):1564–1578.

[52] Tsuji H, Arai T, Kametani F, Nonaka T, Yamashita M, Suzukake M, et al. Molecular analysis and biochemical classification of TDP-43 proteinopathy. Brain. 2012;135(11):3380–3391.

[53] Lace G, Savva GM, Forster G, De Silva R, Brayne C, Matthews FE, et al. Hippocampal tau pathology is related to neuroanatomical connections: an ageing population based study. Brain. 2009;132(5):1324–1334.

[54] Hara M, Hirokawa K, Kamei S, Uchihara T. Isoform transition from four-repeat to three-repeat tau underlies dendrosomatic and regional progression of neurofibrillary pathology. Acta Neuropathologica. 2013;125(4):565–579.

[55] Salehi A, Delcroix JD, Belichenko PV, Zhan K, Wu C, Valletta JS, et al. Increased App expression in a mouse model of Down's syndrome disrupts NGF transport and causes cholinergic neuron degeneration. Neuron. 2006;51(1):29–42.

[56] Wirths O, Weis J, Szczygielski J, Multhaup G, Bayer TA. Axonopathy in an APP/PS1 transgenic mouse model of Alzheimer's disease. Acta Neuropathologica. 2006;111(4):312–319.

[57] Meyer-Luehmann M, Coomaraswamy J, Bolmont T, Kaeser S, Schaefer C, Kilger E, et al. Exogenous induction of cerebral ß-amyloidogenesis is governed by agent and host. Science. 2006;313(5794):1781–1784.

[58] Eisele YS, Obermüller U, Heilbronner G, Baumann F, Kaeser SA, Wolburg H, et al. Peripherally applied Aβ-containing inoculates induce cerebral β-amyloidosis. Science. 2010;330(6006):980–982.

[59] McMillan P, Korvatska E, Poorkaj P, Evstafjeva Z, Robinson L, Greenup L, et al. Tau isoform regulation is region- and cell-specific in mouse brain. Journal of Comparative Neurology. 2008;511(6):788–803.

[60] Nussbaum JM, Schilling S, Cynis H, Silva A, Swanson E, Wangsanut T, et al. Prion-like behaviour and tau-dependent cytotoxicity of pyroglutamylated amyloid-β. Nature. 2012;485(7400):651–655.

[61] Piscopo P, Rivabene R, Adduci A, Mallozzi C, Malvezzi-Campeggi L, Crestini A, et al. Hypoxia induces up-regulation of progranulin in neuroblastoma cell lines. Neurochemistry International. 2010;57(8):893–898.

[62] Pietri M, Caprini A, Mouillet-Richard S, Pradines E, Ermonval M, Grassi J, et al. Overstimulation of PrPC signaling pathways by prion peptide 106-126

causes oxidative injury of bioaminergic neuronal cells. Journal of Biological Chemistry. 2006;281(38):28470–28479.

[63] Klöppel S, Stonnington CM, Chu C, Draganski B, Scahill RI, Rohrer JD, et al. Automatic classification of MR scans in Alzheimer's disease. Brain. 2008;131(3):681–689.

[64] Young AL, Oxtoby NP, Daga P, Cash DM, Fox NC, Ourselin S, et al. A data-driven model of biomarker changes in sporadic Alzheimer's disease. Brain. 2014;137(9):2564–2577.

[65] Rollo JL, Banihashemi N, Vafaee F, Crawford JW, Kuncic Z, Holsinger RMD. Unraveling the mechanistic complexity of Alzheimer's disease through systems biology. Alzheimer's & Dementia. 2016;12(6):708–718.

[66] Lloret-Villas A, Varusai TM, Juty N, Laibe C, Le Novere N, Hermjakob H, et al. The impact of mathematical modeling in understanding the mechanisms underlying neurodegeneration: evolving dimensions and future directions. CPT: Pharmacometrics & Systems Pharmacology. 2017;6(2):73–86.

[67] Pandya S, Mezias C, Raj A. Predictive model of spread of progressive supranuclear palsy using directional network diffusion. Frontiers in Neurology. 2017;8:692.

[68] Mandelli ML, Vilaplana E, Brown JA, Hubbard HI, Binney RJ, Attygalle S, et al. Healthy brain connectivity predicts atrophy progression in non-fluent variant of primary progressive aphasia. Brain. 2016;139(10):2778–2791.

[69] Iturria-Medina Y, Sotero RC, Toussaint PJ, Evans AC, Initiative ADN, et al. Epidemic spreading model to characterize misfolded proteins propagation in aging and associated neurodegenerative disorders. PLoS Computational Biology. 2014;10(11):e1003956.

[70] Weickenmeier J, Jucker M, Goriely A, Kuhl E. A physics based model explains the prion-like features of neurodegeneration in Alzheimer's disease,

Parkinson's disease, and amyotrophic lateral sclerosis. Journal of the Mechanics and Physics of Solids. 2018;124:264–281.

[71] Kerr CC, Van Albada SJ, Neymotin SA, Chadderdon III GL, Robinson PA, Lytton WW. Cortical information flow in Parkinson's disease: a composite network/field model. Frontiers in Computational Neuroscience. 2013;7:39.

[72] Rowan M, Neymotin S, Lytton W. Electrostimulation to reduce synaptic scaling driven progression of Alzheimer's disease. Frontiers in Computational Neuroscience. 2014;8:39.

[73] Bertsch M, Franchi B, Tesi MC, Tosin A. Microscopic and macroscopic models for the onset and progression of Alzheimer's disease. Journal of Physics A: Mathematical and Theoretical. 2017;50(41):414003.

[74] Proctor CJ, Boche D, Gray DA, Nicoll JAR. Investigating interventions in Alzheimer's disease with computer simulation models. PLoS ONE. 2013;8(9):e73631.

[75] Mir M, Kim T, Majumder A, Xiang M, Wang R, Liu SC, et al. Label-free characterization of emerging human neuronal networks. Scientific reports. 2014;4:4434.

[76] Xia CF, Arteaga J, Chen G, Gangadharmath U, Gomez LF, Kasi D, et al. [18F] T807, a novel tau positron emission tomography imaging agent for Alzheimer's disease. Alzheimer's & Dementia. 2013;9(6):666–676.

[77] Young AL, Oxtoby NP, Huang J, Marinescu RV, Daga P, Cash DM, et al. Multiple orderings of events in disease progression. In: International Conference on Information Processing in Medical Imaging. Springer; 2015. p. 711–722.

[78] Georgiadis K, Wray S, Ourselin S, Warren J, Modat M. Simulation of pathogenic protein spread in an artificial neural network. Journal of Neurochemistry. 2016;138:409.

[79] Georgiadis K, Wray S, Ourselin S, Warren JD, Modat M. Computational modelling of pathogenic protein spread in neurodegenerative diseases. PLoS ONE. 2018;13(2):e0192518.

[80] Georgiadis K, Young AL, Hütel M, Razi A, Semedo C, Schott J, et al. Computational Modelling of Pathogenic Protein Behaviour-Governing Mechanisms in the Brain. In: International Conference on Medical Image Computing and Computer-Assisted Intervention. Springer; 2018. p. 532–539.

[81] Georgiadis K, Young AL, Semedo C, Hütel M, Razi A, Rohrer JD, et al. Multiscale modelling of pathogenic protein spread in neurodegenerative diseases; 2020. Under submission to PLoS Computational Biology.

[82] Noback CR, Strominger NL, Demarest RJ, Ruggiero DA. The human nervous system: structure and function. 744. Springer Science & Business Media; 2005.

[83] Lodato S, Arlotta P. Generating neuronal diversity in the mammalian cerebral cortex. Annual Review of Cell and Developmental Biology. 2015;31:699–720.

[84] Mountcastle VB. The columnar organization of the neocortex. Brain. 1997;120(4):701–722.

[85] Markram H, Muller E, Ramaswamy S, Reimann MW, Abdellah M, Sanchez CA, et al. Reconstruction and simulation of neocortical microcircuitry. Cell. 2015;163(2):456–492.

[86] Sansom SN, Livesey FJ. Gradients in the brain: the control of the development of form and function in the cerebral cortex. Cold Spring Harbor Perspectives in Biology. 2009;1(2):a002519.

[87] Thomson AM, Bannister AP. Interlaminar connections in the neocortex. Cerebral Cortex. 2003;13(1):5–14.

[88] Kelly JP. The neural basis of perception and movement. Principles of Neural Science. 1991;p. 283–95.

[89] Shepherd GM, Shepherd GM. The synaptic organization of the brain. vol. 198. oxford university press New York; 1998.

[90] Richardson KA, Fanselow EE, Connors BW. Neocortical anatomy and physiology. Epilepsy A comprehensive textbook. 2008;p. 323–335.

[91] Cardoso MJ. Automated Morphometric Characterization of the Cerebral Cortex for the Developing and Ageing Brain. PhD thesis, University College London; 2012.

[92] Cardoso MJ, Modat M, Wolz R, Melbourne A, Cash D, Rueckert D, et al. Geodesic information flows: spatially-variant graphs and their application to segmentation and fusion. IEEE Transactions on Medical Imaging. 2015;34(9):1976–1988.

[93] Basser PJ, Pajevic S, Pierpaoli C, Duda J, Aldroubi A. In vivo fiber tractography using DT-MRI data. Magnetic Resonance in Medicine. 2000;44(4):625–632.

[94] Logothetis NK, Pauls J, Augath M, Trinath T, Oeltermann A. Neurophysiological investigation of the basis of the fMRI signal. Nature. 2001;412(6843):150–157.

[95] Biswal BB. Resting state fMRI: a personal history. Neuroimage. 2012;62(2):938–944.

[96] Friston KJ. Functional and effective connectivity: a review. Brain Connectivity. 2011;1(1):13–36.

[97] Sporns O. Brain connectivity. Scholarpedia. 2007;2(10):4695. Revision #91084.

[98] Erkkinen MG, Kim MO, Geschwind MD. Clinical neurology and epidemiology of the major neurodegenerative diseases. Cold Spring Harbor Perspectives in Biology. 2018;10(4):a033118.

[99] DeArmond SJ, Prusiner SB. Etiology and pathogenesis of prion diseases. The American Journal of Pathology. 1995;146(4):785–811.

[100] Tschampa HJ, Kallenberg K, Kretzschmar HA, Meissner B, Knauth M, Urbach H, et al. Pattern of cortical changes in sporadic Creutzfeldt-Jakob disease. American Journal of Neuroradiology. 2007;28(6):1114–1118.

[101] Mok TH, Mead S. Prion diseases. Medicine. 2017;45(11):674–677.

[102] Whitwell JL. Progression of atrophy in Alzheimer's disease and related disorders. Neurotoxicity research. 2010;18(3-4):339–346.

[103] Evans DA, Funkenstein HH, Albert MS, Scherr PA, Cook NR, Chown MJ, et al. Prevalence of Alzheimer's disease in a community population of older persons: higher than previously reported. JAMA. 1989;262(18):2551–2556.

[104] Van Duijn CM, Clayton D, Chandra V, Fratiglioni L, Graves AB, Heyman A, et al. Familial aggregation of Alzheimer's disease and related disorders: a collaborative re-analysis of case-control studies. International Journal of Epidemiology. 1991;20(Supplement 2):13–20.

[105] Ryman DC, Acosta-Baena N, Aisen PS, Bird T, Danek A, Fox NC, et al. Symptom onset in autosomal dominant Alzheimer disease: A systematic review and meta-analysis. Neurology. 2014;83(3):253–260.

[106] Farrer LA, Cupples LA, Haines JL, Hyman B, Kukull WA, Mayeux R, et al. Effects of age, sex, and ethnicity on the association between apolipoprotein E genotype and Alzheimer disease: a meta-analysis. JAMA. 1997;278(16):1349–1356.

[107] Birks JS, Chong LY, Grimley Evans J. Rivastigmine for Alzheimer's disease. The Cochrane Library. 2015;(4):CD001191.

[108] Howard R, McShane R, Lindesay J, Ritchie C, Baldwin A, Barber R, et al. Donepezil and memantine for moderate-to-severe Alzheimer's disease. New England Journal of Medicine. 2012;366(10):893–903.

[109] Sieben A, Van Langenhove T, Engelborghs S, Martin JJ, Boon P, Cras P, et al. The genetics and neuropathology of frontotemporal lobar degeneration. Acta Neuropathologica. 2012;124(3):353–372.

[110] Cairns NJ, Bigio EH, Mackenzie IRA, Neumann M, Lee VMY, Hatanpaa KJ, et al. Neuropathologic diagnostic and nosologic criteria for frontotemporal lobar degeneration: consensus of the Consortium for Frontotemporal Lobar Degeneration. Acta Neuropathologica. 2007;114(1):5–22.

[111] Harris JM, Gall C, Thompson JC, Richardson AMT, Neary D, du Plessis D, et al. Classification and pathology of primary progressive aphasia. Neurology. 2013;81(21):1832–1839.

[112] Harris JM, Jones M. Pathology in primary progressive aphasia syndromes. Current Neurology and Neuroscience Reports. 2014;14(8):466.

[113] Rohrer JD, Rosen HJ. Neuroimaging in frontotemporal dementia. International Review of Psychiatry. 2013;25(2):221–229.

[114] Broe M, Hodges J, Schofield E, Shepherd C, Kril J, Halliday G. Staging disease severity in pathologically confirmed cases of frontotemporal dementia. Neurology. 2003;60(6):1005–1011.

[115] Seeley WW, Crawford R, Rascovsky K, Kramer JH, Weiner M, Miller BL, et al. Frontal paralimbic network atrophy in very mild behavioral variant frontotemporal dementia. Archives of Neurology. 2008;65(2):249–255.

[116] Ossenkoppele R, Pijnenburg YAL, Perry DC, Cohn-Sheehy BI, Scheltens NME, Vogel JW, et al. The behavioural/dysexecutive variant of Alzheimer's disease: clinical, neuroimaging and pathological features. Brain. 2015;138(9):2732–2749.

[117] Rosen HJ, Gorno-Tempini ML, Goldman WP, Perry RJ, Schuff N, Weiner M, et al. Patterns of brain atrophy in frontotemporal dementia and semantic dementia. Neurology. 2002;58(2):198–208.

[118] Gorno-Tempini ML, Dronkers NF, Rankin KP, Ogar JM, Phengrasamy L, Rosen HJ, et al. Cognition and anatomy in three variants of primary progressive aphasia. Annals of Neurology. 2004;55(3):335–346.

[119] Madhavan A, Whitwell JL, Weigand SD, Duffy JR, Strand EA, Machulda MM, et al. FDG PET and MRI in logopenic primary progressive aphasia versus dementia of the Alzheimer's type. PLoS ONE. 2013;8(4):e62471.

[120] Onyike CU, Diehl-Schmid J. The epidemiology of frontotemporal dementia. International Review of Psychiatry. 2013;25(2):130–137.

[121] Coyle-Gilchrist ITS, Dick KM, Patterson K, Rodríquez PV, Wehmann E, Wilcox A, et al. Prevalence, characteristics, and survival of frontotemporal lobar degeneration syndromes. Neurology. 2016;86(18):1736–1743.

[122] Rohrer JD, Nicholas JM, Cash DM, van Swieten J, Dopper E, Jiskoot L, et al. Presymptomatic cognitive and neuroanatomical changes in genetic frontotemporal dementia in the Genetic Frontotemporal dementia Initiative (GENFI) study: a cross-sectional analysis. The Lancet Neurology. 2015;14(3):253–262.

[123] Gorno-Tempini ML, Hillis AE, Weintraub S, Kertesz A, Mendez M, Cappa Sea, et al. Classification of primary progressive aphasia and its variants. Neurology. 2011;76(11):1006–1014.

[124] Sink KM, Holden KF, Yaffe K. Pharmacological treatment of neuropsychiatric symptoms of dementia: a review of the evidence. JAMA. 2005;293(5):596–608.

[125] Lebert F, Stekke W, Hasenbroekx C, Pasquier F. Frontotemporal dementia:

a randomised, controlled trial with trazodone. Dementia and Geriatric Cognitive Disorders. 2004;17(4):355–359.

[126] Bottley A, Kondrashov A. Aberrant translation of proteins implicated in Alzheimer's disease pathology. OA Genetics. 2013;1(1):5.

[127] Sposito T, Preza E, Mahoney CJ, Setó-Salvia N, Ryan NS, Morris HR, et al. Developmental regulation of tau splicing is disrupted in stem cell-derived neurons from frontotemporal dementia patients with the 10+16 splice-site mutation in MAPT. Human Molecular Genetics. 2015;24(18):5260–5269.

[128] Hartl FU, Bracher A, Hayer-Hartl M. Molecular chaperones in protein folding and proteostasis. Nature. 2011;475(7356):324–332.

[129] Soti C, Csermely P. Aging and molecular chaperones. Experimental Gerontology. 2003;38(10):1037–1040.

[130] Kopeikina K, Hyman B, Spires-Jones T. Soluble forms of tau are toxic in Alzheimer's disease. Translational Neuroscience. 2012;3(3):223–233.

[131] Tanaka K, Matsuda N. Proteostasis and neurodegeneration: the roles of proteasomal degradation and autophagy. Biochimica et Biophysica Acta (BBA) - Molecular Cell Research. 2014;1843(1):197–204.

[132] Finley D. Recognition and processing of ubiquitin-protein conjugates by the proteasome. Annual Review of Biochemistry. 2009;78:477–513.

[133] Vilchez D, Saez I, Dillin A. The role of protein clearance mechanisms in organismal ageing and age related diseases. Nature Communications. 2014;5:5659.

[134] J Baranello R, L Bharani K, Padmaraju V, Chopra N, K Lahiri D, H Greig N, et al. Amyloid-beta protein clearance and degradation (ABCD) pathways and their role in Alzheimer's disease. Current Alzheimer Research. 2015;12(1):32–46.

[135] Nixon RA. The role of autophagy in neurodegenerative disease. Nature Medicine. 2013;19(8):983–997.

[136] Martinez-Vicente M, Cuervo AM. Autophagy and neurodegeneration: when the cleaning crew goes on strike. The Lancet Neurology. 2007;6(4):352–361.

[137] Goedert M, Masuda-Suzukake M, Falcon B. Like prions: the propagation of aggregated tau and α-synuclein in neurodegeneration. Brain. 2017;140(2):266–278.

[138] Rubinsztein DC, Mariño G, Kroemer G. Autophagy and aging. Cell. 2011;146(5):682–695.

[139] Cuervo AM. Autophagy and aging: keeping that old broom working. Trends in Genetics. 2008;24(12):604–612.

[140] Terman A. The effect of age on formation and elimination of autophagic vacuoles in mouse hepatocytes. Gerontology. 1995;41(Supplement 2):319–326.

[141] Nixon RA, Wegiel J, Kumar A, Yu WH, Peterhoff C, Cataldo A, et al. Extensive involvement of autophagy in Alzheimer disease: an immuno-electron microscopy study. Journal of Neuropathology & Experimental Neurology. 2005;64(2):113–122.

[142] Boland B, Kumar A, Lee S, Platt FM, Wegiel J, Yu WH, et al. Autophagy induction and autophagosome clearance in neurons: relationship to autophagic pathology in Alzheimer's disease. Journal of Neuroscience. 2008;28(27):6926–6937.

[143] Mitra S, Finkbeiner S. The ubiquitin-proteasome pathway in Huntington's disease. The Scientific World Journal. 2008;8:421–433.

[144] Dolan PJ, Johnson GV. A caspase cleaved form of tau is preferentially degraded through the autophagy pathway. Journal of Biological Chemistry. 2010;285(29):21978–21987.

[145] Kaufman SK, Sanders DW, Thomas TL, Ruchinskas AJ, Vaquer-Alicea J, Sharma AM, et al. Tau prion strains dictate patterns of cell pathology, progression rate, and regional vulnerability in vivo. Neuron. 2016;92(4):796–812.

[146] Walker LC, Jucker M. Neurodegenerative diseases: expanding the prion concept. Annual Review of Neuroscience. 2015;38:87–103.

[147] Frost B, Jacks RL, Diamond MI. Propagation of tau misfolding from the outside to the inside of a cell. Journal of Biological Chemistry. 2009;284(19):12845–12852.

[148] Hardy J, Revesz T. The spread of neurodegenerative disease. The New England Journal of Medicine. 2012;366(22):2126–2128.

[149] Masel J, Jansen VAA, Nowak MA. Quantifying the kinetic parameters of prion replication. Biophysical Chemistry. 1999;77(2-3):139–152.

[150] Bessen RA, Kocisko DA, Raymond GJ, Nandan S, Lansbury PT, Caughey B. Non-genetic propagation of strain-specific properties of scrapie prion protein. Nature. 1995;375(6533):698–700.

[151] Telling GC, Parchi P, DeArmond SJ, Cortelli P, Montagna P, Gabizon R, et al. Evidence for the conformation of the pathologic isoform of the prion protein enciphering and propagating prion diversity. Science. 1996;274(5295):2079–2082.

[152] Prusiner SB. Prions. Proceedings of the National Academy of Sciences. 1998;95(23):13363–13383.

[153] Magalhaes AC, Baron GS, Lee KS, Steele-Mortimer O, Dorward D, Prado MAM, et al. Uptake and neuritic transport of scrapie prion protein coincident with infection of neuronal cells. Journal of Neuroscience. 2005;25(21):5207–5216.

[154] Fevrier B, Vilette D, Archer F, Loew D, Faigle W, Vidal M, et al. Cells release prions in association with exosomes. Proceedings of the National Academy of Sciences. 2004;101(26):9683–9688.

[155] Gousset K, Schiff E, Langevin C, Marijanovic Z, Caputo A, Browman DT, et al. Prions hijack tunnelling nanotubes for intercellular spread. Nature Cell Biology. 2009;11(3):328.

[156] Petkova AT, Leapman RD, Guo Z, Yau WM, Mattson MP, Tycko R. Self-propagating, molecular-level polymorphism in Alzheimer's ß-amyloid fibrils. Science. 2005;307(5707):262–265.

[157] Frost B, Ollesch J, Wille H, Diamond MI. Conformational diversity of wild-type Tau fibrils specified by templated conformation change. Journal of Biological Chemistry. 2009;284(6):3546–3551.

[158] Yonetani M, Nonaka T, Masuda M, Inukai Y, Oikawa T, Hisanaga Si, et al. Conversion of wild-type α-synuclein into mutant-type fibrils and its propagation in the presence of A30P mutant. Journal of Biological Chemistry. 2009;284(12):7940–7950.

[159] Li JY, Englund E, Holton JL, Soulet D, Hagell P, Lees AJ, et al. Lewy bodies in grafted neurons in subjects with Parkinson's disease suggest host-to-graft disease propagation. Nature Medicine. 2008;14(5):501–503.

[160] Kordower JH, Chu Y, Hauser RA, Olanow CW, Freeman TB. Transplanted dopaminergic neurons develop PD pathologic changes: a second case report. Movement Disorders. 2008;23(16):2303–2306.

[161] Kordower JH, Chu Y, Hauser RA, Freeman TB, Olanow CW. Lewy body-like pathology in long-term embryonic nigral transplants in Parkinson's disease. Nature Medicine. 2008;14(5):504–506.

[162] Desplats P, Lee HJ, Bae EJ, Patrick C, Rockenstein E, Crews L, et al. Inclusion formation and neuronal cell death through neuron-to-neuron trans-

mission of α-synuclein. Proceedings of the National Academy of Sciences. 2009;106(31):13010–13015.

[163] Powers ET, Morimoto RI, Dillin A, Kelly JW, Balch WE. Biological and chemical approaches to diseases of proteostasis deficiency. Annual Review of Biochemistry. 2009;78:959–991.

[164] Schmidt M, Finley D. Regulation of proteasome activity in health and disease. Biochimica et Biophysica Acta (BBA) - Molecular Cell Research. 2014;1843(1):13–25.

[165] Ferrington DA, Husom AD, Thompson LV. Altered proteasome structure, function, and oxidation in aged muscle. The FASEB Journal. 2005;19(6):644–646.

[166] Lee CK, Klopp RG, Weindruch R, Prolla TA. Gene expression profile of aging and its retardation by caloric restriction. Science. 1999;285(5432):1390–1393.

[167] Ly DH, Lockhart DJ, Lerner RA, Schultz PG. Mitotic misregulation and human aging. Science. 2000;287(5462):2486–2492.

[168] Vernace VA, Arnaud L, Schmidt-Glenewinkel T, Figueiredo-Pereira ME. Aging perturbs 26S proteasome assembly in Drosophila melanogaster. The FASEB Journal. 2007;21(11):2672–2682.

[169] Andersson V, Hanzén S, Liu B, Molin M, Nyström T. Enhancing protein disaggregation restores proteasome activity in aged cells. Aging. 2013;5(11):802–812.

[170] Grune T, Jung T, Merker K, Davies KJ. Decreased proteolysis caused by protein aggregates, inclusion bodies, plaques, lipofuscin, ceroid, and 'aggresomes' during oxidative stress, aging, and disease. The International Journal of Biochemistry & Cell Biology. 2004;36(12):2519–2530.

[171] Bateman RJ, Munsell LY, Morris JC, Swarm R, Yarasheski KE, Holtzman DM. Quantifying CNS protein production and clearance rates in humans using in vivo stable isotope labeling, immunoprecipitation, and tandem mass spectrometry. Nature Medicine. 2006;12(7):856–861.

[172] Proctor CJ, Lorimer IAJ. Modelling the role of the Hsp70/Hsp90 system in the maintenance of protein homeostasis. PLoS ONE. 2011;6(7):e22038.

[173] Mawuenyega KG, Sigurdson W, Ovod V, Munsell L, Kasten T, Morris JC, et al. Decreased clearance of CNS β-amyloid in Alzheimer's disease. Science. 2010;330(6012):1774–1774.

[174] Waters J. The concentration of soluble extracellular amyloid-β protein in acute brain slices from CRND8 mice. PLoS ONE. 2010;5(12):e15709.

[175] Dunning CJR, Reyes JF, Steiner JA, Brundin P. Can Parkinson's disease pathology be propagated from one neuron to another? Progress in Neurobiology. 2012;97(2):205–219.

[176] Wu JW, Hussaini SA, Bastille IM, Rodriguez GA, Mrejeru A, Rilett K, et al. Neuronal activity enhances tau propagation and tau pathology in vivo. Nature Neuroscience. 2016;19(8):1085–1092.

[177] Raj A, Kuceyeski A, Weiner M. A network diffusion model of disease progression in dementia. Neuron. 2012;73(6):1204–1215.

[178] Volpicelli-Daley LA, Luk KC, Patel TP, Tanik SA, Riddle DM, Stieber A, et al. Exogenous α-synuclein fibrils induce Lewy body pathology leading to synaptic dysfunction and neuron death. Neuron. 2011;72(1):57–71.

[179] Spires-Jones TL, Hyman BT. The intersection of amyloid beta and tau at synapses in Alzheimer's disease. Neuron. 2014;82(4):756–771.

[180] Sabry J, O'Connor TP, Kirschner MW. Axonal transport of tubulin in tit pioneer neurons in situ. Neuron. 1995;14(6):1247–1256.

[181] Utton MA, Noble WJ, Hill JE, Anderton BH, Hanger DP. Molecular motors implicated in the axonal transport of tau and α-synuclein. Journal of Cell Science. 2005;118(20):4645–4654.

[182] Ackerley S, Thornhill P, Grierson AJ, Brownlees J, Anderton BH, Leigh PN, et al. Neurofilament heavy chain side arm phosphorylation regulates axonal transport of neurofilaments. The Journal of Cell Biology. 2003;161(3):489–495.

[183] DeArmond SJ, Mobley WC, DeMott DL, Barry RA, Beckstead JH, Prusiner SB. Changes in the localization of brain prion proteins during scrapie infection. Neurology. 1987;37(8):1271–1271.

[184] Borchelt DR, Koliatsos VE, Guarnieri M, Pardo CA, Sisodia SS, Price DL. Rapid anterograde axonal transport of the cellular prion glycoprotein in the peripheral and central nervous systems. Journal of Biological Chemistry. 1994;269(20):14711–14714.

[185] Rodríguez-Martín T, Cuchillo-Ibáñez I, Noble W, Nyenya F, Anderton BH, Hanger DP. Tau phosphorylation affects its axonal transport and degradation. Neurobiology of Aging. 2013;34(9):2146–2157.

[186] Park JY, Kim KS, Lee SB, Ryu JS, Chung KC, Choo YK, et al. On the mechanism of internalization of α-synuclein into microglia: roles of ganglioside GM1 and lipid raft. Journal of Neurochemistry. 2009;110(1):400–411.

[187] Saavedra L, Mohamed A, Ma V, Kar S, de Chaves EP. Internalization of β-amyloid peptide by primary neurons in the absence of apolipoprotein E. Journal of Biological Chemistry. 2007;282(49):35722–35732.

[188] Emmanouilidou E, Melachroinou K, Roumeliotis T, Garbis SD, Ntzouni M, Margaritis LH, et al. Cell-produced α-synuclein is secreted in a calcium-dependent manner by exosomes and impacts neuronal survival. Journal of Neuroscience. 2010;30(20):6838–6851.

[189] Steiner JA, Angot E, Brundin P. A deadly spread: cellular mechanisms of α-synuclein transfer. Cell Death and Differentiation. 2011;18(9):1425.

[190] Vella LJ, Sharples RA, Lawson VA, Masters CL, Cappai R, Hill AF. Packaging of prions into exosomes is associated with a novel pathway of PrP processing. The Journal of Pathology. 2007;211(5):582–590.

[191] Lee HJ, Patel S, Lee SJ. Intravesicular localization and exocytosis of α-synuclein and its aggregates. Journal of Neuroscience. 2005;25(25):6016–6024.

[192] Jang A, Lee HJ, Suk JE, Jung JW, Kim KP, Lee SJ. Non-classical exocytosis of α-synuclein is sensitive to folding states and promoted under stress conditions. Journal of Neurochemistry. 2010;113(5):1263–1274.

[193] Ahn KJ, Paik SR, Chung KC, Kim J. Amino acid sequence motifs and mechanistic features of the membrane translocation of α-synuclein. Journal of Neurochemistry. 2006;97(1):265–279.

[194] Auluck PK, Caraveo G, Lindquist S. α-Synuclein: membrane interactions and toxicity in Parkinson's disease. Annual Review of Cell and Developmental Biology. 2010;26:211–233.

[195] Lee HJ, Suk JE, Bae EJ, Lee JH, Paik SR, Lee SJ. Assembly-dependent endocytosis and clearance of extracellular a-synuclein. The international journal of biochemistry & cell biology. 2008;40(9):1835–1849.

[196] Danzer KM, Haasen D, Karow AR, Moussaud S, Habeck M, Giese A, et al. Different species of α-synuclein oligomers induce calcium influx and seeding. Journal of Neuroscience. 2007;27(34):9220–9232.

[197] Pandya S, Kuceyeski A, Raj A. The brain's structural connectome mediates the relationship between regional neuroimaging biomarkers in Alzheimer's Disease. Journal of Alzheimer's Disease. 2017;55(4):1639–1657.

[198] Zhou J, Greicius MD, Gennatas ED, Growdon ME, Jang JY, Rabinovici GD, et al. Divergent network connectivity changes in behavioural variant frontotemporal dementia and Alzheimer's disease. Brain. 2010;133(5):1352–1367.

[199] Ilieva H, Polymenidou M, Cleveland DW. Non-cell autonomous toxicity in neurodegenerative disorders: ALS and beyond. The Journal of Cell Biology. 2009;187(6):761–772.

[200] L Mickiewicz A, H Kordower J. GDNF family ligands: a potential future for Parkinson's disease therapy. CNS & Neurological Disorders - Drug Targets. 2011;10(6):703–711.

[201] Rangasamy SB, Soderstrom K, Bakay RAE, Kordower JH. Neurotrophic factor therapy for Parkinson's disease. Progress in Brain Research. 2010;184:237–264.

[202] Sakowski SA, Schuyler AD, Feldman EL. Insulin-like growth factor-I for the treatment of amyotrophic lateral sclerosis. Amyotrophic Lateral Sclerosis. 2009;10(2):63–73.

[203] Wyatt TJ, Keirstead HS. Stem cell-derived neurotrophic support for the neuromuscular junction in spinal muscular atrophy. Expert Opinion on Biological Therapy. 2010;10(11):1587–1594.

[204] Zuccato C, Cattaneo E. Brain-derived neurotrophic factor in neurodegenerative diseases. Nature Reviews Neurology. 2009;5(6):311–322.

[205] Brodland GW. How computational models can help unlock biological systems. In: Seminars in Cell & Developmental Biology. vol. 47–48. Elsevier; 2015. p. 62–73.

[206] Bartocci E, Lió P. Computational modeling, formal analysis, and tools for systems biology. PLoS Computational Biology. 2016;12(1):e1004591.

[207] Anderson A, Rejniak K. Single-cell based models in biology and medicine. Springer Science & Business Media; 2007.

[208] Tegnér JN, Compte A, Auffray C, An G, Cedersund G, Clermont G, et al. Computational disease modeling - fact or fiction? BMC Systems Biology. 2009;3(1):56.

[209] Kar S, Leszczynski J. Recent Advances of Computational Modeling for Predicting Drug Metabolism: A Perspective. Current Drug Metabolism. 2017;18(12):1106–1122.

[210] Zienkiewicz OC, Taylor RL. The finite element method for solid and structural mechanics. Elsevier; 2005.

[211] Amaran S, Sahinidis NV, Sharda B, Bury SJ. Simulation optimization: a review of algorithms and applications. Annals of Operations Research. 2016;240(1):351–380.

[212] Rios LM, Sahinidis NV. Derivative-free optimization: a review of algorithms and comparison of software implementations. Journal of Global Optimization. 2013;56(3):1247–1293.

[213] Nelder JA, Mead R. A simplex method for function minimization. The Computer Journal. 1965;7(4):308–313.

[214] Torczon V. On the convergence of pattern search algorithms. SIAM Journal on Optimization. 1997;7(1):1–25.

[215] Kolda TG, Lewis RM, Torczon V. Optimization by direct search: New perspectives on some classical and modern methods. SIAM Review. 2003;45(3):385–482.

[216] Powell MJD. A Direct Search Optimization Method That Models the Objective and Constraint Functions by Linear Interpolation. In: Advances in Optimization and Numerical Analysis. Springer; 1994. p. 51–67.

[217] Winslow TA, Trew RJ, Gilmore P, Kelley CT. Simulated performance optimization of GaAs MESFET amplifiers. In: Proceedings IEEE/Cornell Conference on Advanced Concepts in High Speed Semiconductor Devices and Circuits. IEEE; 1991. p. 393–402.

[218] Shubert BO. A sequential method seeking the global maximum of a function. SIAM Journal on Numerical Analysis. 1972;9(3):379–388.

[219] Huyer W, Neumaier A. Global optimization by multilevel coordinate search. Journal of Global Optimization. 1999;14(4):331–355.

[220] Schonlau M. Computer experiments and global optimization. University of Waterloo. 1997;.

[221] Powell MJD. Recent research at Cambridge on radial basis functions. In: New Developments in Approximation Theory. Springer; 1999. p. 215–232.

[222] Cox DD, John S. A statistical method for global optimization. In: IEEE International Conference on Systems, Man, and Cybernetics. IEEE; 1992. p. 1241–1246.

[223] Booker AJ, Dennis JE, Frank PD, Serafini DB, Torczon V, Trosset MW. A rigorous framework for optimization of expensive functions by surrogates. Structural optimization. 1999;17(1):1–13.

[224] Huyer W, Neumaier A. SNOBFIT - stable noisy optimization by branch and fit. ACM Transactions on Mathematical Software. 2008;35(2):9:1–25.

[225] Metropolis N, Rosenbluth AW, Rosenbluth MN, Teller AH, Teller E. Equation of state calculations by fast computing machines. The Journal of Chemical Physics. 1953;21(6):1087–1092.

[226] Gen M, Lin L. Genetic algorithms. Wiley Encyclopedia of Computer Science and Engineering. 2007;p. 1–15.

[227] Eberhart R, Kennedy J. A new optimizer using particle swarm theory. In: Proceedings of the Sixth International Symposium on Micro Machine and Human Science. IEEE; 1995. p. 39–43.

[228] Juty N, Ali R, Glont M, Keating S, Rodriguez N, Swat MJ, et al. BioModels: content, features, functionality, and use. CPT: Pharmacometrics & Systems Pharmacology. 2015;4(2):55–68.

[229] Büchel F, Saliger S, Dräger A, Hoffmann S, Wrzodek C, Zell A, et al. Parkinson's disease: dopaminergic nerve cell model is consistent with experimental finding of increased extracellular transport of α-synuclein. BMC Neuroscience. 2013;14(1):136.

[230] Puri IK, Li L. Mathematical modeling for the pathogenesis of Alzheimer's disease. PLoS ONE. 2010;5(12):e15176.

[231] Winter F, Bludszuweit-Philipp C, Wolkenhauer O. Mathematical analysis of the influence of brain metabolism on the BOLD signal in Alzheimer's disease. Journal of Cerebral Blood Flow & Metabolism. 2018;38(2):304–316.

[232] Qosa H, Abuasal BS, Romero IA, Weksler B, Couraud PO, Keller JN, et al. Differences in amyloid-β clearance across mouse and human blood-brain barrier models: kinetic analysis and mechanistic modeling. Neuropharmacology. 2014;79:668–678.

[233] Lockwood P, Ewy W, Hermann D, Holford N. Application of clinical trial simulation to compare proof-of-concept study designs for drugs with a slow onset of effect; an example in Alzheimer's disease. Pharmaceutical Research. 2006;23(9):2050–2059.

[234] Masel J, Jansen VAA. Designing drugs to stop the formation of prion aggregates and other amyloids. Biophysical Chemistry. 2000;88(1-3):47–59.

[235] Morris AM, Watzky MA, Agar JN, Finke RG. Fitting neurological protein aggregation kinetic data via a 2-step, minimal/"Ockham's Razor" model: The Finke-Watzky mechanism of nucleation followed by autocatalytic surface growth. Biochemistry. 2008;47(8):2413–2427.

[236] Clarke G, Collins RA, Leavitt BR, Andrews DF, Hayden MR, Lumsden CJ, et al. A one-hit model of cell death in inherited neuronal degenerations. Nature. 2000;406(6792):195–199.

[237] Kuznetsov IA, Kuznetsov AV. A two population model of prion transport through a tunnelling nanotube. Computer Methods in Biomechanics and Biomedical Engineering. 2014;17(15):1705–1715.

[238] Matthäus F. Diffusion versus network models as descriptions for the spread of prion diseases in the brain. Journal of Theoretical Biology. 2006;240(1):104–113.

[239] Stumpf MPH, Krakauer DC. Mapping the parameters of prion-induced neuropathology. Proceedings of the National Academy of Sciences. 2000;97(19):10573–10577.

[240] Hines ML, Carnevale NT. The NEURON simulation environment. Neural Computation. 1997;9(6):1179–1209.

[241] Neymotin SA, Jacobs KM, Fenton AA, Lytton WW. Synaptic information transfer in computer models of neocortical columns. Journal of Computational Neuroscience. 2011;30(1):69–84.

[242] Brette R, Rudolph M, Carnevale T, Hines M, Beeman D, Bower JM, et al. Simulation of networks of spiking neurons: a review of tools and strategies. Journal of Computational Neuroscience. 2007;23(3):349–398.

[243] Rall W. Cable theory for dendritic neurons. In: Methods in Neuronal Modeling. MIT press; 1989. p. 9–92.

[244] McDougal RA, Morse TM, Carnevale T, Marenco L, Wang R, Migliore M, et al. Twenty years of ModelDB and beyond: building essential modeling tools for the future of neuroscience. Journal of Computational Neuroscience. 2017;42(1):1–10.

[245] Shepherd GM. The synaptic organization of the brain. New York: Oxford University Press; 2003.

[246] Ries HM, Nussbaum-Krammer C. Shape matters: the complex relationship between aggregation and toxicity in protein-misfolding diseases. Essays In Biochemistry. 2016;60(2):181–190.

[247] Pooler AM, Polydoro M, Maury EA, Nicholls SB, Reddy SM, Wegmann S, et al. Amyloid accelerates tau propagation and toxicity in a model of early Alzheimer's disease. Acta Neuropathologica Communications. 2015;3(1):14.

[248] Sepulcre J, Grothe MJ, Sabuncu M, Chhatwal J, Schultz AP, Hanseeuw B, et al. Hierarchical organization of tau and amyloid deposits in the cerebral cortex. JAMA Neurology. 2017;74(7):813–820.

[249] Parker TD, Slattery CF, Zhang J, Nicholas JM, Paterson RW, Foulkes AJ, et al. Cortical microstructure in young onset Alzheimer's disease using neurite orientation dispersion and density imaging. Human brain mapping. 2018;39(7):3005–3017.

[250] Karahanoğlu FI, Caballero-Gaudes C, Lazeyras F, Van De Ville D. Total activation: fMRI deconvolution through spatio-temporal regularization. Neuroimage. 2013;73:121–134.

[251] Tournier JD, Calamante F, Connelly A. Improved probabilistic streamlines tractography by 2nd order integration over fibre orientation distributions. In: Proceedings of the International Society for Magnetic Resonance in Medicine. vol. 18; 2010. p. 1670.

[252] Smith RE, Tournier JD, Calamante F, Connelly A. SIFT: spherical-deconvolution informed filtering of tractograms. Neuroimage. 2013;67:298–312.

[253] Friston KJ, Kahan J, Biswal B, Razi A. A DCM for resting state fMRI. Neuroimage. 2014;94:396–407.

[254] Friston KJ, Litvak V, Oswal A, Razi A, Stephan KE, van Wijk BC, et al. Bayesian model reduction and empirical Bayes for group (DCM) studies. Neuroimage. 2016;128:413–431.

[255] Stephan KE, Tittgemeyer M, Knösche TR, Moran RJ, Friston KJ. Tractography based priors for dynamic causal models. Neuroimage. 2009;47(4):1628–1638.

[256] Young AL, Marinescu RV, Oxtoby NP, Bocchetta M, Yong K, Firth NC, et al. Uncovering the heterogeneity and temporal complexity of neurodegenerative diseases with Subtype and Stage Inference. Nature Communications. 2018;9(1):4273.

[257] Xia M, Wang J, He Y. BrainNet Viewer: A Network Visualization Tool for Human Brain Connectomics. PLoS ONE. 2013;8(7):e68910.